Three-body correlations in nuclear matter

B. D. Day
Argonne National Laboratory, Argonne, Illinois 60439
(Received 22 December 1980)

A momentum-space method is developed for the calculation of three-body terms in the Brueckner-Bethe method for nuclear matter. The method is similar to one used earlier for central S-wave potentials. Here we extend it to the full nuclear force, including tensor forces, spin-orbit forces, etc. Furthermore, we show how the method can be used to investigate the possibility of long-range correlations in nuclear matter by summing the generalized ring series. The numerical accuracy obtainable with various mesh parameters and cutoffs in momentum space, and with various truncations of partial-wave expansions, is thoroughly explored. Several angle-average approximations are used, and the estimated numerical accuracy in the three-body cluster energy is 10–15%. The method is applied to a central potential v_2, a semirealistic potential v_6 (Reid), which has a tensor force, and to the Reid potential, augmented by an interaction that is consistent with empirical scattering phase shifts in two-body partial waves with $j \geq 3$. In all cases the three-body contribution to the energy is correctly given in order of magnitude by $\kappa_2 D_2$, where D_2 is the two-body contribution and κ_2 is the usual convergence parameter of the Brueckner-Bethe method. The generalized ring series is found to converge rapidly, indicating that long-range correlations are not very important for the binding energy of nuclear matter. The Reid potential is found to saturate at the right energy but at too high a density.

[NUCLEAR STRUCTURE Method for solving Brueckner-Bethe three-body equations in nuclear matter developed and applied to the Reid potential.]

I. INTRODUCTION

Brueckner-Bethe calculations of nuclear matter are currently formulated using either the hole-line expansion[1–3] or the Bochum truncation[4–6] of the coupled-cluster equations.[6,7] In either case the lowest-order approximation involves a two-body equation, which can be accurately solved. To go beyond lowest order, one has to solve a three-body equation. In the hole-line expansion this gives the three-body cluster term D_3^c, which is the dominant three-hole-line term.[8] The other three-hole-line term, the hole-hole term, is small compared to D_3^c. It involves only two-body quantities and is neglected in this paper. In the Bochum coupled-cluster scheme,[6] one includes at the three-body level the entire generalized ring series.[3,9–11] The first term in this series is D_3^c, and succeeding terms are particular diagrams with four, five,... hole lines.

Near the empirical saturation density, we have $D_3^c \sim -5$ MeV for the Reid potential.[12] Hence this term must be taken into account in any adequate approximation scheme. The first calculations of D_3^c were made by Dahlblom[13] and have been improved by Grangé.[14,15] The calculations are done in coordinate space and involve several approximations whose accuracy has never been quantitatively assessed. Furthermore, this method does not fully treat the tensor force. Depp[16] made an ambitious and useful attempt to do a more accurate calculation of D_3^c in momentum space, but his work was never carried far enough to give useful numerical results. Day, Coester, and Goodman,[17] also working in momentum space and using some of Depp's ideas, showed that accurate calculations could be made for a pure S-wave two-body potential. In this paper we extend this method in two ways: (1) The full nuclear force is treated, and (2) we calculate not only D_3^c but also the sum of the complete generalized ring series.

The generalized ring series arises as follows.[3,9–11] The dominant three-hole-line term is D_3^c and, from

the point of view of the hole-line expansion, there is no point in going beyond D_3^c unless *all* four-hole-line terms are calculated. However, the Bochum truncation of the coupled-cluster equations implies that the diagrams should *not* be grouped strictly according to the number of hole lines. Instead, a partial summation of particular diagrams with three, four, five,... hole lines should be carried out. We call these the generalized ring diagrams because they include all the forward-going ring diagrams, which are known to build up important long-range correlations in the electron gas[18] and in low-density Bose systems.[19] The coupled-cluster equations imply additional partial summations[5,6] that are believed to be less important than the generalized rings and are not considered here. If the generalized ring series converges slowly, this suggests that (1) the hole-line expansion must be modified by summing the generalized ring series, and (2) nuclear matter contains significant long-range correlations. Hence it is important to study the generalized ring series, and we do this in addition to calculating D_3^c.

Thus two separate types of calculation are possible. If one wants only D_3^c, one calculates diagonal matrix elements of the operator $\mathcal{O}$ defined by Eq. (2.44). This is called an $\mathcal{O}$-type calculation. If one wants the generalized ring series (whose first term is D_3^c), one must calculate the matrix $\mathcal{M}$ defined by Eq. (2.62). This is called an $\mathcal{M}$-type calculation and requires more computer time than an $\mathcal{O}$-type calculation. Similar approximations are made in the two types of calculation.

Our main approximation is the use of several angle-average approximations, in particular an angle-average Pauli operator. We make it plausible that the combined effect of all our approximations is to produce an error of 15% or less in D_3^c.

The two-body reaction matrix is calculated in momentum space in each two-body channel. Purely as a numerical technique, this matrix is represented as a sum of separable terms. Truncation of this sum gives an error of order 0.5 MeV in D_3^c at twice the empirical saturation density, and this error decreases rapidly as the density is lowered. Thus the full complexity of the nuclear force can be treated to good accuracy. One exception to this may be two-body potentials with hard cores. The hard core produces a long-range tail in the two-body reaction matrix in momentum space. We use a cutoff at 8 fm^{-1} in momentum space, and whether this procedure is adequate for a potential with a hard core has not been investigated.

The calculations are fairly complicated. Therefore, the formulas and numerical procedures are given in enough detail that the reader could repeat the calculations and get the same numerical results. This should be useful in detecting possible conceptual or numerical errors, and in resolving possible discrepancies with similar calculations done by others in the future. Appreciable computer resources are required for the calculations, e.g., a complete $\mathcal{M}$-type calculation for the Reid potential at one density takes 2 – 3 h on the IBM 370-195. By using different mesh parameters, more severe truncation of partial-wave expansions, etc., one can reduce the computing time at the expense of some loss of accuracy. Detailed tests are made of the accuracy obtainable with various mesh parameters and truncations. This material serves two purposes. First, it allows the reader to judge the accuracy of the present results. Second, for someone contemplating similar calculations, it permits an estimate of the amount of computer resources necessary to achieve a given numerical accuracy.

The general formalism for $\mathcal{O}$-type and $\mathcal{M}$-type calculations is given in Sec. II. In Sec. III we introduce the basis states used in numerical calculations, and in Sec. IV certain important matrix elements are calculated using these basis states. Equations for computation are obtained in Sec. V, and the numerical methods for treating them are given in Sec. VI. Test calculations are described in Sec. VII, and results for the two-body potentials v_2, v_6 (Reid), and full Reid are given in Sec. VIII (these two-body potentials are defined in the Appendix). Section IX contains a summary and a discussion.

For readers who are not interested in following all the details of the calculations, I suggest the following. First read Secs. II A – II C in order to learn precisely which terms are included in D_3^c and in the generalized ring series. Then skip to Sec. VII B, where qualitative arguments are given about the number of partial waves needed in the calculations. Finally, go to Secs. VIII and IX for the numerical results and discussion.

II. GENERAL FORMALISM

We consider a system of A identical nucleons in volume Ω. The nucleons are assumed to obey the nonrelativistic Schrödinger equation with Hamiltonian

$$H = \sum_{i=1}^{A} T_i + \sum_{i<j}^{A} v_{ij} , \tag{2.1}$$

where T_i is the kinetic energy and v_{ij} is the two-body potential. The ground-state energy per particle depends on the density

$$\rho = A/\Omega \tag{2.2}$$

which is held fixed as A and Ω become large. The noninteracting ground state describes a Fermi gas with all single-particle momentum states filled up to the Fermi momentum k_F. Each momentum state can accommodate four nucleons, and the density is related to k_F by

$$\rho = 2k_F^3/3\pi^2 . \tag{2.3}$$

The three-body cluster energy (per particle) D_3^c involves diagonal matrix elements in states with all three particles in the Fermi sea. We reserve the symbols $\vec{p}_1$, $\vec{p}_2$,... for momenta in the Fermi sea, so that

$$p_i = |\vec{p}_i| < k_F .$$

Integrals over $\vec{p}_i$ are understood to run only over the Fermi sea. If summation indices are not explicitly specified for a symbol Σ, then the expression to its right is to be summed over all indices. The notation

$$\delta(ab\ldots|a'b'\ldots) = \delta(a,a')\delta(b,b')\ldots \tag{2.4}$$

is used, where the right-hand side is a product of Kronecker deltas.

We use units in which $\hbar^2/M = 1$, where M is the nucleon mass. Then energy has units fm^{-2}, where $1\ \mathrm{fm}^{-2} = 41.47$ MeV.

In the succeeding subsections we derive the equations needed to calculate D_3^c ($\mathscr{O}$-type calculation) and the generalized ring series ($\mathscr{M}$-type calculation). As mentioned in the Introduction, the equations can be derived either by partial summation of the Brueckner-Goldstone perturbation expansion,[20,2,8] or by truncation of the coupled-cluster equations.[6,7,11] The derivation given here uses the perturbation expansion. However, we emphasize that all the results can be obtained by appropriate truncation of the coupled cluster equations,[6,7,11] which are a system of equations that is equivalent to the many-body Schrödinger equation. In particular, the equations for $\mathscr{O}$-type calculations can be obtained from Eqs. (4.41) and (4.49) of Ref. 11, and those for $\mathscr{M}$-type calculations come from Eqs. (5.23)–(5.25) of Ref. 11. Here, however, we use the perturbation expansion, assuming that the reader has some familiarity with the partial summations of the perturbation expansion that lead to the hole-line expansion.[1,2,8]

A. Basis states and operators

The wave function of a normalized single-particle momentum state is

$$(\vec{r}_1|q) = \Omega^{-1/2}\exp(i\vec{q}\cdot\vec{r}_1) , \tag{2.5}$$

where the allowed momenta $\vec{q}$ are determined by periodic boundary conditions. We regard q as an index that labels the momentum $\vec{q}$ as well as spin and isospin projections. We define $|qs)_{\mathrm{na}}$ by

$$(\vec{r}_1\vec{r}_2|qs)_{\mathrm{na}} = (\vec{r}_1|q)(\vec{r}_2|s) , \tag{2.6}$$

where na stands for "not antisymmetrized." The antisymmetric two-body state $|qs)$ is defined by

$$|qs) = 2^{-1/2}(|qs)_{\mathrm{na}} - |sq)_{\mathrm{na}}) . \tag{2.7}$$

We then find the orthogonality and completeness relations

$$(qs|q's') = \delta(q,q')\delta(s,s') - \delta(q,s')\delta(s,q') , \tag{2.8}$$

$$\tfrac{1}{2}\sum|qs)(qs| = \mathscr{A}_{12} , \tag{2.9}$$

where $\mathscr{A}_{12}$ projects onto antisymmetric two-body states. It is given in terms of the permutation operator P_{12} by

$$\mathscr{A}_{12} = \tfrac{1}{2}(1 - P_{12}) . \tag{2.10}$$

The three-body state $|q,st)$ is defined by

$$(\vec{r}_3\vec{r}_1\vec{r}_2|q,st) = (\vec{r}_3|q)(\vec{r}_1\vec{r}_2|st) . \tag{2.11}$$

It is antisymmetric in particles 1 and 2 but has no simple symmetry under other permutations. The orthogonality and completeness relations are

$$(q,st|q',s't') = \delta(q,q')[\delta(s,s')\delta(t,t') - \delta(s,t')\delta(t,s')] , \tag{2.12}$$

$$\tfrac{1}{2}\sum|q,st)(q,st| = \mathscr{A}_{12} . \tag{2.13}$$

If P_{123} and P_{132} are the two cyclic permutation operators for three particles, we define

$$X = P_{123} + P_{132} . \tag{2.14}$$

One then easily finds

$$\sum|q,st)(s,tq| = \sum|q,st)(t,qs| = \mathscr{A}_{12}X\mathscr{A}_{12} . \tag{2.15}$$

When we take matrix elements of this between states that are antisymmetric in 1,2, as always happens in practice, the factors $\mathscr{A}_{12}$ can be replaced by

unity.

The two-body reaction matrix G is defined by

$$G = v - v(Q/e)G \ , \tag{2.16}$$

where v is the two-body potential. The Pauli operator Q is defined by

$$\begin{aligned} Q\,|st) &= |st), \text{ if } s > k_F \text{ and } t > k_F \\ &= 0, \text{ otherwise} , \end{aligned} \tag{2.17}$$

and e is defined below.

In the three-body problem we define G and Q to act on particles 1 and 2. Two cases then arise: either there is a spectator particle 3 above the Fermi sea, or there is not. We use subscripts a and b, respectively, for these two cases. If particle 3 is not excited above the Fermi sea, we have

$$e_b\,|st) = [E(s) + E(t) - \omega_2]\,|st) \ , \tag{2.18}$$

where $E(s)$ is the single-particle energy and ω_2 is the energy of the initial two-body state in the Fermi sea,

$$\omega_2 = E(p_1) + E(p_2) \ . \tag{2.19}$$

When a spectator particle 3 is above the Fermi sea with momentum q, e_a depends on q and is given by

$$e_a(q)\,|st) = [E(q) + E(s) + E(t) - \omega_3]\,|st) \ , \tag{2.20}$$

where

$$\omega_3 = E(p_1) + E(p_2) + E(p_3) \ . \tag{2.21}$$

The reaction matrices calculated using $e_a(q)$, e_b are denoted $G_a(q)$, G_b, respectively. The Pauli operator Q is the same in the two cases. However, we will later use an angle-average approximation for Q that is different in the two cases. Therefore, when convenient, we often write Q_a or Q_b for Q.

In the three-body basis, Q, e, and G are defined by

$$\begin{aligned} Q\,|q,st) &= |q,st), \text{ if } s > k_F \text{ and } t > k_F \\ &= 0, \text{ otherwise} , \end{aligned} \tag{2.22}$$

$$\begin{aligned} e\,|q,st) &= [E(q) + E(s) + E(t) - \omega_3]\,|q,st), \text{ if } q > k_F \\ &= [E(s) + E(t) - \omega_2]\,|q,st), \text{ if } q < k_F \ , \end{aligned} \tag{2.23}$$

$$\begin{aligned} (q,st\,|\,G\,|\,q',s't') &= \delta(q,q')(st\,|\,G_a(q)\,|\,s't'), \text{ if } q > k_F \\ &= \delta(q,q')(st\,|\,G_b\,|\,s't'), \text{ if } q < k_F \ . \end{aligned} \tag{2.24}$$

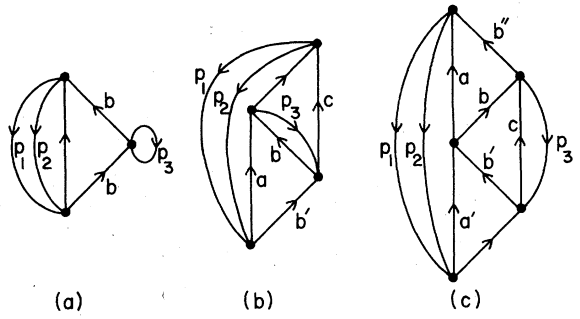

FIG. 1. Direct diagrams for the three-body cluster energy D_3^c. Diagram (a) is called the third-order bubble diagram.

Since the spectator momentum q is one of the labels of a three-body state, it is not necessary to insert subscripts a, b on the left of Eqs. (2.23) and (2.24). However, it is often *convenient* to do so because we use quite different numerical procedures for cases a and b.

Note that the operators Q, e, G, and X are all Hermitian and symmetric in particles 1 and 2. The symmetry in 1,2 allows us to use a basis of three-body states that are antisymmetric in 1,2 because applying Q, e, G, or X to any such state preserves this antisymmetry. Within such a basis the antisymmetrizer $\mathcal{A}_{12}$ in Eqs. (2.13) and (2.15) is unity.

B. Three-body cluster energy

Formulas for the three-body cluster energy D_3^c have been derived earlier using the coupled-cluster equations.[11] Here, for reasons given earlier, we give a more explicit derivation based directly on the three-body cluster diagrams. The three-body cluster diagrams have been discussed earlier in Refs. 2, 8, 13, and 21.

We use Hugenholtz[22] diagrams as shown in Figs. 1 and 2. Upgoing lines are called particle lines and

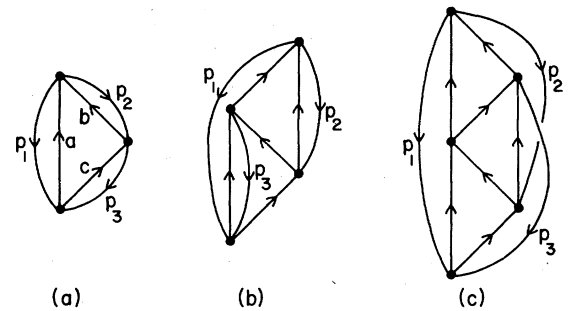

FIG. 2. Exchange diagrams for the three-body cluster energy D_3^c. Diagram (a) is called the third-order ring diagram.

represent occupied states above the Fermi sea. Downgoing lines are called hole lines and represent empty states in the Fermi sea. The dots are called vertices and represent matrix elements of G between the antisymmetric states of Eq. (2.7). Each pair of equivalent lines (i.e., two lines in the same direction that begin at the same vertex and proceed without interaction to end at the same vertex) gives a factor of $\frac{1}{2}$. There is also an overall sign as discussed in Ref. 22. In the diagrams we work from bottom to top, so that the lowest interaction is called the first, and the topmost interaction is called the last.

In this scheme there are exactly two three-body cluster diagrams in each order. Those in Fig. 1 are called direct diagrams and those in Fig. 2 are called exchange diagrams. The arrangement of particle lines is exactly the same in direct and exchange diagrams; only the hole lines differ.

Considering first the direct diagrams (Fig. 1) we let T be an operator such that $(a,bc\,|\,T\,|\,p_3,p_1p_2)$ gives the sum of all diagrams of second or higher order that produce particle lines a,b,c, with b,c emerging from the last interaction, and hole lines p_1,p_2,p_3, with p_1,p_2 entering the first interaction. We first derive an expression for T and then show how the direct contribution $D_3^c(\mathrm{dir})$ is related to T.

We write

$$T=\sum_{n=2}^{\infty}T^{(n)}, \tag{2.25}$$

where $T^{(n)}$ is the contribution of nth order in G. The lowest-order contribution $T^{(2)}$ is seen from the first two interactions of Fig. 1(b) to be

$$(a,bc\,|\,T^{(2)}\,|\,p_3,p_1p_2)=\sum_{b'}(bc\,|\,[Q/e_a(a)]G_a(a)\,|\,b'p_3)\times(ab'\,|\,(Q_b/e_b)G_b\,|\,p_1p_2)\,. \tag{2.26}$$

Using the three-body matrix elements of G defined in Eq. (2.24), we can rewrite this as

$$(a,bc\,|\,T^{(2)}\,|\,p_3,p_1p_2)=\sum_{a'b'c'}(a,bc\,|\,(Q/e_a)G_a\,|\,a',b'c')(c',a'b'\,|\,(Q/e_b)G_b\,|\,p_3,p_1p_2)$$
$$=(a,bc\,|\,(Q_a/e_a)G_aX(Q_b/e_b)G_b\,|\,p_3,p_1p_2)\,. \tag{2.27}$$

The last equality is obtained using Eq. (2.15) and the last paragraph of Sec. II A. Equation (2.27) gives an operator expression for $T^{(2)}$.

To see how $T^{(3)}$ is obtained from $T^{(2)}$ we use the first three interactions of Fig. 1(c) to get

$$(c,ab\,|\,T^{(3)}\,|\,p_3,p_1p_2)=-\sum_{a'b'}(ab\,|\,[Q/e_a(c)]G_a(c)\,|\,a'b')\times(a',b'c\,|\,T^{(2)}\,|\,p_3,p_1p_2)\,, \tag{2.28}$$

where the minus sign comes from the energy denominator $e_a(c)$. Following the derivation of Eq. (2.27), we can rewrite Eq. (2.28) as

$$(c,ab\,|\,T^{(3)}\,|\,p_3,p_1p_2)=-(c,ab\,|\,(Q/e_a)G_aXT^{(2)}\,|\,p_3,p_1p_2)\,. \tag{2.29}$$

This shows how $T^{(3)}$ is related to $T^{(2)}$, and in general we have

$$T^{(n+1)}=-(Q/e_a)G_aXT^{(n)},\quad n\geq 2\,. \tag{2.30}$$

Using this with Eq. (2.27) gives

$$T^{(n)}=(-)^n[(Q/e_a)G_aX]^{n-1}(Q/e_b)G_b\,, \tag{2.31}$$

which is the desired expression for $T^{(n)}$.

Again using Fig. 1(c), we can see how the fifth-order energy contribution $D_3^c(\mathrm{dir},5)$ is obtained from $T^{(3)}$. We find

$$D_3^c(\mathrm{dir},5)=-A^{-1}\tfrac{1}{2}\sum(p_1p_2\,|\,G_b(Q/e_b)\,|\,ab'')(b''p_3\,|\,G_a(a)\,|\,bc)(c,ab\,|\,T^{(3)}\,|\,p_3,p_1p_2)$$
$$=-A^{-1}\tfrac{1}{2}\sum(p_3,p_1p_2\,|\,G_b(Q/e_b)XG_aXT^{(3)}\,|\,p_3,p_1p_2)\,, \tag{2.32}$$

where the method used to derive Eq. (2.27) has been applied. The factor A^{-1} in Eq. (2.32) gives the energy *per particle,* and the factor $\frac{1}{2}$ comes from the pair of equivalent lines p_1p_2.

The same calculation goes through for $D_3^c(\mathrm{dir},n)$ in terms of $T^{(n-2)}$. Using this fact along with Eq. (2.31) gives

$$D_3^c(\mathrm{dir},n)=A^{-1}\tfrac{1}{2}\sum(p_3,p_1p_2\,|\,G_b(Q/e_b)XG_aX\times[-(Q/e_a)G_aX]^{n-3}\times(Q/e_b)G_b\,|\,p_3,p_1p_2)\,. \tag{2.33}$$

We have derived this for $n\geq 4$, but explicit calcula-

tion shows that it holds also for the lowest-order term $n = 3$. So we define

$$\mathcal{O}_{\rm dir} = \sum_{n=0}^{\infty} G_b(Q/e_b)XG_aX[-(Q/e_a)G_aX]^n(Q/e_b)G_b \tag{2.34}$$

and find

$$D_3^c({\rm dir}) = A^{-1}\tfrac{1}{2}\sum(p_3,p_1p_2\,|\,\mathcal{O}_{\rm dir}\,|\,p_3,p_1p_2)\ . \tag{2.35}$$

We next consider the contribution to D_3^c from the exchange diagrams of Fig. 2. In the direct diagrams of Fig. 1, line p_2 always proceeds from the last interaction downwards to its final point at the first interaction, while the final point of line p_3 is always the second interaction. If, in any diagram of Fig. 1, we simply interchange the final points of lines p_2 and p_3, we obtain the corresponding diagram of Fig. 2. Therefore, the contribution from the exchange diagrams (Fig. 2) can be obtained from Eq. (2.35) by omitting the factor $\frac{1}{2}$ (because there are no pairs of equivalent lines in an exchange diagram) and replacing the initial state $|p_3,p_1p_2)$ by $|p_2,p_3p_1)$. Also, we could equally well interchange the final points of lines p_1 and p_3 in the diagrams of Fig. 1, in which case the exchange diagrams would be obtained by replacing the initial state $|p_3,p_1p_2)$ in Eq. (2.35) by $|p_1,p_2p_3)$ rather than by $|p_2,p_3p_1)$. It is convenient to use the average of these two possibilities to get

$$D_3^c({\rm ex}) = A^{-1}\sum(p_3,p_1p_2\,|\,\mathcal{O}_{\rm dir} \times \tfrac{1}{2}[\,|p_1,p_2p_3) + |p_2,p_3p_1)]. \tag{2.36}$$

Noting that

$$X\,|p_3,p_1p_2) = |p_1,p_2p_3) + |p_2,p_3p_1)\ , \tag{2.37}$$

we find

$$D_3^c({\rm ex}) = A^{-1}\tfrac{1}{2}\sum(p_3,p_1p_2\,|\,\mathcal{O}_{\rm ex}\,|p_3,p_1p_2)\ , \tag{2.38}$$

where

$$\mathcal{O}_{\rm ex} = \mathcal{O}_{\rm dir}X\ . \tag{2.39}$$

Thus $D_3 = D_3^c({\rm dir}) + D_3^c({\rm ex})$ is given by

$$D_3^c = A^{-1}\tfrac{1}{2}\sum(p_3,p_1p_2\,|\,\mathcal{O}\,|p_3,p_1p_2)\ , \tag{2.40}$$

where

$$\mathcal{O} = \mathcal{O}_{\rm dir} + \mathcal{O}_{\rm ex} = \mathcal{O}_{\rm dir}(1+X)\ . \tag{2.41}$$

Note that $(1+X)\,|p_3,p_1p_2)$ is antisymmetric in all three particles. Equation (2.40) is the desired expression for D_3^c. It is used in $\mathcal{O}$-type calculations, where we need only D_3^c and not the generalized ring series.

For the subsequent development it is useful to define several additional operators that are related to $\mathcal{O}$. We define

$$D = \sum_{n=0}^{\infty}(-)^n[X(Q/e_a)G_a]^n\ , \tag{2.42}$$

which is formally equivalent to

$$D = 1 - X(Q/e_a)G_aD\ . \tag{2.43}$$

Noting that

$$X[-(Q/e_a)G_aX]^n = [-X(Q/e_a)G_a]^nX\ ,$$

we find from Eqs. (2.34) and (2.41) that

$$\mathcal{O} = G_b(Q/e_b)XG_aDX(Q/e_b)G_b(1+X) \tag{2.44}$$

$$= G_bQCe_b^{-1}G_b(1+X)\ , \tag{2.45}$$

where

$$C = e_b^{-1}XG_aDXQ\ . \tag{2.46}$$

For convenience in numerical work, as explained after Eq. (5.20), we also define

$$\overline{C} = (1/\overline{e}_b)XG_aDXQ\ , \tag{2.47}$$

so that

$$C = (\overline{e}_b/e_b)\overline{C}\ . \tag{2.48}$$

Here, $\overline{e}_b$ is a certain average of e_b and is defined in Sec. IV B, Eq. (4.21).

The lowest-order contributions to $\overline{C}$ and $\mathcal{O}$ are obtained by putting D equal to 1. We define

$$\overline{C}_0 = (1/\overline{e}_b)XG_aXQ\ , \tag{2.49}$$

$$\mathcal{O}_B = G_b(Q/e_b)XG_aX(Q/e_b)G_b\ , \tag{2.50}$$

$$\mathcal{O}_R = \mathcal{O}_BX\ . \tag{2.51}$$

The bubble diagram of Fig. 1(a) is obtained from $\mathcal{O}_B$, and $\mathcal{O}_R$ gives the ring diagram of Fig. 2(a). The higher-order contributions $\overline{C}_H$ and $\mathcal{O}_H$ are defined by

$$\overline{C} = \overline{C}_0 + \overline{C}_H\ , \tag{2.52}$$

$$\mathcal{O} = \mathcal{O}_B + \mathcal{O}_R + \mathcal{O}_H\ . \tag{2.53}$$

The procedure for $\mathcal{O}$-type calculations can now be summarized. Equation (2.43) is solved for D,

which is used in Eq. (2.44) to obtain $\mathscr{O}$. Having $\mathscr{O}$, we obtain the three-body cluster energy D_3^c from Eq. (2.40). In an $\mathscr{M}$-type calculation, on the other hand, we calculate not only D_3^c but also the entire generalized ring series, to which we now turn our attention.

C. Generalized ring series

The results so far are sufficient for an $\mathscr{O}$-type calculation, in which we only calculate the three-body cluster term D_3^c, which has three hole lines. As discussed in the Introduction, the Bochum truncation[4–6,11] of the coupled-cluster equations implies that a set of terms with four, five,... hole lines should be included with D_3^c, giving the generalized ring series.[9–11] In this subsection we define these terms and derive formulas for them.

We start with the pair excitation amplitude $(ab\,|S_2\,|p_1p_2)$, which is given by the sum of all linked diagrams with external particle lines a,b and external hole lines p_1,p_2. The lowest-order (two-hole-line) contribution is

$$(ab\,|S_2^{(2)}\,|p_1p_2) = -(ab\,|Qe_b{}^{-1}G_b\,|p_1p_2)\,. \tag{2.54}$$

Every contribution to S_2 involves an operator with Q at the far left. We define $\overline{S}_2$ to be the result obtained by omitting this factor Q, so that

$$(ab\,|\overline{S}_2^{(2)}\,|p_1p_2) = -(ab\,|e_b{}^{-1}G_b\,|p_1p_2)\,. \tag{2.55}$$

We will derive equations for $\overline{S}_2$ rather than S_2 because it is $\overline{S}_2$ that is most conveniently evaluated by our numerical methods. This is explained after Eq. (3.27).

Removing the last interaction from any three-body cluster diagram gives a three-hole-line contribution to $\overline{S}_2$. An example is shown in Fig. 3(a), which is obtained by removing the last interaction from Fig. 1(b). The sum over all three-body cluster diagrams of such contributions to $\overline{S}_2$ is denoted $\overline{J}^{(3)}$. An additional three-hole-line contribution to $\overline{S}_2$ is obtained from $\overline{J}^{(3)}$ by inserting a particle-particle G matrix as shown in Fig. 3(b). The sum of these three-hole-line contributions can be written formally as

$$\overline{S}_2^{(3)} = (1 - e_b{}^{-1}G_bQ)\overline{J}^{(3)}\,. \tag{2.56}$$

Any contribution to $\overline{J}^{(3)}$ begins with $\overline{S}_2^{(2)}$ and can therefore be written as an operator $\mathscr{M}$ applied to $\overline{S}_2^{(2)}$, as indicated in Fig. 3(a). We now derive formulas for $\overline{J}^{(3)}$ and $\mathscr{M}$. Then the generalized ring series will be generated by repeated application of $\mathscr{M}$.

We begin by noting that

$$D_3^c = A^{-1}\tfrac{1}{2}\sum(p_1p_2\,|G_bQ\overline{J}^{(3)}\,|p_1p_2) \tag{2.57}$$

$$= A^{-1}\tfrac{1}{4}\sum(p_1p_2\,|G_bQ\,|ab)(ab\,|\overline{J}^{(3)}\,|p_1p_2)\,, \tag{2.58}$$

where we have used the completeness relation (2.9). However, D_3^c can also be obtained by putting Eq. (2.45) for $\mathscr{O}$ into Eq. (2.40). After this, we insert the three-body completeness relation (2.13) between Q and C to get

$$D_3^c = A^{-1}\tfrac{1}{4}\sum(p_1p_2\,|G_bQ\,|ab) \times(p_3,ab\,|Ce_b{}^{-1}G_b(1+X)|p_3,p_1p_2)\,. \tag{2.59}$$

Comparing Eqs. (2.58) and (2.59) gives

$$(ab\,|\overline{J}^{(3)}\,|p_1p_2) = \sum_{p_3}(p_3,ab\,|Ce_b{}^{-1} \times G_b(1+X)\,|p_3,p_1p_2)\,, \tag{2.60}$$

which is the desired equation for $\overline{J}^{(3)}$. Inserting Eq. (2.13) just to the right of C and just to the right of G_b in Eq. (2.60) gives

$$(ab\,|\overline{J}^{(3)}\,|p_1p_2) = \tfrac{1}{4}\sum_{a'b'p_1'p_2'}(abp_1p_2\,|\mathscr{M}\,|a'b'p_1'p_2') \times(a'b'\,|\overline{S}_2^{(2)}\,|p_1'p_2')\,, \tag{2.61}$$

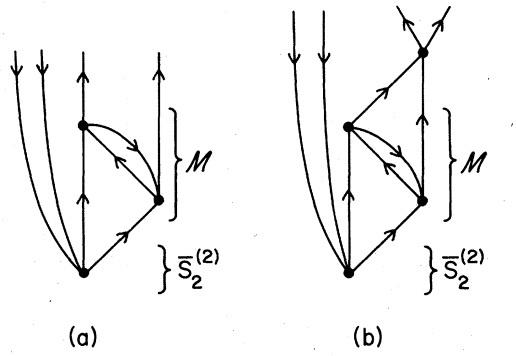

FIG. 3. Diagrams contributing to the pair excitation amplitude $\overline{S}_2$ and illustrating the definition of the matrix $\mathscr{M}$, as discussed in the text.

where

$$(abp_1p_2|\mathcal{M}|a'b'p_1'p_2') = -\sum_{p_3p_3'}(p_3,ab|C|p_3',a'b') \times (p_3',p_1'p_2'|1+X|p_3,p_1p_2) . \quad (2.62)$$

In a more compact notation, we can write Eq. (2.61) as

$$\bar{J}^{(3)} = \mathcal{M}\bar{S}_2^{(2)} , \quad (2.63)$$

where multiplication by the matrix $\mathcal{M}$ involves a sum over both particle and hole indices.

Having the matrix $\mathcal{M}$, we obtain $\bar{J}^{(3)}$, $\bar{S}_2^{(3)}$, and $D_3^{\mathrm{GR}} \equiv D_3^c$ from $\bar{S}_2^{(2)}$ by using Eqs. (2.63), (2.56), and (2.57). The generalized ring series is defined by continuing this process. Thus we define

$$\bar{J}^{(n+1)} = \mathcal{M}\bar{S}_2^{(n)}, \quad n \geq 2 , \quad (2.64)$$

$$\bar{S}_2^{(n)} = (1 - e_b^{-1}G_bQ)\bar{J}^{(n)}, \quad n \geq 3 , \quad (2.65)$$

$$D_n^{\mathrm{GR}} = A^{-1}\tfrac{1}{2}\sum(p_1p_2|G_bQ\bar{J}^{(n)}|p_1p_2), \quad n \geq 3 , \quad (2.66)$$

where GR stands for generalized ring. The quantities $\bar{J}^{(n)}$, $\bar{S}_2^{(n)}$, and D_n^{GR} are represented by diagrams involving exactly n hole lines. In particular, $D_3^{\mathrm{GR}} = D_3^c$, and D_4^{GR} is the four-hole-line contribution of class B1 in the notation of Ref. 8.

The generalized ring series is summed by inverting an appropriate matrix. Defining

$$\bar{J}^{\mathrm{tot}} = \sum_{n=3}^{\infty}\bar{J}^{(n)} , \quad (2.67)$$

$$\bar{S}_2^{\mathrm{tot}} = \sum_{n=2}^{\infty}\bar{S}_2^{(n)} , \quad (2.68)$$

$$D_{\mathrm{tot}}^{\mathrm{GR}} = \sum_{n=3}^{\infty}D_n^{\mathrm{GR}} , \quad (2.69)$$

one easily finds

$$\bar{S}_2^{\mathrm{tot}} = [1 - (1 - e_b^{-1}G_bQ)\mathcal{M}]^{-1}\bar{S}_2^{(2)} , \quad (2.70)$$

$$\bar{J}^{\mathrm{tot}} = \mathcal{M}\bar{S}_2^{\mathrm{tot}} , \quad (2.71)$$

$$D_{\mathrm{tot}}^{\mathrm{GR}} = A^{-1}\tfrac{1}{2}\sum(p_1p_2|G_bQ\bar{J}^{\mathrm{tot}}|p_1p_2) . \quad (2.72)$$

So in order to calculate the generalized ring series ($\mathcal{M}$-type calculation) we must first construct the matrix $\mathcal{M}$ of Eq. (2.62). Then we can iterate the generalized ring series using Eqs. (2.64)–(2.66) and sum the entire series using Eqs. (2.70)–(2.72).

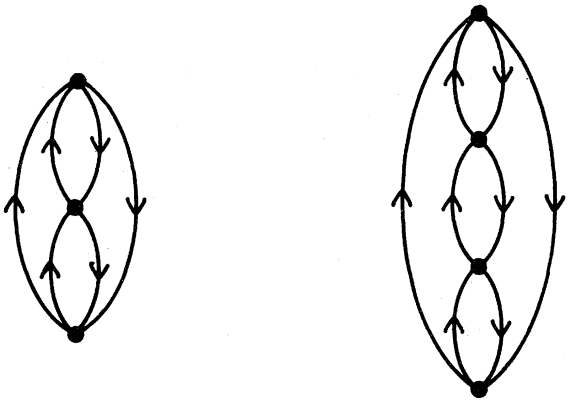

FIG. 4. The first two forward-going ring diagrams.

The ordinary nth order ring diagram is contained in D_n^{GR}. Figure 4 shows the ordinary ring diagrams of third and fourth order. Note that diagram 4(a) is identical to diagram 2(a). The contribution from the ordinary ring diagrams is obtained from our formulas as follows: (1) In Eq. (2.62) for $\mathcal{M}$ we replace C by its lowest-order contribution C_0 from Eqs. (2.48)–(2.49). (2) Also in Eq. (2.62) we include only the X from "$1 + X$." (3) We omit particle-particle interactions; i.e., we replace Eq. (2.65) by $\bar{S}_2^{(n)} = \bar{J}^{(n)}$. Thus the generalized ring series contains all the ordinary ring diagrams of Fig. 4. These diagrams are often called forward-going ring diagrams. The backward-going ring diagrams, of which one example is shown in Fig. 5, are not included in the generalized ring series. The reason that it is preferable to treat the backward-going rings separately from the forward-going rings is discussed in Ref. 6 in connection with Fig. 43.

D. Perturbation theory for $\mathcal{O}$ and C

In numerical work G_b is treated exactly, but G_a is approximated by a sum of separable terms. To

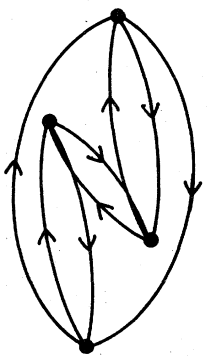

FIG. 5. A backward-going ring diagram.

make the calculation tractable it is necessary to truncate this sum. Thus a small error δG_a is always present because of the omitted terms. We can largely correct for this error by using first-order perturbation theory. From Eqs. (2.45) and (2.62) we see that the basic quantity needed in either an $\mathscr{O}$-type or $\mathscr{M}$-type calculation is C, which involves G_aD [see Eq. (2.46)]. Thus we need a formula for the first-order change in G_aD caused by a change δG_a in G_a. Since G_aD occurs only between three-body states with particle 3 above the Fermi sea, it is sufficient to calculate $Q_3\delta(G_aD)Q_3$, where Q_3 is the projection operator that requires particle 3 to be above the Fermi level.

From Eq. (2.42) we obtain to first order in δG_a

$$\delta(G_aD) = \delta G_a - \delta G_aX(Q/e_a)G_a - G_aX(Q/e_a)\delta G_a + - \cdots . \tag{2.73}$$

Rearranging and inserting factors Q_3 gives

$$Q_3\delta(G_aD)Q_3 = Q_3\sum_{n=0}^{\infty}(-)^n[G_aXQ/e_a]^n\delta G_a \times \sum_{m=0}^{\infty}(-)^m[X(Q/e_a)G_a]^mQ_3 . \tag{2.74}$$

The right-hand sum in Eq. (2.74) gives the operator D. The left-hand sum would be the series for the Hermitian conjugate $D^\dagger$ if we could replace $[G_aXQ/e_a]^n$ by $[G_a(Q/e_a)X]^n$. We will now show that this replacement is justified in Eq. (2.74), so that we get, to first order in δG_a,

$$Q_3\delta(G_aD)Q_3 = Q_3D^\dagger\delta G_aDQ_3 . \tag{2.75}$$

To justify the replacement $XQ/e_a \rightarrow (Q/e_a)X$ in the left-hand sum of Eq. (2.74), we use the formulas

$$Q_3XQ = XQ , \tag{2.76}$$

$$G_aX(Q/e_a)Q_3 = Q_3G_a(Q/e_a)X , \tag{2.77}$$

$$[G_aXQ/e_a]^nQ_3 = Q_3[G_a(Q/e_a)X]^n, \quad n \geq 0 \tag{2.78}$$

$$Q_3^2 = Q_3 . \tag{2.79}$$

Equations (2.76) and (2.77) are easily derived; Eq. (2.78) follows from Eq. (2.77); and Eq. (2.79) expresses the fact that Q_3 is a projection operator. From Eq. (2.76) we see that Eq. (2.74) remains valid if a factor Q_3 is inserted just to the right of δG_a. Since $[\delta G_a, Q_3] = 0$, we can move this factor to the left of δG_a. Then application of Eqs. (2.78) and (2.79) shows that Eq. (2.74) remains valid when $[G_aXQ/e_a]^n$ is replaced by $[G_a(Q/e_a)X]^n$ in the left-hand sum, and this establishes the desired result Eq. (2.75).

The first-order change $\delta\mathscr{O}$ caused by δG_a is

$$\delta\mathscr{O} = G_b(Q/e_b)X\delta(G_aD)X(Q/e_b)G_b(1+X) . \tag{2.80}$$

Using Eq. (2.76) and its Hermitian conjugate, we see that Eq. (2.80) remains valid if we insert Q_3 just to the left and right of $\delta(G_aD)$. We then use Eq. (2.75), after which the factors Q_3 are removed by again using Eq. (2.76). The result is

$$\delta\mathscr{O} = G_b(Q/e_b)XD^\dagger\delta G_aDX(Q/e_b)G_b(1+X) . \tag{2.81}$$

The preceding argument cannot be used to calculate $\delta\overline{C}$ because the absence of a factor Q on the left of Eq. (2.47) prevents the use of Eq. (2.76). We can, however, derive

$$\delta(Q\overline{C}) = Q(1/\overline{e}_b)XD^\dagger\delta G_aDXQ . \tag{2.82}$$

If we now define

$$\Delta\overline{C} = (1/\overline{e}_b)XD^\dagger\delta G_aDXQ , \tag{2.83}$$

then $\Delta\overline{C}$ is *not* the first-order change in $\overline{C}$, but it *is* true that

$$\delta(Q\overline{C}) = Q\Delta\overline{C} . \tag{2.84}$$

Since any interesting quantity involves $Q\overline{C}$ rather than $\overline{C}$ alone, it is sufficient for our purposes to calculate $\Delta\overline{C}$.

E. Transformation to relative and total momentum variables

For nuclear matter all operators of interest conserve total momentum. We take advantage of this by transforming to a representation labeled by relative and total momenta. This also allows us to eliminate explicit factors of A and Ω in favor of $\rho = A/\Omega$.

We first review this process for the two-body energy D_2. The extension to D_3^c, D_n^{GR}, and $\overline{S}_2^{(n)}$ is then straightforward. Spin and isospin variables play no role and are suppressed.

We have[2]

$$D_2 = A^{-1}\tfrac{1}{2}\sum(p_1p_2|\,G_b\,|p_1p_2) , \tag{2.85}$$

where the state $|p_1p_2)$ is defined by Eqs. (2.6) and

(2.7). Defining

$$\vec{k}_0 = \tfrac{1}{2}(\vec{p}_1 - \vec{p}_2)\,, \tag{2.86}$$

$$\vec{P} = \vec{p}_1 + \vec{p}_2\,, \tag{2.87}$$

we use the fact that G conserves $\vec{P}$ to get

$$(p_1p_2\,|\,G_b\,|\,p_1p_2) = \Omega^{-1}(2\pi)^3(\vec{k}_0\,|\,G_b(\vec{P})\,|\,\vec{k}_0)\,, \tag{2.88}$$

where the state $|\,\vec{k}_0)$ of relative motion has the wave function

$$(\vec{r}\,|\,\vec{k}_0) = 2^{-1/2}(2\pi)^{-3/2}(e^{i\vec{k}_0\cdot\vec{r}} - e^{-i\vec{k}_0\cdot\vec{r}})\,, \tag{2.89}$$

and

$$\vec{r} = \vec{r}_1 - \vec{r}_2\,. \tag{2.90}$$

In Eq. (2.88) G_b depends on $\vec{P}$ through e_b and Q (see Sec. IV). Using

$$\sum_{p_1} \to \Omega(2\pi)^{-3}\int d\vec{p}_1 \tag{2.91}$$

and putting Eq. (2.88) into Eq. (2.85) gives

$$D_2 = \tfrac{1}{2}(2\pi)^{-3}\rho^{-1}\int d\vec{p}_1 d\vec{p}_2(\vec{k}_0\,|\,G_b(\vec{P})\,|\,\vec{k}_0)\,, \tag{2.92}$$

where $\vec{k}_0$ and $\vec{P}$ are functions of $\vec{p}_1,\vec{p}_2$ given by Eqs. (2.86) and (2.87), respectively. Equation (2.92) is the desired expression for D_2.

We proceed analogously for D_3^c. For any three single-particle momenta $\vec{k}_1,\vec{k}_2,\vec{k}_3$, we define

$$\vec{\mathscr{K}} = \vec{k}_1 + \vec{k}_2 + \vec{k}_3\,, \tag{2.93}$$

$$\vec{K} = \tfrac{1}{3}(\vec{k}_1 + \vec{k}_2) - \tfrac{2}{3}\vec{k}_3\,, \tag{2.94}$$

$$\vec{k} = \tfrac{1}{2}(\vec{k}_1 - \vec{k}_2)\,, \tag{2.95}$$

$$\vec{P} = \vec{k}_1 + \vec{k}_2 = \tfrac{2}{3}\vec{\mathscr{K}} + \vec{K}\,. \tag{2.96}$$

The inverse transformation is

$$\vec{k}_1 = \tfrac{1}{3}\vec{\mathscr{K}} + \tfrac{1}{2}\vec{K} + \vec{k}\,, \tag{2.97}$$

$$\vec{k}_2 = \tfrac{1}{3}\vec{\mathscr{K}} + \tfrac{1}{2}\vec{K} - \vec{k}\,, \tag{2.98}$$

$$\vec{k}_3 = \tfrac{1}{3}\vec{\mathscr{K}} - \vec{K}\,. \tag{2.99}$$

We also define the coordinate transformation

$$\vec{\mathscr{R}} = \tfrac{1}{3}(\vec{r}_1 + \vec{r}_2 + \vec{r}_3)\,, \tag{2.100}$$

$$\vec{\rho} = \tfrac{1}{2}(\vec{r}_1 + \vec{r}_2) - \vec{r}_3\,, \tag{2.101}$$

$$\vec{r} = \vec{r}_1 - \vec{r}_2\,, \tag{2.102}$$

so that a three-body plane wave can be written

$$\exp i(\vec{k}_1\cdot\vec{r}_1 + \vec{k}_2\cdot\vec{r}_2 + k_3\cdot\vec{r}_3) = \exp i(\vec{\mathscr{K}}\cdot\vec{\mathscr{R}} + \vec{K}\cdot\vec{\rho} + \vec{k}\cdot\vec{r})\,. \tag{2.103}$$

Since $\mathscr{O}$ conserves $\vec{\mathscr{K}}$, we find

$$(p_3,p_1p_2\,|\,\mathscr{O}\,|\,p_3,p_1p_2) = \Omega^{-2}(2\pi)^6(\vec{K}_0\vec{k}_0\,|\,\mathscr{O}(\vec{\mathscr{K}})\,|\,\vec{K}_0\vec{k}_0)\,, \tag{2.104}$$

where $\vec{\mathscr{K}}$, $\vec{K}_0,\vec{k}_0$ are defined by Eqs. (2.93), (2.94), and (2.95), respectively, with $\vec{k}_i \to \vec{p}_i$. In Eq. (2.104) we also have defined

$$|\,\vec{K}_0\vec{k}_0) = |\,\vec{K}_0)\,|\,\vec{k}_0)\,, \tag{2.105}$$

$$(\vec{\rho}\,|\,\vec{K}_0) = (2\pi)^{-3/2}\exp(i\vec{K}_0\cdot\vec{\rho})\,, \tag{2.106}$$

where $|\,\vec{k}_0)$ is defined by Eq. (2.89). The state $|\,\vec{K}_0)$ describes the motion of particle 3 relative to the center of mass of 1 and 2. In Eq. (2.104) $\mathscr{O}(\vec{\mathscr{K}})$ operates in the space (2.105) and depends on $\vec{\mathscr{K}}$ because e_a, Q_a, and G_a depend on $\vec{\mathscr{K}}$ (see Sec. IV). Putting Eq. (2.104) into Eq. (2.40) and using Eq. (2.91) gives

$$D_3^c = \tfrac{1}{2}(2\pi)^{-3}\rho^{-1}\int d\vec{p}_1 d\vec{p}_2 d\vec{p}_3 \times(\vec{K}_0\vec{k}_0\,|\,\mathscr{O}(\vec{\mathscr{K}})\,|\,\vec{K}_0\vec{k}_0)\,, \tag{2.107}$$

which is the desired formula for D_3^c.

We must make a similar treatment of the pair excitation amplitude S_2. The two-hole-line contribution to $\bar{S}_2$ is found from Eq. (2.55) to be

$$(ab\,|\,\bar{S}_2^{(2)}\,|\,p_1p_2) = \Omega^{-1}\delta(\vec{P},\vec{P}')(2\pi)^3(\vec{k}\,|\,\bar{S}_2^{(2)}(\vec{P})\,|\,\vec{k}_0)\,, \tag{2.108}$$

where

$$\vec{k} = \tfrac{1}{2}(\vec{a} - \vec{b})\,, \tag{2.109}$$

$$\vec{P}' = \vec{a} + \vec{b}\,, \tag{2.110}$$

$$(\vec{k}\,|\,\bar{S}_2^{(2)}(\vec{P})\,|\,\vec{k}_0) = -(\vec{k}\,|\,[1/e_b(\vec{P})]G_b(\vec{P})\,|\,\vec{k}_0)\,, \tag{2.111}$$

and $\delta(\vec{P},\vec{P}')$ is a Kronecker delta. Similarly, from Eq. (2.60) we find

$$(ab\,|\,\bar{J}^{(3)}\,|\,p_1p_2) = \Omega^{-1}(2\pi)^3\delta(\vec{P},\vec{P}')(\vec{k}\,|\,\bar{J}^{(3)}(\vec{P})\,|\,\vec{k}_0)\,, \tag{2.112}$$

where

$$(\vec{k}\,|\,\bar{J}^{(3)}(\vec{P})\,|\,\vec{k}_0) = \int d\vec{p}_3(\vec{K}_0\vec{k}\,|\,Ce_b^{-1}G_b(1+X)\,|\,\vec{K}_0\vec{k}_0)\,. \tag{2.113}$$

In this equation the right-hand matrix element depends parametrically on $\vec{\mathscr{K}}$, and $\vec{\mathscr{K}}, \vec{K}_0$ are functions of $\vec{P}, \vec{p}_3$ given by

$$\vec{\mathscr{K}} = \vec{P} + \vec{p}_3 , \tag{2.114}$$

$$\vec{K}_0 = \tfrac{1}{3}\vec{P} - \tfrac{2}{3}\vec{p}_3 . \tag{2.115}$$

III. PARTIAL-WAVE REPRESENTATION

For numerical work we use a partial-wave representation and introduce spin and isospin variables. Several different sets of two-body and three-body states are needed later on, and in this section we define these states and give several useful formulas for transforming from one basis to another.

A. States of the spectator particle

We first consider states of the variable $\vec{\rho}$ of Eq. (2.101) describing the motion of the spectator particle 3 relative to the center of mass of 1 and 2. The state $|\vec{K})$ is defined by giving its wave function

$$(\vec{\rho}\,|K) = (2\pi)^{-3/2}\exp(i\vec{K}\cdot\vec{\rho}) , \tag{3.1}$$

where $\vec{K}$ is defined by Eq. (2.94). The completeness and orthogonality relations are

$$(\vec{K}\,|\,\vec{K}') = \delta(\vec{K} - \vec{K}') , \tag{3.2}$$

$$\int d\vec{K}\,|\,\vec{K})(\vec{K}\,| = 1 . \tag{3.3}$$

The partial-wave state $|KLM)$ is defined by

$$(\vec{\rho}\,|KLM) = i^L(2/\pi)^{1/2}Kj_L(K\rho)Y_{LM}(\hat{\rho}) , \tag{3.4}$$

where j_L is a spherical Bessel function. Equation (3.4) gives

$$(KLM\,|K'L'M') = \delta(LM\,|L'M')\delta(K - K') , \tag{3.5}$$

$$\sum_{LM}\int dK\,|KLM)(KLM\,| = 1 . \tag{3.6}$$

From Eqs. (3.1) and (3.4) we calculate the overlap integral

$$(\vec{K}\,|K'L'M') = K^{-1}\delta(K - K')Y_{L'M'}(\hat{K}) . \tag{3.7}$$

We include spin and isospin by writing

$$(\vec{\rho}\,|\vec{K}\sigma_3\tau_3) = (\vec{\rho}\,|\vec{K})\gamma_{\sigma_3}(3)\mu_{\tau_3}(3) , \tag{3.8}$$

$$(\vec{\rho}\,|KLM\sigma_3\tau_3) = (\vec{\rho}\,|KLM)\gamma_{\sigma_3}(3)\mu_{\tau_3}(3), \tag{3.9}$$

where γ and μ are single-particle spin and isospin functions, respectively. The resulting changes in orthogonality and completeness relations and in the overlap equation (3.7) are obvious.

B. Two-body states

The spatial wave functions of relative motion for particles 1 and 2 are defined by

$$(\vec{r}\,|\,\vec{k})_{\rm na} = (2\pi)^{-3/2}\exp(i\vec{k}\cdot\vec{r}) , \tag{3.10}$$

$$(\vec{r}\,|klm)_{\rm na} = i^l(2/\pi)^{1/2}kj_l(kr)Y_{lm}(\hat{r}) . \tag{3.11}$$

These definitions are analogous to Eqs. (3.1) and (3.4) and lead to similar orthogonality, completeness, and overlap formulas. In Eqs. (3.10) and (3.11) we use nonantisymmetrized states (subscript na). It is only the overall two-body wave function, including spin and isospin, that should be made antisymmetric.

Next we include spin and isospin and then antisymmetrize by applying the operator $2^{-1/2}(1 - P_{12})$. Doing this for the states (3.10) and (3.11) gives

$$(\vec{r}\,|\vec{k}SM_STT_z) = (2\pi)^{-3/2}2^{-1/2} \times[e^{i\vec{k}\cdot\vec{r}} - (-)^{S+T}e^{-i\vec{k}\cdot\vec{r}}] \times \chi^S_{M_S}(1,2)\lambda^T_{T_z}(1,2) , \tag{3.12}$$

$$(\vec{r}\,|klmSM_STT_z) = 2^{1/2}\nu(lST)(\vec{r}\,|klm)_{\rm na} \times \chi^S_{M_S}(1,2)\lambda^T_{T_z}(1,2) , \tag{3.13}$$

where

$$\nu(lST) = [1 - (-)^{l+S+T}]/2 , \tag{3.14}$$

and $\chi^S_{M_S}$ and $\lambda^T_{T_z}$ are two-body spin and isospin functions, respectively.

The two-body states used most often in numerical work are defined by

$$(\vec{r}\,|klSjj_zTT_z) = 2^{1/2}\nu(lST)i^l(2/\pi)^{1/2}kj_l(kr) \times \mathscr{Y}^{j_z}_{jlS}(1,2)\lambda^T_{T_z}(1,2) , \tag{3.15}$$

where

$$\mathscr{Y}^{j_z}_{jlS}(1,2) = \sum_{mM_S}(lSmM_S\,|jj_z)Y_{lm}(\hat{r})\chi^S_{M_S}(1,2) . \tag{3.16}$$

Using the notation

$$f = \{lSjT\} , \tag{3.17}$$

we can write the completeness relation for the states (3.15) in the form

$$\tfrac{1}{2}\sum\int dk\,|kfj_zT_z)(kfj_zT_z| = \mathscr{A}_{12}\,, \qquad (3.18)$$

where $\mathscr{A}_{12}$ is defined by Eq. (2.10). Overlap integrals among the various two-body states are derived straightforwardly. For example, an overlap integral that will be needed in Sec. V A is

$$(\vec{k}SM_STT_z\,|\,k'f'j_z'T_z') = \delta(STT_z\,|\,S'T'T_z')2\nu(l'S'T')k^{-1}\delta(k-k') \times \sum_{m'}(l'S'm'M_S\,|\,j'j_z')Y_{l'm'}(\hat{k})\,. \qquad (3.19)$$

We now introduce a representation that will be used later for the pair excitation amplitude S_2 and the generalized ring series. The lowest-order approximation $\bar{S}_2^{(2)}$ is $-e_b{}^{-1}G_b$ [see Eq. (2.111)]. Using an angle-average Pauli operator, we find in Sec. IV C that G conserves $\{jj_zSTT_z\}$ and is independent of j_z,T_z. In analogy with Eq. (4.30) we can therefore write

$$(kfj_zT_z\,|\,\bar{S}_2^{(2)}\,|\,k_0f_0j_{0z}T_{0z}) = \delta(Sjj_zTT_z\,|\,S_0j_0j_{0z}T_0T_{0z}) \times (kl\,|\,\bar{S}_2^{(2)}(j_0S_0T_0)\,|\,k_0l_0)\,, \qquad (3.20)$$

where

$$(kl\,|\,\bar{S}_2^{(2)}(j_0S_0T_0)\,|\,k_0l_0) = -(kl\,|\,e_b{}^{-1}G_b^{j_0S_0T_0}\,|\,k_0l_0)\,, \qquad (3.21)$$

and we have suppressed the dependence of G_b on P. We now define

$$\bar{S}_2^{(2)}(f_0lkk_0) = (kl\,|\,\bar{S}_2^{(2)}(j_0S_0T_0)\,|\,k_0l_0)\,, \qquad (3.22)$$

with similar definitions for $\bar{S}_2^{(n)}$ and $\bar{J}^{(n)}$. The new representation is now obtained by expanding the dependence of $\bar{S}_2^{(2)}$ on k and k_0 in certain basis functions.

Consider first the dependence on k, and let $p_n(k)$ be a complete set of orthonormal functions,

$$\int p_n(k)p_m(k)dk = \delta(n,m)\,. \qquad (3.23)$$

Any function $F(k)$ can be expanded as

$$F(k) = \sum_n F(n)p_n(k)\,, \qquad (3.24)$$

where

$$F(n) = \int F(k)p_n(k)dk\,. \qquad (3.25)$$

We expand the k dependence of $\bar{S}_2^{(2)}(f_0lkk_0)$ in this way and denote the expansion coefficients by $\bar{S}_2(f_0lnk_0)$. Thus we have

$$\bar{S}_2(f_0lnk_0) = \int dkp_n(k)\bar{S}_2(f_0lkk_0)\,. \qquad (3.26)$$

Other quantities are transformed between the k and n representations in the same way. For example, the matrix element appearing in Eq. (5.19) is defined by

$$(d_0K_0n''l\,|\,\bar{C}(\mathscr{J}\mathscr{P}\mathscr{T})\,|\,d_0'K_0'n'l') = \int dk''dk'p_{n''}(k'')(d_0K_0k''l\,|\,\bar{C}(\mathscr{J}\mathscr{P}\mathscr{T}) \times |\,d_0'K_0'k'l')p_{n'}(k')\,. \qquad (3.27)$$

We can now see the reason for working with $\bar{S}_2$ rather than with $S_2 = Q\bar{S}_2$. Equation (3.22) for $\bar{S}_2^{(2)}$ is a smooth function of k and is therefore suitable for expansion in the polynomials $p_n(k)$. However, S_2 is obtained by multiplying $\bar{S}_2$ by the angle-average Pauli operator $Q(P,k)$ of Eq. (4.3), which has a discontinuous first derivative with respect to k. Thus S_2 is not a smooth function of k, and it would be inefficient to expand it in $p_n(k)$. Instead, we calculate $\bar{S}_2$ as an expansion in $p_n(k)$ and multiply by $Q(P,k)$ at the end of the calculation.

Next consider the dependence of $\bar{S}_2^{(2)}$ on k_0. We can approximate any function $F(k_0)$ by

$$F(k_0) \simeq \sum_{m=1}^{p} F(m)k_0^{m-1}\,. \qquad (3.28)$$

We determine the coefficients $F(m)$ by requiring that Eq. (3.28) be exact at p grid points $k_{01},\ldots k_{0p}$. This gives

$$F(m) = \sum_{i=1}^{p} Y(m,i)F(k_{0i}),\quad m = 1,2\cdots p\,, \qquad (3.29)$$

where the matrix Y is the inverse of the matrix K defined by

$$K(i,m) = k_{0i}^{m-1},\quad i,m = 1,2,\ldots p\,. \qquad (3.30)$$

In Eq. (3.28) the first term contains the zeroth power of k_0. If we want the leading term to be k_0^r, we simply apply the above procedure to $k_0{}^{-r}F(k_0)$ instead of to $F(k_0)$. In particular, for $\bar{S}_2^{(n)}$ and $\bar{J}^{(n)}$, we define the transformation between the k_0 and m representations by

$$\bar{S}_2^{(n)}(f_0lkk_0) = \sum_{m\geq 1}\bar{S}_2^{(n)}(f_0lkm)k_0^{l_0+m}\,, \qquad (3.31)$$

$$\bar{S}_2^{(n)}(f_0lkm) = \sum_{i\geq 1}k_{0i}^{-l_0-1}Y(m,i)\bar{S}_2^{(n)}(f_0lkk_{0i})\,. \qquad (3.32)$$

We have used the fact that $\overline{S}_2^{(n)}$ is proportional to $k_0^{l_0+1}$ as $k_0 \to 0$. This dependence on k_0 comes from the factor $k_0 j_{l_0}(k_0 r)$ in Eq. (3.15) for the wave function of the inital state.

In deriving equations for computation of the generalized ring series, we will frequently transform between the k and n representations and also between the k_0 and m representations.

C. Three-body states

Three-body states are obtained as products of states of particle 3 with states of relative motion of particles 1 and 2. For example, the state $|\vec{K}\sigma_3\tau_3,\vec{k}SM_S TT_z)$ is simply the product of the states (3.8) and (3.12). After taking the product, it is often useful to recouple angular momentum and isospin. Applying this procedure to Eqs. (3.9) and (3.15) gives the three-body state

$$|Kk[(L\tfrac{1}{2})J(lS)j]\mathscr{J}\mathscr{J}_z(\tfrac{1}{2}T)\mathscr{T}\mathscr{T}_z) \equiv |dKkl,\ \mathscr{J}\mathscr{J}_z\mathscr{P}\mathscr{T}\mathscr{T}_z)\ , \quad (3.33)$$

where

$$d \equiv \{LJjST\}\ , \quad (3.34)$$

$$\mathscr{P} = (-)^{L+l}\ . \quad (3.35)$$

In Eq. (3.33) L is coupled to the spin of particle 3 to give J, and the isospin of particle 3 is coupled to T to give $\mathscr{T}$. The other couplings are self-explanatory. In numerical work, as a result of approximations explained in Sec. IV, total angular momentum $\mathscr{J}$, total isospin $\mathscr{T}$, and parity $\mathscr{P}$ are all conserved. Since $\mathscr{P}$ is conserved, it is convenient to write it explicitly in Eq. (3.33), even though it is redundant because of Eq. (3.35). The orthogonality and completeness relations for the states of Eq. (3.33) are

$$(dKkl,\mathscr{J}\mathscr{J}_z\mathscr{P}\mathscr{T}\mathscr{T}_z\,|\,d'K'k'l',\mathscr{J}'\mathscr{J}_z'\mathscr{P}'\mathscr{T}'\mathscr{T}_z') = 2\nu(lST)\delta(K-K')\delta(k-k') \times \delta(dl\mathscr{J}\mathscr{J}_z\mathscr{T}\mathscr{T}_z\,|\,d'l'\mathscr{J}'\mathscr{J}_z'\mathscr{T}'\mathscr{T}_z')\ , \quad (3.36)$$

$$\tfrac{1}{2}\sum\int dK\,dk\,|dKkl,\mathscr{J}\mathscr{J}_z\mathscr{P}\mathscr{T}\mathscr{T}_z) \times (dKkl,\mathscr{J}\mathscr{J}_z\mathscr{P}\mathscr{T}\mathscr{T}_z| = \mathscr{A}_{12}\ , \quad (3.37)$$

where $\mathscr{A}_{12}$ is defined by Eq. (2.10).

If we start with Eq. (3.33) but couple the angular momenta differently we obtain the state

$$|Kk[(Ll)\mathscr{L}(\tfrac{1}{2}S)\mathscr{S}]\mathscr{J}\mathscr{J}_z(\tfrac{1}{2}T)\mathscr{T}\mathscr{T}_z)\ . \quad (3.38)$$

The states (3.33) and (3.38) are related by

$$|dKkl,\mathscr{J}\mathscr{J}_z\mathscr{P}\mathscr{T}\mathscr{T}_z) = \sum_{\mathscr{L}\mathscr{S}}[\hat{\mathscr{L}}\hat{\mathscr{S}}\hat{J}\hat{j}]^{1/2}\begin{Bmatrix} L & \frac{1}{2} & J \\ l & S & j \\ \mathscr{L} & \mathscr{S} & \mathscr{J}\end{Bmatrix} \times |Kk[(Ll)\mathscr{L}(\tfrac{1}{2}S)\mathscr{S}]\mathscr{J}\mathscr{J}_z(\tfrac{1}{2}T)\mathscr{T}\mathscr{T}_z)\ , \quad (3.39)$$

where the curly bracket on the right of Eq. (3.39) is a $9j$ symbol, and we use the notation

$$\hat{a} = 2a + 1\ . \quad (3.40)$$

Matrix elements of G take a simple form in states (3.33) while matrix elements of X are more conveniently calculated in states (3.38).

Two other overlap integrals that are used later on, and whose derivations are straightforward, are

$$(\vec{K}'\sigma_3'\tau_3'\vec{k}'S'M_S'T'T_z'\,|\,dKkl,\mathscr{J}\mathscr{J}_z\mathscr{P}\mathscr{T}\mathscr{T}_z) = 2\nu(lST)\delta(S'T'|ST)K^{-1}\delta(K-K')k^{-1}\delta(k-k') \times \sum_{MJ_zmj_z}(L\tfrac{1}{2}M\sigma_3'|JJ_z)(lSmM_S'|jj_z)(JjJ_zj_z|\mathscr{J}\mathscr{J}_z)(\tfrac{1}{2}T\tau_3'T_z'|\mathscr{T}\mathscr{T}_z)Y_{LM}(\hat{K}')Y_{lm}(\hat{k}')\ , \quad (3.41)$$

$$(\vec{K}'\sigma_3'\tau_3',k'f'j_z'T_z'\,|\,dKkl,\mathscr{J}\mathscr{J}_z\mathscr{P}\mathscr{T}\mathscr{T}_z) = 2\nu(lST)K^{-1}\delta(K-K')\delta(k-k')\delta(f,f')(\tfrac{1}{2}T\tau_3'T_z'|\mathscr{T}\mathscr{T}_z) \times \sum_{MJ_z}(L\tfrac{1}{2}M\sigma_3'|JJ_z)(JjJ_zj_z'|\mathscr{J}\mathscr{J}_z)Y_{LM}(\hat{K}')\ . \quad (3.42)$$

The following identities among spherical harmonics and Clebsch-Gordan coefficients will also be used later:

$$\sum_M Y_{LM}(\hat{K})Y_{LM}^*(\hat{K}) = (4\pi)^{-1}\hat{L}\ , \quad (3.43)$$

$$\sum_{mn}(abmn|ck)(abmn|c'k') = \delta(ck|c'k')\ , \quad (3.44)$$

$$\sum_{nk}(abmn|ck)(a'bm'n|ck) = \delta(am|a'm')\hat{c}/\hat{a} \quad (3.45)$$

The separable representation for G_a, given by Eq. (4.32), motivates the definition of a different type of three-body state. Using the fact that G_a does not affect the quantum numbers $(KLJ\tau_3)$ of particle 3, and using Eqs. (4.30) and (4.32), we find

$$(dKkl,\mathcal{J}\mathcal{J}_z\mathcal{P}\mathcal{T}\mathcal{T}_z\,|\,G_a\,|\,d'K'k'l',\mathcal{J}'\mathcal{J}_z'\mathcal{P}'\mathcal{T}'\mathcal{T}_z') = \delta(d\mathcal{J}\mathcal{J}_z\mathcal{T}\mathcal{T}_z\,|\,d'\mathcal{J}'\mathcal{J}_z'\mathcal{T}'\mathcal{T}_z')\delta(K-K') \times \sum_\beta g_{\beta l}^{jST}(k,K)\lambda_\beta^{jST}(K)g_{\beta l'}^{jST}(k',K)\,. \quad (3.46)$$

We now define the state $|\,d\beta K,\mathcal{J}\mathcal{J}_z\mathcal{P}\mathcal{T}\mathcal{T}_z)$ by giving its overlap with the complete set of states (3.33):

$$(d'K'k'l',\mathcal{J}'\mathcal{J}_z'\mathcal{P}'\mathcal{T}'\mathcal{T}_z'\,|\,d\beta K,\mathcal{J}\mathcal{J}_z\mathcal{P}\mathcal{T}\mathcal{T}_z) = \delta(K-K')\delta(d'\mathcal{J}'\mathcal{J}_z'\mathcal{T}'\mathcal{T}_z'\,|\,d\mathcal{J}\mathcal{J}_z\mathcal{T}\mathcal{T}_z) \times g_{\beta l'}^{jST}(k',K)\,. \quad (3.47)$$

Then we find the convenient formula

$$G_a = \sum_{\mathcal{J}\mathcal{J}_z\mathcal{T}\mathcal{T}_z}\sum_{d\beta}\int dK\,|\,d\beta K,\mathcal{J}\mathcal{J}_z\mathcal{P}\mathcal{T}\mathcal{T}_z) \times\lambda_\beta^{jST}(K)(d\beta K,\mathcal{J}\mathcal{J}_z\mathcal{P}\mathcal{T}\mathcal{T}_z|\,. \quad (3.48)$$

This representation of G_a plays a central role in reducing the equations to a form suitable for numerical work. Also in connection with this equation, it is convenient to introduce the following notation, which will be used later:

$$\alpha = \{d\beta K\}\,, \quad (3.49)$$

$$\sum_\alpha = \sum_{d\beta}\int dK\,, \quad (3.50)$$

$$\delta(\alpha,\alpha') = \delta(d,d')\delta(\beta,\beta')\delta(K-K')\,. \quad (3.51)$$

IV. MATRIX ELEMENTS OF Q, e, v, G, X

We plan to write the equations of Sec. II using the basis states defined in Sec. III. To do that we need matrix elements of the operators Q, e, G, and X in these basis states. In this section we derive formulas for these matrix elements. We also introduce several approximations that are necessary to make the numerical work tractable. These include use of an angle-average approximation for Q, and the use of constant average values for $|\vec{\mathscr{K}}|$ and ω_3, instead of letting these quantities depend on $\vec{p}_1,\vec{p}_2,\vec{p}_3$.

A. Matrix elements of Q

The operator Q requires $|\vec{k}_1| > k_F$ and $|\vec{k}_2| > k_F$. It is diagonal in a representation labeled by $\vec{K},\vec{k}$, and depends parametrically on $\vec{\mathscr{K}}$, with eigenvalues

$$Q(\vec{\mathscr{K}},\vec{K},\vec{k}) = 1,\ \text{if } k_1 > k_F \text{ and } k_2 > k_F = 0,\ \text{otherwise}\,, \quad (4.1)$$

where $\vec{k}_1$ and $\vec{k}_2$ are given by Eqs. (2.97) and (2.98). However, in numerical work we use a partial-wave basis. In the basis constructed from Eqs. (3.4) and (3.11) we find

$${}_{\rm na}(KLMklm\,|\,Q(\vec{\mathscr{K}})\,|\,K'L'M'k'l'm')_{\rm na} = \int d\vec{K}_a d\vec{k}_a (KLM\,|\,\vec{K}_a)_{\rm na}(klm\,|\,k_a)Q(\vec{\mathscr{K}},\vec{K}_a,\vec{k}_a)(\vec{K}_a\,|\,K'L'M')(\vec{k}_a\,|\,k'l'm')_{\rm na}\,,$$
$$= \delta(K-K')\delta(k-k')\int d\hat{K}_a d\hat{k}_a Q(\vec{\mathscr{K}},\vec{K}_a,\vec{k}_a)Y_{LM}^*(\hat{K}_a)Y_{L'M'}(\hat{K}_a)Y_{lm}^*(\hat{k}_a)Y_{l'm'}(\hat{k}_a)\,. \quad (4.2)$$

The integral in Eq. (4.2) is to be evaluated using $|\vec{K}_a| = K$, $|\vec{k}_a| = k$. The complicated angular dependence of $Q(\vec{\mathscr{K}},\vec{K}_a,\vec{k}_a)$ prevents use of the orthogonality properties of the spherical harmonics. Thus no further simplification is possible, and Q does not conserve any of the quantum numbers $(LMlm)$. Also, since $Q(\vec{\mathscr{K}},\vec{K}_a,\vec{k}_a) \neq Q(\vec{\mathscr{K}},-\vec{K}_a,-\vec{k}_a)$, Q does not conserve parity $\mathscr{P} = (-)^{L+l}$.

In this paper we avoid these complications by using an angle-average approximation[23] for Q. Consider a state where particles 1 and 2 have magnitudes P and k of total and relative momentum, respectively [see Eqs. (2.95) and (2.96)]. The angle-average approximation to Q is diagonal in this representation with eigenvalues

$$Q(P,k) = 0,\ k^2 + \tfrac{1}{4}P^2 < k_F^2 = \min\{1,(k^2+\tfrac{1}{4}P^2-k_F^2)/Pk\},\ \text{otherwise}\,. \quad (4.3)$$

This formula has usually been derived for $P < 2k_F$, but it holds for any value of P.

The volume of $\vec{k}$ space excluded by Q depends on P but is never larger than the volume of two Fermi spheres. This is a very small fraction of the important region of $\vec{k}$ space, which is a sphere

whose radius is about 4 fm^{-1}. Largely for this reason, the use of the angle-average approximation for Q has been found quite accurate[24] for calculation of the two-body energy D_2. In the calculation of D_2 one always has $P < 2k_F$, so that Eq. (4.3) is exact for $k > k_F + \frac{1}{2}P$. In the three-body equations, however, values of P larger than $2k_F$ occur. In this case, as pointed out by Ioannides (private communication), Eq. (4.3) remains approximate even at fairly large values of k. Thus the fraction of $\vec{k}$ space in which Eq. (4.3) is exact becomes smaller as P increases, even though the volume in $\vec{k}$ space excluded by Q remains fixed. For this reason it would be worthwhile to check the accuracy of G-matrix elements calculated using Eq. (4.3) for large P, but this has not yet been done.

The angle-average approximation (4.3) is applied differently in the two cases (a) particle 3 is above the Fermi sea and (b) particle 3 is in the Fermi sea. In case (a) we shall want to apply Q_a to three-body states in the basis of Eq. (3.33), labeled by K,k with parameter $\vec{\mathscr{K}} = \vec{\mathscr{K}}_0$. From Eq. (2.96) we see that P depends on the angle between $\vec{\mathscr{K}}_0$ and $\vec{\mathrm{K}}$; so P does not have a definite value in the basis of Eq. (3.33). However, we force Q to be diagonal in this basis by choosing an appropriate average value of P and using Eq. (4.3). Thus we define

$$Q_a(K,k) = Q(P_a,k)\,, \tag{4.4}$$

where

$$P_a = (4\mathscr{K}_0^2/9 + K^2)^{1/2} \tag{4.5}$$

is the rms average of P over the angle between $\mathscr{K}_0$ and $\vec{\mathrm{K}}$.

In numerical calculations we have neglected the dependence of $\vec{\mathscr{K}}$ on $\vec{p}_1,\vec{p}_2,\vec{p}_3$ and instead have used the fixed, average value

$$\mathscr{K}_0 = (\tfrac{9}{5})^{1/2}k_F\,. \tag{4.6}$$

Since $\mathscr{K}_0$ does not vary, the dependence of Q_a on $\mathscr{K}_0$ is suppressed in Eq. (4.4).

In case (b) we apply Q_b either to a two-body state [as in Eq. (2.26)] or to a three-body state of type (3.33) that occurs just before the last or just after the first interaction in a three-body diagram [as in Eq. (2.27)]. In neither case do we treat the dependence on P in detail. We know from momentum conservation that

$$\vec{\mathrm{P}} = \vec{p}_1 + \vec{p}_2\,, \tag{4.7}$$

and we simply replace P by its rms value over two-body states in the Fermi sea. Thus we define

$$Q_b(k) = Q(P_b,k)\,, \tag{4.8}$$

where

$$P_b = (\tfrac{6}{5})^{1/2}k_F\,. \tag{4.9}$$

B. Matrix elements of e

The energy denominator e depends on the single-particle spectrum, which we take to be

$$\begin{aligned} E(k) &= \tfrac{1}{2}k^2, \quad k > k_F \\ &= \tfrac{1}{2}k^2/m^* - E_0, \quad k < k_F\,. \end{aligned} \tag{4.10}$$

The parameters m^* and E_0 are obtained from self-consistent two-body calculations.

As explained in Sec. II A, we distinguish the two operators e_a (particle 3 above the sea) and e_b (particle 3 below the sea). From Eq. (2.20) or Eq. (2.23) we find

$$e_a = \tfrac{1}{2}(k_1^2 + k_2^2 + k_3^2) - \omega_3\,, \tag{4.11}$$

where k_i is the momentum of particle i above the Fermi sea. We rewrite this in terms of $\mathscr{K},K,k$ using Eqs. (2.97)–(2.99). For $\mathscr{K}$ we use the average value $\mathscr{K}_o$ of Eq. (4.6). We also replace ω_3 by its average value $\overline{\omega}_3$, which is seen from Eq. (4.10) to be

$$\overline{\omega}_3 = 0.9k_F^2/m^* - 3E_0\,. \tag{4.12}$$

Thus we find

$$e_a(K,k) = \gamma_a^2 + k^2\,, \tag{4.13}$$

where

$$\gamma_a^2 = \tfrac{1}{6}\mathscr{K}_0^2 + \tfrac{3}{4}K^2 - \overline{\omega}_3\,. \tag{4.14}$$

The operator e_a is diagonal in the basis (3.33) and takes the value (4.13).

The operator e_b is used for a state of two particles with momenta $\vec{k}_1,\vec{k}_2$ above the Fermi sea and two holes $\vec{p}_1,\vec{p}_2$ in the sea. Equation (4.10) and either Eq. (2.18) or Eq. (2.23) give

$$e_b = \tfrac{1}{2}(k_1^2 + k_2^2) - E(p_1) - E(p_2)\,. \tag{4.15}$$

Introducing relative and total momenta via Eqs. (2.86), (2.87), (2.95), and (2.96), and using the spectrum (4.10), gives

$$e_b = k^2 + \tfrac{1}{4}P^2(1 - 1/m^*) - k_0^2/m^* + 2E_0\,. \tag{4.16}$$

Just as in our treatment of Q_b in Sec. IV A we

now replace P^2 by an average value. We average $P^2 = (\vec{p}_1 + \vec{p}_2)^2$ over $\vec{p}_1$ and $\vec{p}_2$, subject to the constraint $|\vec{p}_1 - \vec{p}_2| = 2k_0$. The result depends on k_0 and is given by

$$P^2(k_0) = 2.4k_F^2(1-x)[1 + x^2/(3x+6)] , \tag{4.17}$$

where

$$x = k_0/k_F . \tag{4.18}$$

Thus we finally get

$$e_b(k,k_0) = k^2 + \gamma_b^2 , \tag{4.19}$$

$$\gamma_b^2 = \tfrac{1}{4}P^2(k_0)(1 - 1/m^*) - k_0^2/m^* + 2E_0 . \tag{4.20}$$

We now define $\overline{e}_b$ by averaging Eq. (4.20) over k_0. This average is most easily obtained by replacing P^2 and k_0^2 in Eq. (4.16) by their average values $6k_F^2/5$ and $3k_F^2/10$, respectively. The result is

$$\overline{e}_b(k) = k^2 + \overline{\gamma}_b^2 , \tag{4.21}$$

$$\overline{\gamma}_b^2 = 0.3(1 - 2/m^*)k_F^2 + 2E_0 . \tag{4.22}$$

Equations (4.19)—(4.22) are used for both two-body and three-body states.

C. Matrix elements of v and G

Since the two-body potential v conserves jST and is independent of j_z,T_z, we can write

$$(klSjj_zTT_z \,|\, v \,|\, k'l'Sjj_zTT_z) = (kl \,|\, v^{jST} \,|\, k'l') . \tag{4.23}$$

For a given two-body (jST), the potentials considered in this paper can be written

$$v^{jST} = v_c^{jST}(r) + v_T^{jST}(r)S_{12} + v_{LS}^{jST}(r)\vec{l}\cdot\vec{S} , \tag{4.24}$$

where the tensor operator is

$$S_{12} = 3(\vec{\sigma}_1\cdot\hat{r})(\vec{\sigma}_2\cdot\hat{r}) - \vec{\sigma}_1\cdot\vec{\sigma}_2 . \tag{4.25}$$

Using Eq. (3.15) we then find

$$(kl \,|\, v^{jST} \,|\, k'l') = i^{l-l'}\nu(lST)(4kk'/\pi)\int_0^\infty j_l kr\,[\,\delta(l,l')v_c^{jST}(r) + \langle lSj \,|\, S_{12} \,|\, l'Sj\rangle v_T^{jST}(r) + \delta(l,l')\langle lSj \,|\, \vec{l}\cdot\vec{S} \,|\, lSj\rangle v_{LS}^{jST}(r)]\,j_{l'}(k'r)r^2dr , \tag{4.26}$$

where, for $A = S_{12}$ or $A = \vec{l}\cdot\vec{S}$, we have defined

$$\langle lSj \,|\, A \,|\, l'Sj\rangle = \langle \mathscr{Y}_{jlS}^{j_z}(1,2) \,|\, A \,|\, \mathscr{Y}_{jl'S}^{j_z}(1,2)\rangle , \tag{4.27}$$

and $\mathscr{Y}_{jls}^{j_z}$ is defined by Eq. (3.16). The factor $i^{l-l'}$ in Eq. (4.26) should be noted.

The equation for G is

$$G = v - v(Q/e)G \tag{4.28}$$

and we solve this in the $|klSjj_zTT_z)$ representation for the relative motion of particles 1 and 2. We use the angle-average $Q(P,k)$ of Eq. (4.3), and we have

$$e = k^2 + \gamma^2 . \tag{4.29}$$

Thus G depends on the two parameters P and γ^2. As discussed in the preceding two subsections, the choice of P and γ^2 is different in the cases (a) and (b). Since Q and e are diagonal and depend only on k, G conserves jST and is independent of j_z,T_z. Therefore, we can write in analogy with Eq. (4.23) (we suppress P and γ^2)

$$(klSjj_zTT_z \,|\, G \,|\, k'l'Sjj_zTT_z) = (kl \,|\, G^{jST} \,|\, k'l') . \tag{4.30}$$

Putting the completeness relation (3.18) into Eq. (4.28), we find

$$(kl \,|\, G^{jST} \,|\, k'l') = (kl \,|\, v^{jST} \,|\, k'l') - \tfrac{1}{2}\sum_{l''}\int dk''(kl \,|\, v^{jST} \,|\, k''l'') \times Q(P,k'')(k''^2 + \gamma^2)^{-1} \times (k''l'' \,|\, G^{jST} \,|\, k'l') . \tag{4.31}$$

For fixed values of $(jST,P\gamma^2)$ we solve this equation numerically in momentum space to obtain matrix elements of G.

We will represent G_a as a sum of separable terms,

$$(kl \,|\, G_a^{jST} \,|\, k'l') = \sum_\beta g_{\beta l}^{jST}(k,K)\lambda_\beta^{jST}(K)g_{\beta l'}^{jST}(k',K) . \tag{4.32}$$

The values of P_a,γ_a^2 depend on K, $\mathscr{K}_0$, and $\overline{\omega}_3$

through Eqs. (4.5) and (4.14). Since $\mathscr{K}_0$ and $\overline{\omega}_3$ are held fixed in numerical work, we suppress them in Eq. (4.32) and only indicate the dependence of G on K. Note that in tensor-coupled channels the strength λ_β is independent of l and l'.

The strengths λ and form factors g in Eq. (4.32) are found as follows. The variables j,S,T,K appear only as parameters, and we suppress them. We first set up a discrete grid k_i, $i = 1,2 \ldots R$. In practice we use

$$k_i = 0(0.25)5(0.5)10 \text{ fm}^{-1} \ , \tag{4.33}$$

so that $R = 31$. Since we use a cutoff in momentum, values of k larger than 10 fm^{-1} do not appear in the three-body equations. Then we solve Eq. (4.31) to get the matrix $(k_i l \mid G \mid k_j l')$ of dimension $B = RN(l)$, where $N(l) = 1$ or 2 for uncoupled or tensor-coupled channels, respectively. This is a real, symmetric matrix, and a separable representation can be obtained from its eigenvectors and eigenvalues. However, we expect larger values of k to be relatively less important in the three-body equations, and we therefore define

$$(il \mid L \mid jl') = w(k_i)(k_i l \mid G \mid k_j l')w(k_j) \ , \tag{4.34}$$

where $w(k)$ is a weight function that makes large k less prominent in the matrix L. In practice we have used $w(k) = (k^2 + \gamma^2)^{-1}$. If ν_β and $u_\beta(k_i l)$ are the eigenvalues and orthonormal eigenvectors of L, we have

$$\sum_{jl'} (il \mid L \mid jl')u_\beta(k_j l') = \nu_\beta u_\beta(k_i l), \qquad \beta = 1,2 \ldots B \tag{4.35}$$

$$(il \mid L \mid jl') = \sum_{\beta=1}^{B} u_\beta(k_i l)\nu_\beta u_\beta(k_j l') \ . \tag{4.36}$$

Equations (4.34) and (4.36) give

$$(k_i l \mid G \mid k_j l') = \sum_{\beta=1}^{B} g_{\beta l}(k_i)\lambda_\beta g_{\beta l'}(k_j) \ , \tag{4.37}$$

where

$$g_{\beta l}(k_i) = K_\beta^{-1} u_\beta(k_i l)/w(k_i) \ , \tag{4.38}$$

$$\lambda_\beta = K_\beta^2 \nu_\beta \ . \tag{4.39}$$

We choose K_β so that

$$\sum_{il} [g_{\beta l}(k_i)]^2 = B/2 \ , \tag{4.40}$$

and this means the rms value of g is $\frac{1}{2}$, independent of β. This is convenient because the size of $|\lambda_\beta|$ then determines the relative importance of each term β in Eq. (4.37).

Equation (4.37) gives the desired separable representation of G_a when the initial and final momenta coincide with mesh points. For other values of k,k', we obtain $(kl \mid G \mid k'l')$ by interpolation of the form factors $g_{\beta l}(k)$. In practice a cubic spline interpolation formula has been used. The entire procedure just described is carried out separately for each set jST and each mesh point K_i that occurs in the three-body calculation.

D. Matrix elements of X

In numerical calculations we need matrix elements of X in the basis (3.33). We calculate these by first deriving matrix elements of X in the basis (3.38) and then changing basis using Eq. (3.39). The state (3.38) can be written

$$|Kk[(Ll)\mathscr{L}(\tfrac{1}{2}S)\mathscr{S}]\mathscr{J}\mathscr{J}_z(\tfrac{1}{2}T)\mathscr{T}\mathscr{T}_z) = \sum_{\mathscr{L}_z\mathscr{S}_z} (\mathscr{L}\mathscr{S}\mathscr{L}_z\mathscr{S}_z \mid \mathscr{J}\mathscr{J}_z)2^{1/2}\nu(lST) \mid Kk(Ll)\mathscr{L}\mathscr{L}_z)_{\text{na}} \mid (\tfrac{1}{2}S)\mathscr{S}\mathscr{S}_z) \mid (\tfrac{1}{2}T)\mathscr{T}\mathscr{T}_z) \ , \tag{4.41}$$

where $|Kk(Ll)\mathscr{L}\mathscr{L}_z)_{\text{na}}$ is the product of states (3.4) and (3.11), coupled to $\mathscr{L}\mathscr{L}_z$. On the right of Eq. (4.41) we have products of space, spin, and isospin wave functions, and we therefore need space, spin, and isospin matrix elements of X.

First consider the spin wave function, which can be written more explicitly as

$$|(\tfrac{1}{2}S)\mathscr{S}\mathscr{S}_z) = |\{\tfrac{1}{2}(3)[\tfrac{1}{2}(1)\tfrac{1}{2}(2)]S\}\mathscr{S}\mathscr{S}_z) \ , \tag{4.42}$$

where the notation $\frac{1}{2}(i)$ means spin $\frac{1}{2}$ for particle i. We have $X = P_{123} + P_{132}$, and we first consider matrix elements of P_{123} between states of Eq. (4.42). The operators $\mathscr{S}$ and $\mathscr{S}_z$ are completely symmetric and therefore commute with all permutation operators. Hence all permutation operators are diagonal in $\mathscr{S}$ and $\mathscr{S}_z$. Also, all permutation operators commute with the raising and lowering operators for $\mathscr{S}_z$, and this means all matrix elements of permutation operators are independent of $\mathscr{S}_z$. As a

result, the only matrix elements of P_{123} that occur are

$$[(\tfrac{1}{2}S)\mathcal{S}\mathcal{S}_z \,|\, P_{123} \,|\, (\tfrac{1}{2}S')\mathcal{S}\mathcal{S}_z] \equiv \mathcal{R}(\mathcal{S},SS') \ . \tag{4.43}$$

States with $\mathcal{S} = \frac{3}{2}$ are totally symmetric, so that

$$\mathcal{R}(\tfrac{3}{2},11) = 1 \ . \tag{4.44}$$

To evaluate $\mathcal{R}(\frac{1}{2},SS')$ we note that

$$P_{123} \,|\, (\tfrac{1}{2}S')\mathcal{S}\mathcal{S}_z) = \,|\, \{\tfrac{1}{2}(1)[\tfrac{1}{2}(2)\tfrac{1}{2}(3)]S'\}\mathcal{S}\mathcal{S}_z) \ , \tag{4.45}$$

which leads to

$$\mathcal{R}(\tfrac{1}{2},SS') = \tfrac{1}{2}\begin{bmatrix} -1 & 3^{1/2} \\ -3^{1/2} & -1 \end{bmatrix} \ , \tag{4.46}$$

where the first row or column corresponds to $S = 0$ and the second to $S = 1$.

This takes care of spin matrix elements of P_{123}. To treat P_{132} we note that

$$P_{132} = P_{12}P_{123}P_{12} \ , \tag{4.47}$$

so that

$$[(\tfrac{1}{2}S)\mathcal{S}\mathcal{S}_z \,|\, P_{132} \,|\, (\tfrac{1}{2}S')\mathcal{S}\mathcal{S}_z)] = (-)^{S+S'}\mathcal{R}(\mathcal{S},SS') \ . \tag{4.48}$$

We now have all the ingredients for spin matrix elements of X. The discussion for isospin is exactly the same.

We now turn to spatial matrix elements of X, and again we first consider P_{123}. By an argument similar to that for spin, matrix elements of P_{123} are diagonal to $\mathcal{L},\mathcal{L}_z$ and are independent of $\mathcal{L}_z$. Using the completeness relation

$$\int d\vec{K}\, d\vec{k} \,|\, \vec{K}\,\vec{k})_{\rm na\,na}(\vec{K}\,\vec{k}\,| = 1 \ , \tag{4.49}$$

where $|\,\vec{K}\,\vec{k})_{\rm na}$ is a product of the states (3.1) and (3.10), we find

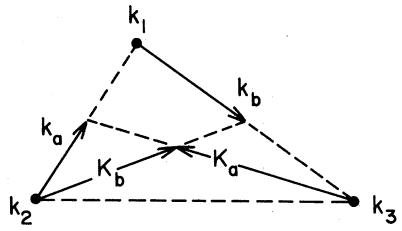

FIG. 6. Diagram illustrating Eqs. (4.51)–(4.53). The vertices of the triangle lie at the tips of the vectors $\vec{k}_1,\vec{k}_2,\vec{k}_3$. The vectors $\vec{K}_a,\vec{k}_a$ are defined by Eqs. (2.94) and (2.95), respectively. The vectors $\vec{K}_a$ and $\vec{K}_b$ intersect at the median of the triangle.

$$_{\rm na}(KLMklm \,|\, P_{123} \,|\, K'L'M'k'l'm')_{\rm na} = \int d\vec{K}_a d\vec{k}_a \ {}_{\rm na}(KLMklm \,|\, P_{123} \,|\, \vec{K}_a\vec{k}_a)_{\rm na} \times {}_{\rm na}(\vec{K}_a\vec{k}_a \,|\, K'L'M'k'l'm')_{\rm na} \ . \tag{4.50}$$

In state $|\,\vec{K}_a\vec{k}_a)_{\rm na}$ we suppose that particles 1,2,3 have momenta $\vec{k}_1,\vec{k}_2,\vec{k}_3$, respectively, so that $\vec{K}_a$ and $\vec{k}_a$ are given by Eqs. (2.94) and (2.95), respectively. Then in the state $P_{123}\,|\,\vec{K}_a\vec{k}_a)_{\rm na}$ particles 1,2,3 have the respective momenta $\vec{k}_3,\vec{k}_1,\vec{k}_2$. Using Eqs. (2.94) and (2.95) then gives

$$P_{123}\,|\,\vec{K}_a\vec{k}_a)_{\rm na} = \,|\,\vec{K}_b\vec{k}_b)_{\rm na} \ , \tag{4.51}$$

where

$$\vec{K}_b = -\tfrac{1}{2}\vec{K}_a + \vec{k}_a \ , \tag{4.52}$$

$$\vec{k}_b = -\tfrac{3}{4}\vec{K}_a - \tfrac{1}{2}\vec{k}_a \ . \tag{4.53}$$

Figure 6 is useful in deriving the last two formulas.

We now put Eq. (4.51) into Eq. (4.50) and change variables from $\vec{K}_a\vec{k}_a$ to $\vec{K}_b\vec{k}_b$ using Eqs. (4.52) and (4.53). We also perform the angular momentum couplings $(Ll)\mathcal{L}\mathcal{L}_z$ and $(L'l')\mathcal{L}\mathcal{L}_z$ and use the formula

$$_{\rm na}(\vec{K}'\vec{k}' \,|\, KLMklm)_{\rm na} = (Kk)^{-1}\delta(K-K')\delta(k-k') \times Y_{LM}(\hat{K}')Y_{lm}(\hat{k}') \ . \tag{4.54}$$

The result is

$$_{\rm na}[Kk(Ll)\mathcal{L}\mathcal{L}_z \,|\, P_{123} \,|\, K'k'(L'l')\mathcal{L}\mathcal{L}_z]_{\rm na} = (KkK'k')^{-1}\int d\vec{K}_b d\vec{k}_b \delta(K_b-K)\delta(k_b-k)\delta(K'-K_a)\delta(k'-k_a) \times \sum_{Mm}(LlMm \,|\, \mathcal{L}\mathcal{L}_z)Y^*_{LM}(\hat{K}_b)Y^*_{lm}(\hat{k}_b) \times \sum_{M'm'}(L'l'M'm' \,|\, \mathcal{L}\mathcal{L}_z)Y_{L'M'}(\hat{K}_a)Y_{l'm'}(\hat{k}_a) \ , \tag{4.55}$$

where $\vec{K}_a$ and $\vec{k}_a$ are functions of $\vec{K}_b,\vec{k}_b$ given by the inverse of Eqs. (4.52) and (4.53).

Equation (4.55) is evaluated following Balian and Brézin,[25] and the result is

$$ {}_{\rm na}(Kk(Ll)\mathscr{L}\mathscr{L}_z\,|P_{123}\,|K'k'(L'l')\mathscr{L}\mathscr{L}_z)_{\rm na} $$
$$ = 2\delta(\tfrac{3}{4}K^2 + k^2 - \tfrac{3}{4}K'^2 - k'^2)\theta(1 - |\cos\theta_2|)(KLkl\,|f(\mathscr{L})\,|K'L'k'l') \ , \quad (4.56) $$

where $\theta(x)$ is the unit step function and

$$ (KLkl\,|f(\mathscr{L})\,|K'L'k'l') = 16\pi^2\hat{\mathscr{L}}^{-1}\hat{L}^{1/2}(4\pi)^{-1/2}\sum_{mm'}(-)^m(Ll0m\,|\,\mathscr{L}m)(L'l'm - m'm'\,|\,\mathscr{L}m) $$
$$ \times Y_{lm}(\cos\theta_1,0)Y_{L'm-m'}(\cos\theta_2,0)Y_{l'm'}(\cos\theta_3,0) \ , \quad (4.57) $$

$$ \cos\theta_1 = (K'^2 - \tfrac{1}{4}K^2 - k^2)/Kk \ , \quad (4.58) $$

$$ \cos\theta_2 = (k^2 - \tfrac{1}{4}K^2 - K'^2)/KK' \ , \quad (4.59) $$

$$ \cos\theta_3 = (K^2 + k'^2 - \tfrac{1}{4}K'^2)/2Kk' \ . \quad (4.60) $$

Noting that

$$ P_{12}\,|Kk(Ll)\mathscr{L}\mathscr{L}_z)_{\rm na} = (-)^l\,|Kk(Ll)\mathscr{L}\mathscr{L}_z)_{\rm na} \ , \quad (4.61) $$

we use $P_{132} = P_{12}P_{123}P_{12}$ to get

$$ {}_{\rm na}(Kk(Ll)\mathscr{L}\mathscr{L}_z\,|P_{132}\,|K'k'(L'l')\mathscr{L}\mathscr{L}_z)_{\rm na} $$
$$ = (-)^{l+l'}{}_{\rm na}(Kk(Ll)\mathscr{L}\mathscr{L}_z\,|P_{123}\,| $$
$$ \times K'k'(L'l')\mathscr{L}\mathscr{L}_z)_{\rm na} \ . \quad (4.62) $$

Equations (4.56)–(4.62) determine the required spatial matrix elements of X.

A very important property of X is that it conserves parity $\mathscr{P} = (-)^{L+l}$. This follows from

$$ [P_{123},\mathscr{P}] = 0 \ , \quad (4.63) $$

which is most easily derived in the basis $|\vec{K}\vec{k})_{\rm na}$. The effect of P_{123} in this basis is given by Eqs. (4.51)–(4.53). Using these equations along with

$$ \mathscr{P}\,|\vec{K}\vec{k})_{\rm na} = |-\vec{K},-\vec{k})_{\rm na} \ , \quad (4.64) $$

one easily verifies Eq. (4.63).

Later on we shall have to integrate expressions like Eq. (4.56) over two momentum variables while holding the other two fixed. Two cases arise:

(1) Integrate over k,k' for fixed K,K'. The delta function in Eq. (4.56) is used to evaluate the integral over k. The requirement $|\cos\theta_2| < 1$ then determines the limits on k' to be

$$ |K - \tfrac{1}{2}K'| < k' < K + \tfrac{1}{2}K' \ . \quad (4.65) $$

(2) Integrate over K,k for fixed K',k'. The delta function in Eq. (4.56) is used to integrate over k. The limits on K are then

$$ |k' - \tfrac{1}{2}K'| < K < k' + \tfrac{1}{2}K' \ . \quad (4.66) $$

Figure 6 is useful in understanding Eqs. (4.65)–(4.66).

We can now assemble our results to obtain the matrix elements of X in the basis (3.33). From Eqs. (4.48) and (4.62) we see that matrix elements of P_{123} differ from those of P_{132} by a factor $(-)^{l+S+T}(-)^{l'+S'+T'}$. Since we consider only states that are antisymmetric in particles 1 and 2, this factor is unity. Thus matrix elements of X are just twice those of P_{123}. Equations (4.44), (4.46), and (4.56) determine the matrix elements of X in the basis (3.38), which is related to the basis (3.33) by Eq. (3.39). A simple calculation gives

$$ (dKkl,\mathscr{J}\mathscr{J}_z\mathscr{P}\mathscr{T}\mathscr{T}_z\,|X\,|d'K'k'l',\mathscr{J}'\mathscr{J}'_z\mathscr{P}'\mathscr{T}'\mathscr{T}'_z) $$
$$ = 8\delta(\mathscr{J}\mathscr{J}_z\mathscr{P}\mathscr{T}\mathscr{T}_z\,|\mathscr{J}'\mathscr{J}'_z\mathscr{P}'\mathscr{T}'\mathscr{T}'_z)\sum_{\mathscr{L}\mathscr{S}}\hat{\mathscr{L}}\hat{\mathscr{S}}[\hat{J}\hat{j}\hat{J}'\hat{j}']^{1/2}\begin{Bmatrix} L & \frac{1}{2} & J \\ l & S & j \\ \mathscr{L} & \mathscr{S} & \mathscr{J} \end{Bmatrix}\begin{Bmatrix} L' & \frac{1}{2} & J' \\ l' & S' & j' \\ \mathscr{L} & \mathscr{S} & \mathscr{J} \end{Bmatrix} $$
$$ \times \delta(\tfrac{3}{4}K^2 + k^2 - \tfrac{3}{4}K'^2 - k'^2)\theta(1 - |\cos\theta_2|) $$
$$ \times (KLkl\,|f(\mathscr{L})\,|K'L'k'l')\mathscr{R}(\mathscr{S},SS')\mathscr{R}(\mathscr{T},TT') \ . \quad (4.67) $$

V. FORMULAS FOR COMPUTATION

In this section we put the matrix elements of Sec. IV into the formal expressions of Sec. II to get practical formulas for computation. We also introduce two additional angle-average approximations that arise when we change integration variables from $\vec{p}_i$ to $\vec{K}_0,\vec{k}_0$ in Eqs. (2.107) and (2.113).

We have seen that X conserves $\mathcal{J}\mathcal{J}_z\mathcal{P}\mathcal{T}\mathcal{T}_z$ and has matrix elements independent of $\mathcal{J}_z$, $\mathcal{T}_z$. Because of our angle-average approximations, this is also true for Q, e, and G. Therefore, the same is true of operators such as $\mathcal{O}$, C, and D that are built from Q, e, g, and X. We use this fact in our notation, writing, for example,

$$(dKkl,\mathcal{J}\mathcal{J}_z\mathcal{P}\mathcal{T}\mathcal{T}_z\,|\,\mathcal{O}\,|\,d'K'k'l',\mathcal{J}\mathcal{J}_z\mathcal{P}\mathcal{T}\mathcal{T}_z)\equiv(dKkl\,|\,\mathcal{O}(\mathcal{J}\mathcal{P}\mathcal{T})\,|\,d'K'k'l')\ , \tag{5.1}$$

where it is understood that the initial and final states in the right-hand matrix element have quantum numbers $\mathcal{J}\mathcal{P}\mathcal{T}$. Both D_3^c and $\mathcal{M}$ will be given by sums of independent contributions from different sets of $\mathcal{J}\mathcal{P}\mathcal{T}$. The variables $\mathcal{K}$ and ω_3 have been suppressed in Eq. (5.1) because, as mentioned in Secs. IV A and IV B, we use fixed average values for them.

A. Formula for D_2 and D_n^{GR}

The two-body energy D_2 is given by Eq. (2.92). The same formula also gives D_n^{GR} if G_b is replaced by $G_bQ\overline{J}^{(n)}$. Putting spin and isospin into Eq. (2.92) gives

$$D_2=\tfrac{1}{2}(2\pi)^{-3}\rho^{-1}\sum\int d\vec{p}_1d\vec{p}_2(\vec{k}_0SM_sTT_z\,|\,G_b(\vec{P})\,|\,\vec{k}_0SM_sTT_z)\ , \tag{5.2}$$

where $|k_0SM_sTT_z)$ is defined by Eq. (3.12). We transform to the $k_0f_0j_{0z}T_{0z}$ representation by using Eqs. (3.18) and (3.19) to get

$$\sum(\vec{k}_0SM_sTT_z\,|\,G_b(P)\,|\,\vec{k}_0SM_sTT_z)=\sum_{f_0}\nu(f_0)\hat{j}_0\hat{T}_0(4\pi)^{-1}k_0{}^{-2}(k_0l_0\,|\,G_b^{j_0S_0T_0}(P)\,|\,k_0l_0)\ , \tag{5.3}$$

where $f_0=\{\,l_0S_0j_0T_0\,\}$. In deriving Eq. (5.3) we used the fact that G_b conserves jj_zSTT_z and is independent of j_z,T_z, along with Eqs. (3.43), (3.45) and (4.30).

Putting Eq. (5.3) into Eq. (5.2) gives

$$D_2=\sum_{f_0}\nu(f_0)\hat{j}_0\hat{T}_0(k_F{}^3/24)\langle k_0{}^{-2}(k_0f_0\,|\,G_b(P)\,|\,k_0f_0)\rangle_2\ , \tag{5.4}$$

where, for any function $h(\vec{p}_1,\ldots,\vec{p}_n)$, we define

$$\langle h\rangle_n=(4\pi k_F{}^3/3)^{-n}\int d\vec{p}_1\ldots d\vec{p}_nh(\vec{p}_1,\ldots,\vec{p}_n)\ . \tag{5.5}$$

As a result of an approximation to be introduced in Sec. V C, $G_bQ\overline{J}^{(n)}$ conserves jj_zSTT_z and is independent of j_z,T_z. Hence Eq. (5.3) is valid for $G_bQ\overline{J}^{(n)}$, so that D_n^{GR} is given by Eq. (5.4) with G_b replaced by $G_bQ\overline{J}^{(n)}$.

B. Formula for D_3^c in terms of $\mathcal{O}$

In an $\mathcal{O}$-type calculation we evaluate D_3^c using Eq. (2.107). In order to include spin and isospin in Eq. (2.107), we replace $|\vec{K}_0\vec{k}_0)$ by the product of the states (3.8) and (3.12) to get

$$D_3^c=\tfrac{1}{2}(2\pi)^{-3}\rho^{-1}\sum\int d\vec{p}_1d\vec{p}_2d\vec{p}_3(\vec{K}_0\sigma_3\tau_3\vec{k}_0SM_STT_z\,|\,\mathcal{O}\,|\,\vec{K}_0\sigma_3\tau_3\vec{k}_0SM_STT_z)\ . \tag{5.6}$$

We now insert Eq. (3.37) on either side of $\mathcal{O}$, use the fact that $\mathcal{O}$ conserves $\mathcal{J}\mathcal{J}_z\mathcal{P}\mathcal{T}\mathcal{T}_z$ and has matrix elements independent of $\mathcal{J}_z$, $\mathcal{T}_z$, and change variables from $\vec{p}_1,\vec{p}_2,\vec{p}_3$ to $\vec{\mathcal{K}},\vec{K}_0,\vec{k}_0$ via Eqs. (2.93)–(2.95). The

result is

$$D_3^c = \tfrac{1}{2}(2\pi)^{-3}\rho^{-1}\sum\int dK\,dk\,dK'dk'\int d\vec{\mathscr{K}}(d_0'K'k'l_0'\,|\,Q_{3h}(\vec{\mathscr{K}}\mathscr{J}\mathscr{P}\mathscr{T})\,|\,d_0Kkl_0)$$
$$\times(d_0Kkl_0\,|\,\mathscr{O}(\mathscr{J}\mathscr{P}\mathscr{T})\,|\,d_0'K'k'l_0')\ , \tag{5.7}$$

where

$$(d_0'K'k'l_0'\,|\,Q_{3h}(\vec{\mathscr{K}}\mathscr{J}\mathscr{P}\mathscr{T})\,|\,d_0Kkl_0)=\tfrac{1}{4}\sum_{ST}\sum_{\text{mag}}\int_{(3h)}d\vec{\mathrm{K}}_0d\vec{\mathrm{k}}_0(d_0'K'k'l_0',\mathscr{J}\mathscr{J}_z\mathscr{P}\mathscr{T}\mathscr{T}_z\,|\,\vec{\mathrm{K}}_0\sigma_3\tau_3\vec{\mathrm{k}}_0SM_STT_z)$$
$$\times(\vec{\mathrm{K}}_0\sigma_3\tau_3\vec{\mathrm{k}}_0SM_STT_z\,|\,d_0Kkl_0,\mathscr{J}\mathscr{J}_z\mathscr{P}\mathscr{T}\mathscr{T}_z)\ . \tag{5.8}$$

In the integral the notation (3h) stands for "three-hole" and means that, for the given value of $\vec{\mathscr{K}}$, the vectors $K_0,\vec{\mathrm{k}}_0$ are restricted so that all three single-particle momenta from Eqs. (2.97)–(2.99) are in the Fermi sea. Also, $\sum_{\text{mag}}$ means summation over all magnetic quantum numbers.

Substituting Eq. (3.41) into Eq. (5.8), we can perform the sum over $\tau_3,T_z,\mathscr{T}_z$ to get

$$(d_0'K'k'l_0'\,|\,Q_{3h}(\vec{\mathscr{K}}\mathscr{J}\mathscr{P}\mathscr{T})\,|\,d_0Kkl_0)$$
$$=\nu(l_0'S_0T_0)\nu(l_0S_0T_0)\delta(S_0'T_0'\,|\,S_0T_0)\delta(K-K')\delta(k-k')\hat{\mathscr{T}}$$
$$\times\int_{(3h)}d\vec{\mathrm{K}}_0d\vec{\mathrm{k}}_0K_0^{-2}k_0^{-2}\delta(K_0-K)\delta(k_0-k)$$
$$\times\sum_{\text{mag}}(L_0\tfrac{1}{2}M_0\sigma_3\,|\,J_0J_{0z})(L_0'\tfrac{1}{2}M_0'\sigma_3\,|\,J_0'J_{0z}')(l_0S_0m_0M_S\,|\,j_0j_{0z})(l_0'S_0m_0'M_S\,|\,j_0'j_{0z}')$$
$$\times(J_0j_0J_{0z}j_{0z}\,|\,\mathscr{J}\mathscr{J}_z)(J_0'j_0'J_{0z}'j_{0z}'\,|\,\mathscr{J}\mathscr{J}_z)Y^*_{L_0'M_0'}(\hat{K}_0)Y_{L_0M_0}(\hat{K}_0)Y^*_{l_0'm_0'}(\hat{k}_0)Y_{l_0m_0}(k_0)\ , \tag{5.9}$$

where the sum is over all magnetic quantum numbers. Equation (5.9) cannot be simplified further because the angular integrations are restricted by the requirement that all three single-particle momenta be in the Fermi sea, so that we cannot use the orthogonality of the spherical harmonics. To proceed, we make the angle-average approximation

$$\int d\hat{k}_0Y^*_{l_0'm_0'}(\hat{k}_0)Y_{l_0m_0}(\hat{k}_0)\to\int d\hat{k}_0(4\pi)^{-1}\delta(l_0m_0\,|\,l_0'm_0')\ . \tag{5.10}$$

When this is put into Eq. (5.9), all sums over magnetic quantum numbers can be done using Eqs. (3.43)–(3.45), and the result is

$$(d_0'K'k'l_0'\,|\,Q_{3h}(\vec{\mathscr{K}}\mathscr{J}\mathscr{P}\mathscr{T})\,|\,d_0Kkl_0)=\nu(l_0S_0T_0)\delta(d_0'l_0'\,|\,d_0l_0)\delta(K-K')\delta(k-k')\hat{\mathscr{J}}\hat{\mathscr{T}}$$
$$\times(4\pi)^{-2}\int_{(3h)}d\vec{\mathrm{K}}_0d\vec{\mathrm{k}}_0K_0^{-2}k_0^{-2}\delta(K_0-K)\delta(k_0-k)\ . \tag{5.11}$$

Putting this into Eq. (5.7) gives

$$D_3^c=\sum\hat{\mathscr{J}}\hat{\mathscr{T}}(k_F^6/72)\langle K_0^{-2}k_0^{-2}(d_0K_0k_0l_0\,|\,\mathscr{O}(\mathscr{J}\mathscr{P}\mathscr{T})\,|\,d_0K_0k_0l_0)\rangle_3\ , \tag{5.12}$$

where the angular bracket is defined by Eq. (5.5)

Equation (5.12) is our basic formula for D_3^c in terms of $\mathscr{O}$. It has been obtained using the approximation (5.10), which we expect to cause only a small error for several reasons:

(1) The most important contributions to D_3^c are from terms with $l_0=l_0'=0$. In this case Eq. (5.10) is exact.

(2) If l_0 and l_0' have opposite parity, the most important case being $l_0=0$, $l_0'=1$, the integrand of Eq. (5.9) is an odd function of $\hat{k}_0$. But if $\hat{k}_0$ is allowed by the condition $p_i<k_F$, $i=1,2,3$, then $-\hat{k}_0$ is also allowed because changing the sign of $\hat{k}_0$ simply interchanges particles 1 and 2. Hence the integral over $\hat{k}_0$ in Eq. (5.9) vanishes, and Eq. (5.10) is again exact.

(3) D_3^c is largest for $L_0=L_0'=0$. In this case we have $L_0=L_0'$, $M_0=M_0'$, and Eq. (5.9) can be reduced

to Eq. (5.11) without using the approximation (5.10) at all.

(4) If L_0 and L_0' have opposite parity, the most important case being $L_0 = 0$, $L_0' = 1$, then, since $\mathcal{O}$ conserves $\mathcal{P} = (-)^{L_0+l_0}$, l_0 and l_0' must have opposite parity, and Eq. (5.10) is exact as discussed in point (2) above.

C. Formula for $\mathcal{M}$ in terms of $\overline{C}$

In an $\mathcal{M}$-type calculation we use the matrix $\mathcal{M}$ to obtain the generalized ring series. To obtain $\mathcal{M}$, we start with Eq. (2.113) for $\overline{J}^{(3)}$. We introduce spin and isospin by using the states of Eqs. (3.8) and (3.15) to get

$$(kfj_zT_z\,|\,\overline{J}^{(3)}(\vec{\mathrm{P}})\,|\,k_0f_0j_{0z}T_{0z}) = \sum_{\sigma_3\tau_3}\int d\vec{\mathrm{p}}_3(\vec{\mathrm{K}}_0\sigma_3\tau_3kfj_zT_z\,|\,(\overline{e}_b/e_b)\overline{C}e_b{}^{-1}G_b(1+X)\,|\,\vec{\mathrm{K}}_0\sigma_3\tau_3k_0f_0j_{0z}T_{0z})\ , \tag{5.13}$$

where

$$\vec{\mathrm{K}}_0 = \tfrac{1}{3}\vec{\mathrm{P}} - \tfrac{2}{3}\vec{\mathrm{p}}_3\ , \tag{5.14}$$

and we have introduced $\overline{C}$ in place of C through Eq. (2.48). We must first rewrite Eq. (5.13) using the basis $|dKkl,\mathcal{J}\mathcal{J}_z\mathcal{P}\mathcal{T}\mathcal{T}_z)$. The result will then be expressed as a matrix applied to $e_b{}^{-1}G_b = \overline{S}_2^{(2)}$. This matrix is the $\mathcal{M}$ matrix [see Eqs. (2.61) and (2.63)].

The transformation of the right-hand side of Eq. (5.13) to the $|dKkl)$ basis is carried out using Eqs. (3.37) and (3.42). After using Eq. (3.45) for the isospin Clebsch-Gordan coefficients we find

$$\begin{aligned}(kfj_zT_z\,|\,\overline{J}^{(3)}(P)\,|\,k_0f_0j_{0z}T_{0z})&\\ = \delta(TT_z\,|\,T_0T_{0z})\sum_{\mathcal{J}\mathcal{T}LJL_0J_0\sigma_3}\sum_{\mathcal{J}_z\mathcal{J}_{0z}MM_0}&(\hat{\mathcal{T}}/\hat{T}_0)\nu(lST_0)\nu(l_0S_0T_0)\\ &\times\int d\vec{\mathrm{p}}_3K_0{}^{-2}Y_{LM}(\hat{K}_0Y^*_{L_0M_0}(\hat{K}_0)(L\tfrac{1}{2}M\sigma_3\,|\,JJ_z)(L_0\tfrac{1}{2}M_0\sigma_3\,|\,J_0J_{0z})\\ &\times(JjJ_zj_z\,|\,\mathcal{J}\mathcal{J}_z)(J_0j_0J_{0z}j_{0z}\,|\,\mathcal{J}\mathcal{J}_z)\\ &\times(dK_0kl\,|\,(\overline{e}_b/e_b)\overline{C}(\mathcal{J}\mathcal{P}\mathcal{T})e_b{}^{-1}G_b(1+X)\,|\,d_0K_0k_0l_0)\ .\end{aligned} \tag{5.15}$$

Suppose now that we change variables from $\vec{\mathrm{p}}_3$ to $\vec{\mathrm{K}}_0$, using Eq. (5.14). Then for a given magnitude K_0, the requirement $p_3 < k_F$ restricts the allowed directions of $\vec{\mathrm{K}}_0$, so that we cannot use the orthogonality of the spherical harmonics in Eq. (5.15). Nevertheless, inside the integral of Eq. (5.15), we make the angle-average approximation

$$Y_{LM}(K_0)Y^*_{L_0M_0}(K_0)\to(4\pi)^{-1}\delta(LM\,|\,L_0M_0)\ . \tag{5.16}$$

All sums over magnetic quantum numbers can now be carried out, and one finds an expression in which $L = L_0$. Parity conservation then implies that $(-)^l = (-)^{l_0}$. Since we also have $T = T_0$ and $(-)^{l+S+T} = (-)^{l_0+S_0+T_0}$, it follows that $S = S_0$. The result is that $\overline{J}^{(3)}$ conserves $j_0S_0T_0j_{0z}T_{0z}$ and is independent of j_{0z},T_{0z}. Thus we can use the notation of Eq. (3.20) for $\overline{J}^{(3)}$. The final result is

$$\begin{aligned}(kl\,|\,\overline{J}^{(3)}(\vec{\mathrm{P}},j_0S_0T_0)\,|\,k_0l_0) = \sum_{\mathcal{J}\mathcal{T}L_0J_0}&\hat{\mathcal{J}}\hat{\mathcal{T}}[j_0\hat{T}_0]^{-1}\nu(l_0S_0T_0)(4\pi)^{-1}\\ &\times\int d\vec{\mathrm{p}}_3K_0{}^{-2}(d_0K_0kl\,|\,(\overline{e}_b/e_b)\overline{C}(\mathcal{J}\mathcal{P}\mathcal{T})e_b{}^{-1}G_b(1+X)\,|\,d_0K_0k_0l_0)\ .\end{aligned} \tag{5.17}$$

This is the desired expression of Eq. (5.13) in the $|dKkl)$ basis.

Having $\overline{J}^{(3)}$, we can calculate D_3^c by constructing $G_bQ\overline{J}^{(3)}$ and using it in place of G_b in Eq. (5.4). The resulting formula for D_3^c turns out to be equivalent to Eq. (5.12). Thus the angle-average approximations (5.10) and (5.16) lead to the same approximation for D_3^c.

Equation (5.17) depends on P through the relation (5.14) between $\vec{K}_0$ and $\vec{p}_3$. In numerical calculations, an appropriate average over P is made (see Sec. VI B). In calculations of D_2 it is found that a similar average over P produces errors of a few percent, and we expect a comparable percentage error here and in the higher-order terms in the generalized ring series.

Thus the dependence on P disappears, and we write the left-hand side of Eq. (5.17) as $\overline{J}^{(3)}(f_0 l,k,k_0)$, using the notation introduced in Eq. (3.22). To extract the $\mathscr{M}$ matrix, we express the right-hand side of Eq. (5.17) as a matrix (the $\mathscr{M}$ matrix) applied to $\overline{S}_2^{(2)}$. In Eq. (5.17) we insert the completeness relation (3.37) on either side of $e_b{}^{-1}G_b$, and then we transform to the $(f_0 lnm)$ representation as discussed in Sec. III B. The result is

$$\overline{J}^{(3)}(f_0 lnm) = \sum_{f_0' l' n' m'} (f_0 lnm \,|\mathscr{M}|\, f_0' l' n' m')\overline{S}_2^{(2)}(f_0' l' n' m') \ , \tag{5.18}$$

where

$$\begin{aligned}(f_0 lnm \,|\mathscr{M}|\, f_0' l' n' m') &= -\tfrac{1}{4}\nu(f_0)\nu(f_0')\sum_i k_{0i}^{-l_0-1} Y(m,i)\sum_{n''}(n\,|[\overline{e}_b/e_b(k_{0i})]\,|\,n'') \\ &\times \sum_{\mathscr{J}\mathscr{T}L_0J_0L_0'J_0'} \hat{\mathscr{J}}\hat{\mathscr{T}}(\hat{j}_0\hat{T}_0)^{-1}(4\pi)^{-1}\int d\vec{p}_3 K_0^{-2}\int dK_0' dk_0' \\ &\times (d_0 K_0 n'' l \,|\,\overline{C}(\mathscr{J}\mathscr{P}\mathscr{T})\,|\,d_0' K_0' n' l')k_0{}^{l_0'+m'} \\ &\times (d_0' K_0' k_0' l_0' \,|\,1+X\,|\,d_0 K_0 k_{0i} l_0) \ , \end{aligned} \tag{5.19}$$

and

$$(n\,|[\overline{e}_b/e_b(k_0)]\,|\,n'') = \int dk p_n(k)(\overline{\gamma}_b{}^2 + k^2)(\gamma_b{}^2 + k^2)^{-1} p_{n''}(k) \ . \tag{5.20}$$

Equation (5.20) depends on k_0 through $\gamma_b{}^2$, which is defined by Eq. (4.20).

The reason for splitting C into the two factors $\overline{e}_b/e_b$ and $\overline{C}$ is that matrix elements of C depend on k_{0i} through the factor $e_b{}^{-1}$ on the left, while matrix elements of $\overline{C}$ are independent of k_{0i}. Since a major part of the computational effort goes into calculating matrix elements of C or $\overline{C}$, it saves computing time to use $\overline{C}$ so that these matrix elements do not have to be recomputed for each new mesh point k_{0i}.

D. Formulas for the generalized ring series

Equation (5.18) is the explicit statement of Eq. (2.63) in the $(f_0 lnm)$ representation. In numerical work the iterations implied by Eqs. (2.64)–(2.66) and the matrix inversion of Eq. (2.70) for $\overline{S}_2^{\rm tot}$ are carried out in the $(f_0 lnm)$ representation. In this subsection we derive several formulas, in addition to Eq. (5.19) for $\mathscr{M}$, that are needed to carry out these calculations. We make extensive use of the transformations discussed in Sec. III B between the k and n representations, and between the k_0 and m representations.

To evaluate Eq. (2.70) for $\overline{S}_2^{\rm tot}$ we need the matrix $e_b{}^{-1}G_b Q_b \mathscr{M}$. We start with the equation

$$(f_0 lkk_0\,|\,e_b{}^{-1}G_b Q_b \mathscr{M}\,|\,f_0' l' n' m') = \tfrac{1}{2}\sum_{l''}\int dk''(kl\,|\,e_b{}^{-1}(k,k_0)G_b^{j_0 S_0 T_0} Q_b\,|\,k'' l'')(f_0 l'' k'' k_0\,|\,\mathscr{M}\,|\,f_0' l' n' m') \ , \tag{5.21}$$

which is obtained by inserting the completeness relation (3.18) between Q_b and $\mathscr{M}$. In Eq. (5.21) both $e_b{}^{-1}$ and G_b depend on k_0, and this fact must be taken into account in transforming from (k,k_0) to (n,m). The result is

$$\begin{aligned}(f_0 lnm\,|\,e_b{}^{-1}G_b Q_b \mathscr{M}\,|\,f_0' l' n' m') &= \tfrac{1}{2}\sum_i Y(m,i)k_{0i}^{-l_0-1}\sum_{l''n''}(nl\,|\,e_b{}^{-1}(k_{0i})G_b^{j_0 S_0 T_0}(k_{0i})Q_b\,|\,n'' l'') \\ &\times \sum_{m''} k_{0i}^{l_0+m''}(f_0 l'' n'' m''\,|\,\mathscr{M}\,|\,f_0' l' n' m') \ . \end{aligned} \tag{5.22}$$

Given the matrix $\mathscr{M}$ in the (f_0lnm) representation, Eq. (5.22) shows how to calculate the matrix $e_b^{-1}G_bQ\mathscr{M}$ in the same representation.

In Eq. (2.65) we must apply $e_b^{-1}G_bQ$ to the vector $\overline{J}^{(n)}(f_0lnm)$ to get a new vector $K(f_0lnm)$,

$$K(f_0lnm) = [e_b^{-1}G_bQ\overline{J}^{(n)}](f_0lnm) \ . \tag{5.23}$$

The operator $e_b^{-1}G_bQ$ depends on k_0 through the energy denominators; so we transform $\overline{J}^{(n)}$ from m to k_0 before operating with $e_b^{-1}G_bQ$. A derivation similar to that of Eq. (5.22) gives

$$K(f_0lnm) = \sum_i Y(m,i)k_{0i}^{-l_0-1}\tfrac{1}{2}\sum_{l'n'}(nl\,|\,e_b^{-1}(k_{0i})G_b^{j_0S_0T_0}(k_{0i})Q_b\,|\,n'l')\sum_{m'}\overline{J}^{(n)}(f_0l'n'm')k_{0i}^{l_0+m'} . \tag{5.24}$$

Finally, we must evaluate the energy D_n^{GR} of the nth term in the generalized ring series. From Sec. V A we have

$$D_n^{\mathrm{GR}} = \sum_{f_0}\nu(f_0)\hat{j}_0\hat{T}_0(k_F^3/24) \times\langle k_0^{-2}(k_0f_0\,|\,G_bQ\overline{J}^{(n)}\,|\,k_0f_0)\rangle_2 \ . \tag{5.25}$$

Assuming $\overline{J}^{(n)}(f_0lnm)$ to be known, we calculate the matrix element in Eq. (5.25) from

$$(k_0f_0\,|\,G_bQ\overline{J}^{(n)}\,|\,k_0f_0) = \tfrac{1}{2}\sum_{lnm}(k_0l_0\,|\,G_b^{j_0S_0T_0}Q_b\,|\,nl)\overline{J}^{(n)}(f_0lnm)k_0^{l_0+m} \ . \tag{5.26}$$

E. Third order bubble diagram

Equations (5.12) and (5.19) give formulas for D_3^c and $\mathscr{M}$ in terms of $\mathscr{O}$ and $\overline{C}$, respectively. The bubble contribution $D_3^c(B)$ of Fig. 1(a) to D_3^c is obtained by replacing $\mathscr{O}$ by $\mathscr{O}_B$ in Eq. (5.12), where $\mathscr{O}_B$ is defined by Eq. (2.50). The bubble contribution to $\mathscr{M}$ is obtained from Eq. (5.19) by using the 1 from $1+X$ and by replacing $\overline{C}$ by $\overline{C}_0$, defined in Eq. (2.49). It turns out that these methods are numerically inefficient for calculating the contribution of the bubble diagram to either D_3^c or $\mathscr{M}$. In this subsection we derive a formula that is more efficient for calculating the bubble contribution to $\mathscr{M}$. The corresponding contribution to D_3^c can then be obtained as the first term in the generalized ring series. A simpler calculation of $D_3^c(B)$, using the ideas given below but not calculating $\mathscr{M}$, is feasible but has not been implemented numerically.

The contribution of the bubble diagram to $\mathscr{M}$ is obtained from Fig. 7 and from a similar diagram where the p_3 bubble is inserted into the line k_1. The effect of the bubble interaction is simply to multiply $(k_1k_2\,|\,\overline{S}_2^{(2)}\,|\,p_1p_2)$ by

$$-e_b^{-1}\sum_{p_3}[(k_1p_3\,|\,G_a\,|\,k_1p_3)+(k_2p_3\,|\,G_a\,|\,k_2p_3)] \ , \tag{5.27}$$

where we use the two-body states defined by Eq. (2.7). Consider the second term of this expression. Eliminating the volume Ω, introducing spin and isospin, and applying Eq. (5.3) to G_a gives for this term

$$-e_b^{-1}U(k_2,\delta E) \ , \tag{5.28}$$

where

$$U(k_2,\delta E) = \tfrac{1}{4}\sum_f\nu(f)\hat{j}\,\hat{T} \times\int d\vec{p}_3(k'l\,|\,G_a(f,P',\gamma^2)\,|\,k'l)/(4\pi k'^2) \ , \tag{5.29}$$

and

$$k' = \tfrac{1}{2}|\vec{k}_2-\vec{p}_3| \ , \tag{5.30}$$

$$P' = |\vec{k}_2+\vec{p}_3| \ , \tag{5.31}$$

$$\gamma^2 = \tfrac{1}{4}P^2 - E(p_3) + \delta E \ , \tag{5.32}$$

$$\delta E = E(k_1) - E(p_1) - E(p_2) \ . \tag{5.33}$$

In the calculation of $G_a(f,P',\gamma^2)$ the energy denom-

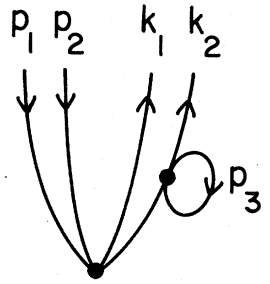

FIG. 7. Diagram showing the bubble contribution $\mathscr{M}_B$ to the matrix $\mathscr{M}$, as discussed in the text.

inator of an intermediate state of relative momentum k is $k^2+\gamma^2$.

In our approximation scheme for the generalized ring series we have $\bar{S}_2=\bar{S}_2(f_0lkk_0)$, where

$$k=\tfrac{1}{2}|\vec{k}_1-\vec{k}_2| \ , \tag{5.34}$$

$$k_0=\tfrac{1}{2}|\vec{p}_1-\vec{p}_2| \ . \tag{5.35}$$

Therefore, before multiplying $\bar{S}_2$ by $U(k_2,\delta E)$, we must take an average of $U(k_2,\delta E)$ over $\vec{k}_1,\vec{k}_2,\vec{p}_1,\vec{p}_2$, subject to the constraints of Eqs. (5.34), (5.35), and to momentum conservation,

$$\vec{k}_1+\vec{k}_2=\vec{p}_1+\vec{p}_2 \ . \tag{5.36}$$

This average can be written

$$\bar{U}(k,k_0)=\int_{k_i>k_F} d\vec{k}_1 d\vec{k}_2 d\vec{p}_1 d\vec{p}_2 \delta(k-\tfrac{1}{2}|\vec{k}_1-\vec{k}_2|)\delta(k_0-\tfrac{1}{2}|\vec{p}_1-\vec{p}_2|)\delta(\vec{k}_1+\vec{k}_2-\vec{p}_1-\vec{p}_2)U(k_2,\delta E)$$
$$\times\left[\int_{k_i>k_F} d\vec{k}_1 d\vec{k}_2 d\vec{p}_1 d\vec{p}_2 \delta(k-\tfrac{1}{2}|\vec{k}_1-\vec{k}_2|)\right.$$
$$\left.\times\,\delta(k_0-\tfrac{1}{2}|\vec{p}_1-\vec{p}_2|)\delta(\vec{k}_1+\vec{k}^2-\vec{p}_1\vec{p}_2)\right]^{-1} \ . \tag{5.37}$$

Equation (5.37) is evaluated by transforming to the variables $\vec{P},\vec{k},\vec{k}_0$ defined by

$$\vec{P}=\vec{k}_1+\vec{k}_2=\vec{p}_1+\vec{p}_2 \ , \tag{5.38}$$

$$\vec{k}=\tfrac{1}{2}(\vec{k}_1-\vec{k}_2) \ , \tag{5.39}$$

$$\vec{k}_0=\tfrac{1}{2}(\vec{p}_1-\vec{p}_2) \ . \tag{5.40}$$

Using Eqs. (5.33), (5.38)–(5.40), and (4.10), we find

$$k_1=(\tfrac{1}{4}P^2+k^2+kPz)^{1/2} \ , \tag{5.41}$$

$$k_2=(\tfrac{1}{4}P^2+k^2-kPz)^{1/2} \ , \tag{5.42}$$

$$\delta E=\tfrac{1}{2}k_1^2-(k_0^2+\tfrac{1}{4}P^2)/m^*+2E_0 \ , \tag{5.43}$$

where

$$z=\hat{P}\cdot\hat{k} \ . \tag{5.44}$$

Therefore, $U(k_2,\delta E)$ depends on k,k_0,P,z, and Eq. (5.37) can be reduced to integrals over P and z. The result is

$$\bar{U}(k,k_0)=\int w(k_0,P)dP\int_{-1}^{1}dz\,\theta(k_1-k_F)\theta(k_2-k_F)U(k_2,\delta E)$$
$$\times\left[\int w(k_0,P)dP\int_{-1}^{1}dz\,\theta(k_1-k_F)\theta(k_2-k_F)\right]^{-1} \ , \tag{5.45}$$

where

$$w(k_0,P)=P^2, \text{ if } 0<P<2(k_F-k_0)$$
$$=(P/k_0)(k_F^2-k_0^2-\tfrac{1}{4}P^2), \text{ if } 2(k_F-k_0)<P<2(k_F^2-k_0^2)^{1/2}$$
$$=0, \text{ if } P>2(k_F^2-k_0^2)^{1/2} \ . \tag{5.46}$$

The first term of Eq. (5.27) gives an identical contribution. Therefore, denoting the bubble contribution to $\mathcal{M}$ by $\mathcal{M}_B$, we have

$$(\mathcal{M}_B\bar{S}_2)(f_0lkk_0)=-[2\bar{U}(k,k_0)/e_b(k,k_0)](kl\,|\,\bar{S}_2(f_0)\,|\,k_0l_0) \ . \tag{5.47}$$

Transforming to the (f_0lmn) representation, we find

$$(f_0lnm\,|\,\mathcal{M}_B\,|\,f_0'l'n'm')=\delta(f_0,f_0')\delta(l,l')\sum_i Y(m,i)k_{0i}^{m'-1}\int dk p_n(k)[-2\bar{U}(k,k_{0i})/e_b(k,k_{0i})]p_{n'}(k) \ . \tag{5.48}$$

In numerical work we evaluate $\bar{U}(k,k_0)$ from Eq. (5.45) and substitute the result into Eq. (5.48) to obtain $\mathscr{M}_B$.

F. Calculation of G_aD

Both $\mathscr{O}$ and $\bar{C}$ involve the operator G_aD, where D is determined by Eq. (2.43). To calculate G_aD we use the basis $|dKkl,\mathscr{J}\mathscr{J}_z\mathscr{P}\mathscr{T}\mathscr{T}_z)$ of Eq. (3.33). We suppress the conserved quantum numbers $\mathscr{J}\mathscr{J}_z\mathscr{P}\mathscr{T}\mathscr{T}_z$ and use the notation of Eqs. (3.49)–(3.51). We can then write Eq. (3.48), within a given $\mathscr{J}\mathscr{P}\mathscr{T}$ manifold, in the form

$$G_a = \sum_\alpha |\alpha)\lambda_\alpha(\alpha| \quad . \tag{5.49}$$

Applying $(\alpha|$ to Eq. (2.43) and using Eq. (5.49) gives

$$(\alpha|D = (\alpha| - \sum_{\alpha'} (\alpha|XQ_a/e_a|\alpha')\lambda_{\alpha'}(\alpha'|D \quad , \tag{5.50}$$

whose solution is

$$\lambda_\alpha(\alpha|D = \sum_{\alpha'} N^{-1}(\alpha,\alpha')(\alpha'| \quad , \tag{5.51}$$

where

$$N(\alpha,\alpha') = \lambda_\alpha^{-1}\delta(\alpha,\alpha') + (\alpha|XQ_a/e_a|\alpha') \quad . \tag{5.52}$$

From Eqs. (5.49)–(5.51) we find

$$G_aD = \sum_{\alpha\alpha'} |\alpha)N^{-1}(\alpha,\alpha')(\alpha'| \quad , \tag{5.53}$$

which is the desired solution for G_aD.

In practice the number of states α that can be treated in this way is limited by the requirement that the matrix $N(\alpha,\alpha')$ not become unmanageably large. Additional states α can be approximately included by first-order perturbation theory. Let G_a and D be calculated from the unperturbed set of α that are treated exactly. Let α_1 label the states to be treated by perturbation theory, so that

$$\delta G_a = \sum_{\alpha_1} |\alpha_1)\lambda_{\alpha_1}(\alpha_1| \quad . \tag{5.54}$$

The perturbation corrections $\delta\mathscr{O}$ and $\Delta\bar{C}$ from Eqs. (2.81) and (2.83), respectively, both contain the operator

$$D^\dagger\delta G_aD = \sum_{\alpha_1} D^\dagger|\alpha_1)\lambda_{\alpha_1}(\alpha_1|D \quad . \tag{5.55}$$

To evaluate Eq. (5.55) we substitute Eq. (5.49) for G_a into Eq. (2.43) for D and apply $(\alpha_1|$ from the left to get

$$(\alpha_1|D = (\alpha_1| - \sum_\alpha N(\alpha_1,\alpha)\lambda_\alpha(\alpha|D \quad , \tag{5.56}$$

where the sum includes only the unperturbed α. Since $N(\alpha_1,\alpha)$ and λ_α are real, the Hermitian conjugate of this equation is

$$D^\dagger|\alpha_1) = |\alpha_1) - \sum_\alpha N(\alpha_1,\alpha)\lambda_\alpha D^\dagger|\alpha). \tag{5.57}$$

We now put Eq. (5.51) and its Hermitian conjugate into Eqs. (5.56) and (5.57), respectively. These equations are then put into Eq. (5.55), which in turn is used in Eqs. (2.81) and (2.83) for $\delta\mathscr{O}$ and $\Delta\bar{C}$, respectively.

So our procedure for calculating G_aD is as follows. The most important states α are treated exactly by constructing $N(\alpha,\alpha')$ from Eq. (5.52), inverting it, and using Eq. (5.53). A set of less important states α_1 is then included by first-order perturbation theory.

G. Calculation of $\mathscr{O}$

For the $\mathscr{O}$-type calculation of D_3^c from Eq. (5.12), we need diagonal matrix elements of $\mathscr{O}$ in the $|d_0K_0k_0l_0)$ representation. Consider first the contributions $\mathscr{O}_B$ and $\mathscr{O}_R$ from the bubble and ring diagrams of Figs. 1(a) and 2(a), respectively. For a given set of conserved quantum numbers $\mathscr{J}\mathscr{P}\mathscr{T}$, which we suppress, we use Eqs. (2.50), (2.51), and (5.49) to get

$$(d_0K_0k_0l_0|\mathscr{O}_B|d_0K_0k_0l_0) = \sum_\alpha F_0^{\rm dir}(\alpha)\lambda_\alpha F_0^{\rm dir}(\alpha) \quad , \tag{5.58}$$

$$(d_0K_0k_0l_0|\mathscr{O}_R|d_0K_0k_0l_0) = \sum_\alpha F_0^{\rm dir}(\alpha)\lambda_\alpha F_0^{\rm ex}(\alpha) \quad , \tag{5.59}$$

where

$$F_0^{\rm dir}(\alpha) = (\alpha|X(Q_b/e_b)G_b|d_0K_0k_0l_0) \quad , \tag{5.60}$$

$$F_0^{\rm ex}(\alpha) = (\alpha|X(Q_b/e_b)G_bX|d_0K_0k_0l_0) \quad . \tag{5.61}$$

For ease of writing we suppress the dependence of $F_0^{\rm dir}$ and $F_0^{\rm ex}$ on $(d_0K_0k_0l_0)$. The lowest-order contribution to D_3^c is the sum of Eqs. (5.58) and (5.59). The higher-order contribution comes from

$$(d_0K_0k_0l_0\,|\,\mathcal{O}_H\,|\,d_0K_0k_0l_0) = (d_0K_0k_0l_0\,|\,\mathcal{O}-\mathcal{O}_B-\mathcal{O}_R\,|\,d_0K_0k_0l_0)\ . \tag{5.62}$$

To calculate $\mathcal{O}$, we put Eq. (5.49) for G_a into Eq. (2.44) to get

$$(d_0K_0k_0l_0\,|\,\mathcal{O}\,|\,d_0K_0k_0l_0)=\sum_\alpha F_0^{\rm dir}(\alpha)F(\alpha), \tag{5.63}$$

where

$$F(\alpha)=\lambda_\alpha(\alpha\,|\,DX(Q_b/e_b)G_b(1+X)\,|\,d_0K_0k_0l_0)\ . \tag{5.64}$$

Putting Eq. (5.50) into Eq. (5.64), we find that $F(\alpha)$ satisfies the linear equation

$$\lambda_\alpha^{-1}F(\alpha)=F_0^{\rm dir}(\alpha)+F_0^{\rm ex}(\alpha)-\sum_{\alpha'}(\alpha\,|\,XQ_a/e_a\,|\,\alpha')F(\alpha')\ , \tag{5.65}$$

which can also be written

$$\sum_{\alpha'}N(\alpha,\alpha')F(\alpha')=F_0^{\rm dir}(\alpha)+F_0^{\rm ex}(\alpha)\ ,$$

where $N(\alpha,\alpha')$ is defined by Eq. (5.52).

The states α included in the matrix $N(\alpha,\alpha')$ are called unperturbed states. First-order perturbation theory can be used to treat an additional set of states α_1. For reasons given below, perturbation theory is used only for the higher-order contribution $\delta\mathcal{O}_H=\delta\mathcal{O}-\delta\mathcal{O}_B-\delta\mathcal{O}_R$. Using Eq. (2.81) for $\delta\mathcal{O}$ gives

$$\begin{aligned}(d_0K_0k_0l_0\,|\,\delta\mathcal{O}_H\,|\,d_0K_0k_0l_0)&=\sum_{\alpha_1}(d_0K_0k_0l_0\,|\,G_b(Q_b/e_b)XD^\dagger\,|\,\alpha_1)\\&\quad\times\lambda_{\alpha_1}(\alpha_1|\,DX(Q_b/e_b)G_b(1+X)\,|\,d_0K_0k_0l_0)\\&\quad-\sum_{\alpha_1}F_0^{\rm dir}(\alpha_1)\lambda_{\alpha_1}[F_0^{\rm dir}(\alpha_1)+F_0^{\rm ex}(\alpha_1)]\ .\end{aligned} \tag{5.67}$$

Using Eqs. (5.56) and (5.51), we find the matrix element in Eq. (5.67) to be

$$\begin{aligned}(\alpha_1\,|\,DX(Q_b/e_b)G_b(1+X)\,|\,d_0K_0k_0l_0)&=F_0^{\rm dir}(\alpha_1)+F_0^{\rm ex}(\alpha_1)\\&\quad-\sum_{\alpha\alpha'}N(\alpha_1,\alpha)N^{-1}(\alpha,\alpha')[F_0^{\rm dir}(\alpha')+F_0^{\rm ex}(\alpha')]\ ,\end{aligned} \tag{5.68}$$

where α,α' are summed over the unperturbed states. A similar result holds for the other matrix element on the right of Eq. (5.67). Thus it is sufficient to calculate the inverse matrix $N^{-1}(\alpha,\alpha')$ only in the unperturbed space in order to calculate the first-order perturbation correction.

The above procedure is straightforward, but some modifications are necessary in practical calculations. In practice the steps to be followed are:

(1) The ring contribution is calculated using Eq. (5.59). Since no matrix inversion is involved, one can include as many states α as required for the desired numerical accuracy.

(2) The bubble contribution to D_3^c is calculated as described in Sec. V E, not from Eq. (5.58). However, Eq. (5.58) must still be evaluated because it is subtracted from $\mathcal{O}$ to get $\mathcal{O}_H$ in Eq. (5.62).

(3) A set of unperturbed α is chosen, Eq. (5.65) is solved for $F(\alpha)$, and the result is used in Eqs. (5.63) and (5.62) to get the unperturbed contribution to $\mathcal{O}_H$.

(4) A set of perturbation states α_1 is chosen, and Eqs. (5.67) and (5.68) are used to calculate the first-order correction $\delta\mathcal{O}_H$, which is added to the unperturbed contribution from step 3.

We have not implemented the perturbation calculation of $\delta\mathcal{O}_H$ in $\mathcal{O}$-type calculations. The corresponding calculation of $\Delta\overline{C}$ *has* been implemented, however, in $\mathcal{M}$-type calculations, and this is described in the next subsection.

H. Calculation of $\overline{C}$

Equation (5.19) for $\mathcal{M}$ requires matrix elements of $\overline{C}$ in the (d_0K_0nl) representation (we suppress the conserved quantum numbers $\mathcal{J}\mathcal{P}\mathcal{T}$). The lowest-order contribution $\overline{C}_0$ is defined by Eq. (2.49). Putting Eq. (5.49) into this equation gives

$$\begin{aligned}(d_0K_0nl\,|\,\overline{C}_0\,|\,d_0'K_0'n'l')&=\sum_\alpha(d_0K_0nl\,|\,(1/\overline{e}_b)X\,|\,\alpha)\\&\quad\times\lambda_\alpha(\alpha\,|\,XQ_b\,|\,d_0'K_0'n'l')\ .\end{aligned} \tag{5.69}$$

To get the higher-order contribution $\overline{C}_H=\overline{C}-\overline{C}_0$, we put Eq. (5.53) into Eq. (2.47) and subtract $\overline{C}_0$ to get

$$\begin{aligned}(d_0K_0nl\,|\,\overline{C}_H\,|\,d_0'K_0'n'l')&=\sum_{\alpha\alpha'}(d_0K_0nl\,|\,(1/\overline{e}_b)X\,|\,\alpha)\\&\quad\times[N^{-1}(\alpha,\alpha')-\lambda_\alpha\delta(\alpha,\alpha')]\\&\quad\times(\alpha'\,|\,XQ_b\,|\,d_0'K_0'n'l')\ .\end{aligned} \tag{5.70}$$

Equation (5.70) is used for the contribution to $\overline{C}_H$ from unperturbed states α. The first-order correction $\Delta\overline{C}_H$ from perturbation states α_1 is found from Eqs. (2.83) and (5.54) to be

$$(d_0K_0nl\,|\,\Delta\bar{C}_H\,|\,d_0'K_0'n'l')=\sum_{\alpha_1}(d_0K_0nl\,|\,(1/\bar{e}_b)XD^\dagger\,|\,\alpha_1)\lambda_{\alpha_1}(\alpha_1\,|\,DXQ_b\,|\,d_0'K_0'n'l')$$
$$-\sum_{\alpha_1}(d_0K_0nl\,|\,(1/\bar{e}_b)X\,|\,\alpha_1)\lambda_{\alpha_1}(\alpha_1\,|\,XQ_b\,|\,d_0'K_0'n'l')\ . \tag{5.71}$$

From Eqs. (5.56) and (5.51) we find

$$(\alpha_1\,|\,DXQ_b\,|\,d_0'K_0'n'l')$$
$$=(\alpha_1\,|\,XQ_b\,|\,d_0'K_0'n'l')$$
$$-\sum_{\alpha\alpha'}N(\alpha_1,\alpha)N^{-1}(\alpha,\alpha')(\alpha'\,|\,XQ_b\,|\,d_0'K_0'n'l'), \tag{5.72}$$

where α,α' are summed over the unperturbed states. Equation (5.72) gives one of the required matrix elements of Eq. (5.71). The other one is

$$(d_0K_0nl\,|\,(1/\bar{e}_b)XD^\dagger\,|\,\alpha_1)=(\alpha_1\,|\,DX/\bar{e}_b\,|\,d_0K_0nl) \tag{5.73}$$

and is obtained from Eq. (5.72) with Q_b replaced by $(1/\bar{e}_b)$.

We can now summarize the procedure used in practical calculations of $\bar{C}$ and $\mathscr{M}$:

(1) Equation (5.69) for $\bar{C}_0$ is evaluated, using as many states α as required for the desired numerical accuracy.

(2) The result for $\bar{C}_0$ is put into Eq. (5.19), and only the X is used from $1+X$ in this equation. This gives the lowest-order ring contribution $\mathscr{M}_R$ to $\mathscr{M}$.

(3) The bubble contribution $\mathscr{M}_B$ is calculated as described in Sec. V E.

(4) A set of unperturbed states α is chosen and Eq. (5.70) for $\bar{C}_H$ is evaluated.

(5) The perturbation correction $\Delta\bar{C}_H$ is calculated from Eq. (5.71) and is added to $\bar{C}_H$. The sum is put into Eq. (5.19) to get $\mathscr{M}_H$.

I. Symmetrization of kernel

The lowest-order (bubble and ring) contributions to either $\mathscr{O}$ or $\bar{C}$ are obtained by putting the operator D of Eq. (2.42) equal to its leading term, $D=1$. Higher-order contributions come from the higher-order terms in D, the term of nth order being

$$(-)^n[X(Q/e_a)G_a]^n\ . \tag{5.74}$$

This is the origin of the matrix $(\alpha\,|\,XQ_a/e_a\,|\,\alpha')$ that appears in Eqs. (5.52), (5.53), (5.65), and (5.70). We now show that D_3^c and the $\mathscr{M}$ matrix are unaffected if XQ_a/e_a is replaced by $(Q_a/e_a)X$ in this matrix.

Note first that in formulas for $\mathscr{O}$ and $Q\bar{C}$ the operator D occurs only between three-body states with particle 3 above the Fermi sea. This follows from Eqs. (2.44) and (2.47). Hence it is sufficient to restrict our attention to Q_3DQ_3, where the projection operator Q_3 requires particle 3 to be above the Fermi sea. Using the Hermitian conjugate of Eq. (2.77), it is easy to show that

$$Q_3[X(Q/e_a)G_a]^nQ_3=Q_3[(Q/e_a)XG_a]^nQ_3\ . \tag{5.75}$$

This means that in the nth term of Q_3DQ_3 we can replace $X(Q/e_a)$ by $(Q/e_a)X$, and, correspondingly, we can make the same replacement in Eqs. (5.52) and (5.65) without affecting either $\mathscr{O}$ or $\mathscr{M}$.

From the relation

$$(\alpha\,|\,(Q/e_a)X\,|\,\alpha')=(\alpha'\,|\,XQ/e_a\,|\,\alpha) \tag{5.76}$$

one sees that replacing $X(Q/e_a)$ by $(Q/e_a)X$ in the matrix of Eq. (5.52) is equivalent to replacing that matrix by its transpose. In calculations using an angle-average approximation for Q_a, this change is found to give a nonzero but very small change in $D_3^c(H)$. (See Sec. VII E.) Symmetrizing the matrix of Eq. (5.52) is also found to change $D_3^c(H)$ only slightly. Using a symmetric matrix is convenient for numerical work because it reduces the storage needed in the computer. Therefore, in all numerical calculations we have symmetrized the matrix (5.52) before using it to calculate $\mathscr{O}_H$ or $\bar{C}_H$.

VI. NUMERICAL METHODS

In this section we give the methods we have used to evaluate the expressions of Sec. V on the computer.

A. $\mathscr{O}$-type calculations

In an $\mathscr{O}$-type calculation the formulas of Sec. V G are used to calculate diagonal matrix elements of $\mathscr{O}$, and these are put ino Eq. (5.12) to obtain D_3^c. A separate calculation is done for each set of conserved quantum numbers $\mathscr{J}\mathscr{P}\mathscr{T}$, and these in-

dependent contributions are summed in Eq. (5.12).

In Sec. V G we encounter $\sum_\alpha \equiv \sum_{d\beta} \int dK$. The integral is evaluated by using Gauss points K_i, $i = 1,2,\ldots N(K)$, on the interval $K_{\min} < K < K_{\max}$. The cutoff $K_{\max}$ must be large enough to give a good approximation to the integral over $K_{\min} < K < \infty$, and $K_{\max} = 8$ fm^{-1} is found to be adequate. Standard values of mesh parameters, cutoff momenta, etc., are given in Table I. The lower limit $K_{\min}$ is taken to be

$$K_{\min} = (k_F^2 - \mathscr{K}_0^2/9)^{1/2} \ , \tag{6.1}$$

where $\mathscr{K}_0$ is the fixed, average value of total three-body momentum; see Eq. (4.6). The choice (6.1) is somewhat arbitrary and is discussed in Ref. 17. It must be checked that D_3^c is insensitive to reasonable changes in $K_{\min}$.

Let us now consider the evaluation of $F_0^{\rm dir}(d\beta K)$ from Eq. (5.60), where we replace α by the more explicit notation $d\beta K$ of Eqs. (3.49)–(3.51). In Eq. (5.60) we insert the completeness relation (3.37) on both sides of X and use Eq. (3.47) to get

$$F_0^{\rm dir}(d\beta K) = \tfrac{1}{4} \sum_{ll'} \int dk\, dk' g_{\beta l'}^{jST}(k',K)(dKk'l' \,|\, X \,|\, d_0 K_0 k l) \times Q(P_b,k)(kl \,|\, e_b{}^{-1} G_b^{j_0 S_0 T_0} \,|\, k_0 l_0) \ . \tag{6.2}$$

We use Eq. (4.67) for the matrix element of X, and we use the delta function in this formula to integrate over k'. The limits on $\int dk$ are then determined by Eq. (4.65), except that (1) we require $k < k_{\max}$, where the cutoff $k_{\max} = 8$ fm^{-1} has been found adequate, and (2) the factor $Q(P_b,k)$ vanishes for k less than $(k_F^2 - P_b^2/4)^{1/2}$, see Eq. (4.3). Thus Eq. (6.2) becomes

$$F_0^{\rm dir}(d\beta K) = \sum_{ll'} \int_{L_0}^{U_0} k'^{-1} dk g_{\beta l'}^{jST}(k',K) Q(P_b,k)(kl \,|\, e_b{}^{-1} G_b^{j_0 S_0 T_0} \,|\, k_0 l_0) \times \sum_{\mathscr{L}\mathscr{S}} \mathscr{R}(\mathscr{S},SS_0)\mathscr{R}(\mathscr{T},TT_0) \begin{Bmatrix} L & \frac{1}{2} & J \\ l' & S & j \\ \mathscr{L} & \mathscr{S} & \mathscr{J} \end{Bmatrix} \begin{Bmatrix} L_0 & \frac{1}{2} & J_0 \\ l & S_0 & j_0 \\ \mathscr{L} & \mathscr{S} & \mathscr{J} \end{Bmatrix} \times \hat{\mathscr{L}}\hat{\mathscr{S}}[\hat{J}\hat{j}\hat{J}_0\hat{j}_0]^{1/2}(KLk'l' \,|\, f(\mathscr{L}) \,|\, K_0 L_0 k l) \ , \tag{6.3}$$

where

$$k' = (\tfrac{3}{4}K_0^2 + k^2 - \tfrac{3}{4}K^2)^{1/2} \ , \tag{6.4}$$

$$U_0 = \min\{ k_{\max}, K + \tfrac{1}{2}K_0 \} \ , \tag{6.5}$$

$$L_0 = \max\{ (k_F^2 - \tfrac{1}{4}P_b^2)^{1/2}, |K - \tfrac{1}{2}K_0| \} \ . \tag{6.6}$$

The integral over k in Eq. (6.3) is evaluated by changing variables from k to y, where

$$k^2 = K^2 + KK_0 y + \tfrac{1}{4}K_0^2 \ . \tag{6.7}$$

We use $N(k)$ Gauss points in the variable y, where $N(k) = 6$ has been found to be adequate. We have found it unnecessary to make any special provision for the discontinuous derivative in $Q(P_b,k)$ at $k = k_F + \frac{1}{2}P_b$.

Equation (6.3) is evaluated at the $N(K)$ Gauss points K_i, at $N(K_0)$ mesh points K_{0i} on the interval $[0,4k_F/3]$, and at $N(k_0)$ mesh points k_{0i} on the in-

TABLE I. Standard values of parameters used in numerical calculations, as discussed in the text.

Parameter	Value
$N(K)$	8
$K_{\max}$	8 fm^{-1}
$N(k)$	6
$k_{\max}$	8 fm^{-1}
$N(K_0)$	3
$N_{\rm ex}(K_0)$	6
$N(k_0)$	3
$n_{\max}$	8
l_0	0,1,2
L_0	$l_0 + L_0 \le 2$
$K_{\min}$	$(k_F^2 - \mathscr{K}_0^2/9)^{1/2}$
P_b	$(\frac{6}{5})^{1/2}k_F$
$\mathscr{K}_0$	$(\frac{9}{5})^{1/2}k_F$
$\bar{\omega}_3$	$9k_F^2/10m^* - 3E_0$

terval $[0,k_F]$. For each pair of mesh points (K_i,K_{0j}) we have a separate set of $N(k)$ mesh points k, each with a corresponding value of k' from Eq. (6.4). Using the standard values of Table I, we then find

$$N(K)N(K_0)N(k) = 8 \times 3 \times 6 = 144$$

distinct sets (K,K_0,k,k'). We refer to each set as a grid point, so that 144 grid points are used in evaluating Eq. (6.3) when the standard parameters of Table I are used.

The form factors $g_{\beta l'}^{jST}(k',K)$ are calculated beforehand, as described in Sec. IV C, and stored in an array with rows corresponding to grid points and with one column for each distinct set of variables $(jSTl'\beta)$. Matrix elements of $e_b^{-1}G_b$ are treated similarly, with columns labeled by $(l_0S_0j_0T_0l'k_0)$. To treat matrix elements of $f(\mathscr{L})$ in Eq. (6.3), we use Eqs. (4.57)–(4.60) and note that each grid point determines values of $\cos\theta_1$, $\cos\theta_2$, and $\cos\theta_3$. Arrays of Y_{lm} for these arguments are calculated and stored, and these are used to evaluate matrix elements of $f(\mathscr{L})$ from Eq. (4.57) as needed. The result for $F_0^{\rm dir}$ is a two-dimensional array with rows labeled by $(d\beta K)$ and columns labeled by $(d_0K_0k_0l_0)$. The size of this array depends on $\mathscr{J}\mathscr{P}\mathscr{T}$ and is typically about 300×100.

To evaluate $F_0^{\rm ex}(\alpha)$ we start with Eq. (5.61) and insert the completeness relation (3.37) between G_b and X. We then encounter an integration of type 2 [see Eq. (4.66)], and the final result is

$$F_0^{\rm ex}(d\beta K) = 2\sum_{d_0'l_0'}\int_{L_{\rm ex}}^{U_{\rm ex}} k_0'^{-1}dK_0'F_0^{\rm dir}(d\beta K,d_0'K_0'k_0'l_0')$$
$$\times \sum_{\mathscr{L}\mathscr{S}} \mathscr{R}(\mathscr{S},S_0'S_0)\mathscr{R}(\mathscr{T},T_0'T_0)\hat{\mathscr{L}}\hat{\mathscr{S}}[\hat{J}_0'\hat{j}_0'\hat{J}_0\hat{j}_0]^{1/2}$$
$$\times \begin{Bmatrix} L_0' & \frac{1}{2} & J_0' \\ l_0' & S_0' & j_0' \\ \mathscr{L} & \mathscr{S} & \mathscr{J} \end{Bmatrix} \begin{Bmatrix} L_0 & \frac{1}{2} & J_0 \\ l_0 & S_0 & j_0 \\ \mathscr{L} & \mathscr{S} & \mathscr{J} \end{Bmatrix} (K_0'L_0'k_0'l_0' \,|f(\mathscr{L})|\, K_0L_0k_0l_0) \ , \qquad (6.8)$$

where

$$k_0' = (\tfrac{3}{4}K_0^2 + k_0^2 - \tfrac{3}{4}K_0'^2)^{1/2} \ , \qquad (6.9)$$

$$L_{\rm ex} = |\tfrac{1}{2}K_0 - k_0| \ , \qquad (6.10)$$

$$U_{\rm ex} = \tfrac{1}{2}K_0 + k_0 \ . \qquad (6.11)$$

In Eq. (6.8) we have indicated that $F_0^{\rm dir}$ is calculated with initial state $|d_0'K_0'k_0'l_0')$ which differs from the initial state $|d_0K_0k_0l_0)$ of $F_0^{\rm ex}$.

The integral over K_0' in Eq. (6.8) is evaluated by transforming to the variable y defined by

$$K_0'^2 = \tfrac{1}{4}K_0^2 + K_0k_0y + k_0^2 \ . \qquad (6.12)$$

Then Gauss integration in y is used with $N_{\rm ex}(K_0)$ Gauss points, where $N_{\rm ex}(K_0) = 6$ is the standard value. A grid point in Eq. (6.8) is defined by each distinct set (K_0,k_0,K_0',k_0'). The total number of grid points is

$$N(K_0)N(k_0)N_{\rm ex}(K_0) = 3 \times 3 \times 6 = 54$$

when the standard parameters of Table I are used. Values of $F_0^{\rm dir}$ are available from evaluating Eq. (6.3) on the grid points (K_{0i},k_{0j}), $i = 1,2,\ldots N(K_0)$, $j = 1,2,\ldots N(k_0)$. To obtain $F_0^{\rm dir}$ at the points (K_0',k_0') required in Eq. (6.8), we use the interpolation formula

$$F_0^{\rm dir}(d\beta K,d_0'K_0'k_0'l_0') \cong \sum_{m=1}^{N(K_0)}\sum_{n=1}^{N(k_0)} B(m,n)K_0'^m k_0'^n \ , \qquad (6.13)$$

where the coefficients $B(m,n)$ are chosen so that Eq. (6.13) is exact on the grid points (K_{0i},k_{0j}). A different set of $B(m,n)$ is required for each distinct set of the variables $(d\beta Kd_0'l_0')$. The leading term in Eq. (6.13) has been chosen to be linear in K_0' and k_0' because the initial state $|d_0'K_0'k_0'l_0')$ has this property for $L_0' = l_0' = 0$. The array $F_0^{\rm ex}(d\beta K,d_0K_0k_0l_0)$ has the same size as $F_0^{\rm dir}$.

We next evaluate $(\alpha\,|XQ_a/e_a\,|\,\alpha')$, which appears in the Eq. (5.65) that determines $F(\alpha)$. We insert the completeness relation (3.37) on either side of X and then use Eq. (3.47). Using Eq. (4.67) for X, we find an integral of type 1 [see Eq. (4.65)], and the final result is

$$(d'\beta'K'\,|\,XQ_a/e_a\,|\,d\beta K) = \sum_{ll'} \int_L^U k'^{-1} dk\, g^{j'S'T'}_{\beta' l'}(k',K') g^{jST}_{\beta l}(k,K)[Q_a(K,k)/e_a(K,k)]$$

$$\times \sum_{\mathscr{L}\mathscr{S}} \mathscr{R}(\mathscr{S},S'S)\mathscr{R}(\mathscr{T},T'T)\hat{\mathscr{L}}\hat{\mathscr{S}}[\hat{J}'\hat{j}'\hat{J}\hat{j}]^{1/2} \begin{Bmatrix} L' & \frac{1}{2} & J' \\ l' & S' & j' \\ \mathscr{L} & \mathscr{S} & \mathscr{J} \end{Bmatrix} \begin{Bmatrix} L & \frac{1}{2} & J \\ l & S & J \\ \mathscr{L} & \mathscr{S} & \mathscr{J} \end{Bmatrix}$$

$$\times (K'L'k'l'\,|\,f(\mathscr{L})\,|\,KLkl) \ , \tag{6.14}$$

where

$$k' = (\tfrac{3}{4}K^2 + k^2 - \tfrac{3}{4}K'^2)^{1/2} \ , \tag{6.15}$$

$$L = \max\{\,(k_F^2 - \tfrac{1}{4}P_a^2)^{1/2}, |K' - \tfrac{1}{2}K\,|\,\}, \quad \text{if } P_a < 2k_F$$

$$= |K' - \tfrac{1}{2}K\,|, \text{ if } P_a > 2k_F \tag{6.16}$$

$$U = \min\{\,k_{\max}, K' + \tfrac{1}{2}K\,\} \ , \tag{6.17}$$

and $Q_a(K,k)$, $e_a(K,k)$, and P_a are defined by Eqs. (4.4), (4.13), and (4.5), respectively. The lower limit L is determined as follows. For $P_a > 2k_F$, $Q_a(K,k) = Q(P_a,k)$ does not vanish for any value of k, and L is determined from Eq. (4.65). For $P_a < 2k_F$, $Q_a(K,k)$ vanishes for $k < k_F^2 - \frac{1}{4}P_a^2)^{1/2}$, and this fact is used in Eq. (6.16).

Equation (6.14) is evaluated in essentially the same way as Eq. (6.3). The integration is done using $N(k)$ Gauss points in the variable y defined by

$$k^2 = K'^2 + KK'y + \tfrac{1}{4}K^2 \ . \tag{6.18}$$

The form factors and matrix elements of $f(\mathscr{L})$ are handled in the same way as for Eq. (6.3). The number of grid points $(K'Kk'k)$ is

$$N(K)N(K)N(k) = 8 \times 8 \times 6 = 384$$

when the standard parameters of Table I are used. Equation (6.14) is a square matrix whose dimension $N(d\beta K)$ is typically in the range 200 to 400.

Having calculated $F_0^{\rm dir}$, $F_0^{\rm ex}$, and $(\alpha\,|\,XQ_a/e_a\,|\,\alpha')$, we put these quantities into Eq. (5.65) and solve for $F(\alpha)$. For each set $(d_0K_0k_0l_0)$, Eq. (5.65) is a set of $N(d\beta K)$ linear equations which are solved numerically. Having $F(\alpha)$ we can use the equations of Sec. V G to calculate diagonal matrix elements of $\mathscr{O}$ in the $(d_0K_0k_0l_0)$ representation (we have not carried out the perturbation calculation described in Sec. V G).

The diagonal matrix elements of $\mathscr{O}_H, \mathscr{O}_B, \mathscr{O}_R$ are now put into Eq. (5.12) for D_3^c, which involves an average over three-body states in the Fermi sea. Since we use a fixed value $\mathscr{K} = \mathscr{K}_0$, the only remaining dependence on $\vec{p}_1, \vec{p}_2, \vec{p}_3$ in Eq. (5.12) is through (K_0,k_0). Matrix elements of $\mathscr{O}$ are calculated on the grid points (K_{0i},k_{0j}) $i = 1,2\ldots N(K_0)$, $j = 1,2\ldots N(k_0)$. We make the approximation

$$K_0^{-2}k_0^{-2}(d_0K_0k_0l_0\,|\,\mathscr{O}(\mathscr{J}\mathscr{P}\mathscr{T})\,|\,d_0K_0k_0l_0)$$

$$\simeq \sum_{m=1}^{N(K_0)N(k_0)} \sum_{n=1} A(m,n) K_0^{m-1} k_0^{n-1} \ , \tag{6.19}$$

where $\mathscr{O}$ can be any of $\mathscr{O}_H, \mathscr{O}_B, \mathscr{O}_R$, and the coefficients $A(m,n)$ are chosen so that Eq. (6.19) is exact on the grid points (K_{0i},k_{0j}). The three-body average of each term is then calculated analytically (see Table III of Ref. 17). The grid points K_{0i} and k_{0j} have been chosen to be Gauss points on the intervals $(0,4k_F/3)$ and $(0,k_F)$, respectively.

B. $\mathscr{M}$-type calculation

$\mathscr{M}$-type calculations are done in the (f_0lnm) representation, which depends on the choice of the orthornormal expansion functions $p_n(k)$. These functions are defined on the interval $k_{\min} < k < k_{\max}$, where

$$k_{\min} = (k_F^2 - \tfrac{1}{4}P_b^2)^{1/2} \ . \tag{6.20}$$

The cutoff $k_{\max}$ must be chosen large enough that contributions from $k_{\max} < k < \infty$ are negligible, and $k_{\max} = 8$ fm^{-1} has been found adequate. Expression (6.20) for $k_{\min}$ is the point where $Q(k,P_b)$ vanishes. The main quantity of interest is $S_2 = Q_b\overline{S}_2$, which is nonzero only for $k > k_{\min}$.

We have taken the $p_n(k)$ to be orthonormal polynomials

$$p_n(k) = N_n P_{n-1}[-1 + 2(k - k_{\min})/(k_{\max} - k_{\min})], \quad n \geq 1 \tag{6.21}$$

where P_n is a Legendre polynomial and N_n is

chosen so that

$$\int_{k_{\min}}^{k_{\max}} p_n^2(k)dk = 1 \ . \tag{6.22}$$

All expansions are truncated after $n_{\max}$ functions $p_n(k)$, where $n_{\max} = 8$ has been found adequate. The method permits much greater flexibility than this. For example, we could use different values of $n_{\max}$ for different two-body channels (f_0,l). We could even use different expansion functions $p_n(k)$ for different (f_0,l). However, we have not explored either of these possibilities, nor have we tried a choice of $p_n(k)$ different from Eq. (6.21).

The formulas in Sec. V H for $\overline{C}$ involve the matrix elements $(d\beta K \mid XQ_b \mid d_0K_0nl)$ and $(d\beta K \mid X/\overline{e}_b \mid d_0K_0nl)$. To evaluate the former, we insert the completeness relation (3.37) to the left of X and use Eq. (3.47). Inserting Eq. (4.67) for matrix elements of X, we find an integral of type 1, see Eq. (4.65). The result is

$$(d\beta K \mid XQ_b \mid d_0K_0nl) = 2\sum_{l'} \int_{L_0}^{U_0} k'^{-1}dk g_{\beta l'}^{jST}(k',K)Q(P_b,k)p_n(k)$$
$$\times \sum_{\mathscr{L}\mathscr{S}} \mathscr{R}(\mathscr{S},SS_0)\mathscr{R}(\mathscr{T},TT_0)\hat{\mathscr{L}}\hat{\mathscr{S}}[\hat{J}\hat{j}\hat{J}_0\hat{j}_0]^{1/2} \begin{Bmatrix} L & \frac{1}{2} & J \\ l' & S & j \\ \mathscr{L} & \mathscr{S} & \mathscr{J} \end{Bmatrix} \begin{Bmatrix} L_0 & \frac{1}{2} & J_0 \\ l & S_0 & j_0 \\ \mathscr{L} & \mathscr{S} & \mathscr{J} \end{Bmatrix}$$
$$\times (KLk'l' \mid f(\mathscr{L}) \mid K_0L_0kl) \ , \tag{6.23}$$

where the matrix element of $f(\mathscr{L})$ is given by Eq. (4.57). The momentum k' and the limits of integration U_0,L_0 are given by Eqs. (6.4)–(6.6). The numerical evaluation of Eq. (6.23) is done in exactly the same way as that of Eq. (6.3) for F_0^{dir}. We obtain $(d\beta K \mid X/\overline{e}_b \mid d_0K_0nl)$ in the same way except that in Eq. (6.23) $Q(P_b,k)$ is replaced by $(k^2+\overline{\gamma}_b^2)^{-1}$, where $\overline{\gamma}_b^2$ is given by Eq. (4.22). These results along with Eq. (6.14) for $(d\beta K \mid XQ_a/e_a \mid d'\beta'K')$ are sufficient to evaluate the formulas for $\overline{C}$ given in Sec. V H.

Once the matrix elements of $\overline{C}$ have been calculated, we can evaluate $\mathscr{M}$ starting with Eq. (5.19). It is useful to rewrite Eq. (5.19) as

$$(f_0lnm \mid \mathscr{M} \mid f_0'l'n'm') = \sum_i k_{0i}^{-l_0-1}Y(m,i)\sum_{n''}(n \mid \overline{e}_b/e_b(k_{0i}) \mid n'')(f_0nl''k_{0i} \mid \overline{\mathscr{M}} \mid f_0'l'n'm') \ , \tag{6.24}$$

which defines $\overline{\mathscr{M}}$. We then write $\overline{\mathscr{M}} = \overline{\mathscr{M}}^{\text{dir}} + \overline{\mathscr{M}}^{\text{ex}}$, where $\overline{\mathscr{M}}^{\text{dir}}$ is calculated using the 1 from the term $1+X$ in Eq. (5.19) and $\mathscr{M}^{\text{ex}}$ uses the X. We obtain

$$(f_0lnk_{0i} \mid \overline{\mathscr{M}}^{\text{dir}} \mid f_0'l'n'm') = -\tfrac{1}{2}\nu(f_0)\nu(f_0')\delta(f_0,f_0') \sum_{\mathscr{J}\mathscr{T}L_0J_0} \hat{\mathscr{J}}\hat{\mathscr{T}}[\hat{j}_0\hat{T}_0]^{-1}(4\pi)^{-1}$$
$$\times \int d\vec{p}_3 K_0^{-2}(d_0K_0nl \mid \overline{C}(\mathscr{J}\mathscr{P}\mathscr{T}) \mid d_0K_0n'l')k_{oi}^{l_o+m'} \ . \tag{6.25}$$

To evaluate $\overline{\mathscr{M}}^{\text{ex}}$, we put Eq. (4.67) into Eq. (5.19) and note that we have an integral of type 2, see Eq. (4.66). The result is

$$(f_0lnk_{0i} \mid \overline{\mathscr{M}}^{\text{ex}} \mid f_0'l'n'm')$$
$$= -\nu(f_0)\nu(f_0') \sum_{\mathscr{J}\mathscr{T}L_0J_0L_0'J_0'} \hat{\mathscr{J}}\hat{\mathscr{T}}(\hat{j}_0\hat{T}_0)^{-1}(4\pi)^{-1}\int d\vec{p}_3 K_0^{-2}$$
$$\times \int_{L_{\text{ex}}}^{U_{\text{ex}}} k_o'^{-1}dK_o'(d_0K_0nl \mid \overline{C}(\mathscr{J}\mathscr{P}\mathscr{T}) \mid d_0'K_0'n'l')k_0'^{l_0'+m'}$$
$$\times \sum_{\mathscr{L}\mathscr{S}} \mathscr{R}(\mathscr{S},S_0'S_0)\mathscr{R}(\mathscr{T},T_0'T_0)\hat{\mathscr{L}}\hat{\mathscr{S}}[\hat{J}_0'\hat{j}_0'\hat{J}_0\hat{j}_0]^{1/2} \begin{Bmatrix} L_0' & \frac{1}{2} & J_0' \\ l_0' & S_0' & j_0' \\ \mathscr{L} & \mathscr{S} & \mathscr{J} \end{Bmatrix} \begin{Bmatrix} L_0 & \frac{1}{2} & J_0 \\ l_0 & S_0 & j_0 \\ \mathscr{L} & \mathscr{S} & \mathscr{J} \end{Bmatrix}$$
$$\times (K_0'L_0'k_0'l_0' \mid f(\mathscr{L}) \mid K_0L_0k_{0i}l_0) \ , \tag{6.26}$$

where L_{ex}, U_{ex}, and k_0' are given by Eqs. (6.9)–(6.11). Except for the integral over $\vec{p}_3$, the numerical evaluation of Eq. (6.26) is similar to that of Eq. (6.8) for F_0^{ex}. Matrix elements of $\bar{C}$ are needed at the mesh points K_{0i}' used in the integration. They are obtained by interpolation from values calculated at the $N(K_0)$ mesh points K_{0i}. The interpolation formula is

$$(d_0K_0nl\,|\,\bar{C}(\mathscr{J}\mathscr{P}\mathscr{T})\,|\,d_0'K_0'n'l') \simeq \sum_{k=1}^{N(K_0)} A(k)K_0'^{L_0'+k} \quad , \tag{6.27}$$

where the coefficients $A(k)$ are determined so that Eq. (6.27) is exact whenever K_0' coincides with one of the mesh points K_{0i}. A different set of coefficients is calculated for each distinct set of quantum numbers $(d_0K_0nl\,d_0'\,n'l'\mathscr{J}\mathscr{P}\mathscr{T})$. The mesh points K_{0i} are chosen for convenience in carrying out $\int d\vec{p}_3$ in Eq. (6.26) as described below.

We now turn to the integral over $\vec{p}_3$ that occurs in Eqs. (6.25) and (6.26). The integrand depends on $\vec{p}_3$ through K_0 and $\mathscr{K}$, which are defined by

$$\vec{K}_0 = \tfrac{1}{3}\vec{P} - \tfrac{2}{3}\vec{p}_3 \quad , \tag{6.28}$$

$$\vec{\mathscr{K}} = \vec{P} + \vec{p}_3 \quad , \tag{6.29}$$

where $\vec{P} = \vec{p}_1 + \vec{p}_2$. In our approximate treatment we use a fixed, average value of $\mathscr{K}$, so the integrand depends on K_0 but not on $\mathscr{K}$. Thus the integral $I(P)$ to be evaluated has the form

$$I(P) = \int d\vec{p}_3 f(K_0) \quad , \tag{6.30}$$

where $f(K_0)$ can be read off from either Eq. (6.25) or (6.26).

One approach now is to change variables from $\vec{p}_3$ to $\vec{K}_0$ and perform the angular integrations analytically. The result is

$$I(P) = \int v(K_0,P)f(K_0)dK_0 \quad , \tag{6.31}$$

where

$$\begin{aligned} v(K_0,P) &= 27\pi K_0^2/2, \quad 0 < K_0 < \tfrac{2}{3}k_F - \tfrac{1}{3}P \\ &= (9\pi/8)K_0(-9K_0^2/P + 6K_0 \\ &\quad + 4k_F^2/P - P) \quad , \\ &\qquad \tfrac{2}{3}k_F - \tfrac{1}{3}P < K_0 < \tfrac{2}{3}k_F + \tfrac{1}{3}P \\ &= 0, \quad \text{otherwise} \quad . \end{aligned} \tag{6.32}$$

We can choose a reasonable average value of P and evaluate expression (6.31) numerically. The procedure we have actually used is somewhat different. Instead of evaluating Eq. (6.31) for an average value of P, we have averaged the entire integral over P, i.e., we make the replacement $I(P) \to \bar{I}$, where

$$\bar{I} = \int d\vec{p}_1 d\vec{p}_2 I(P = |\vec{p}_1 + \vec{p}_2|) \Big/ \int d\vec{p}_1 d\vec{p}_2 \quad . \tag{6.33}$$

Putting Eq. (6.30) into Eq. (6.33) and using Eq. (6.28) gives

$$\bar{I} = \int w(K_0)f(K_0)dK_0 \quad , \tag{6.34}$$

where

$$w(K_0) = \int d\vec{p}_1 d\vec{p}_2 d\vec{p}_3 \delta(K_0 - |\tfrac{1}{3}(\vec{p}_1 + \vec{p}_2) - \tfrac{2}{3}\vec{p}_3|) \Big/ \int d\vec{p}_1 d\vec{p}_2 \quad . \tag{6.35}$$

Formula (6.35) can be evaluated analytically to give

$$w(K_0) = (81\pi k_F^2/2) \sum_{n=1}^{8} A_n x^n \quad , \tag{6.36}$$

where

$$x = K_0/k_F \quad . \tag{6.37}$$

The coefficients A_n are different in the two cases $0 < x < \frac{2}{3}$ and $\frac{2}{3} < x < \frac{4}{3}$. They are given in Table II.

To evaluate the integral of Eq. (6.34), we use the methods of Ref. 26 to find Gauss points K_{0i} and corresponding Gauss weights appropriate to the weight function $w(K_0)$. Thus the integrand of Eq. (6.25) or (6.26) is evaluated at $N(K_0)$ Gauss points K_{0i}, where $N(K_0) = 3$ is usually used.

TABLE II. The coefficients A_n to be used in Eq. (6.36) are given as rational fractions. Column (a) is used for $0 < x < \frac{2}{3}$ and column (b) for $\frac{2}{3} < x < \frac{4}{3}$. The A_n are zero for other values of x.

n	(a)	(b)
1	0	$-\frac{16}{35}$
2	$\frac{1}{3}$	$\frac{8}{3}$
3	0	$-\frac{18}{5}$
4	0	0
5	$-\frac{27}{16}$	$\frac{45}{16}$
6	$\frac{243}{160}$	$-\frac{243}{160}$
7	0	0
8	$-\frac{243}{2240}$	$\frac{243}{2240}$

Now we turn to the numerical evaluation of $\mathcal{M}_B$, using the formulas of Sec. V E. The interval of integration in Eq. (5.48) is divided into the two intervals

$$(k_F^2 - \tfrac{1}{4}P_b^2)^{1/2} < k < k_F + \tfrac{1}{2}P_b \ , \quad (6.38)$$

$$k_F + \tfrac{1}{2}P_b < k < k_{\max} \ , \quad (6.39)$$

with 8 and 16 Gauss points being used, respectively, on these two intervals. Thus, for each discrete value k_{0i}, Eq. (5.45) for $\bar{U}(k,k_{0i})$ must be evaluated for 24 mesh points k. This is done using Gauss integration, choosing subintervals in z and P with due regard to discontinuities in the θ functions and in the derivative with respect to P of Eq. (5.46) for $w(k_0,P)$.

The values of $U(k_2,\delta E)$ needed in Eq. (5.45) are obtained by interpolation from a previously computed table. The table of $U(k_2,\delta E)$ is calculated for seven equally spaced values of δE and for k_2 on the grid

$$k_2 - k_F = 0(0.5)4(1.0)k_{\max} \ , \quad (6.40)$$

where all numerical values are in fm^{-1}. Interpolation is done as follows. For each value of δE in the table, cubic spline interpolation is done in k_2. The resulting seven values of U are then interpolated in δE by fitting them with a sixth-order polynomial.

The table of values $U(k_2,\delta E)$ is calculated using Eq. (5.29). The integral over $\vec{p}_3$ reduces to a two-dimensional integral over $|\vec{p}_3|$ and $\cos\theta(\vec{p}_3,\vec{k}_2)$. Two Gauss points are used in $|\vec{p}_3|$ and three in $\cos\theta(\vec{p}_3,\vec{k}_2)$.

The sum over two-body channels $f = (lsjT)$ in Eq. (5.29) is carried out as follows. For each channel with $l \leq 3$ the reaction matrix G_a is explicitly calculated. All channels with $l \geq 4$ are included using the approximation $G_a \approx v$. In this approximation it is possible to sum analytically over all channels using the formulas

$$\sum_{l=0}^{\infty} (2l+1)j_l^2(kr) = 1 \ , \quad (6.41)$$

$$\sum_{\text{even } l} (2l+1)j_l^2(kr) = \tfrac{1}{2}[1 + j_0(2kr)] \ . \quad (6.42)$$

The numerical accuracy of the procedures described above is about 0.2 MeV in $D_3^c(B)$ at $k_F = 1.8$ fm^{-1}. As k_F is decreased below 1.8 fm^{-1}, $D_3^c(B)$ gets rapidly smaller (see Table XXXIII), and we expect the numerical error in $D_3^c(B)$ to also decrease rapidly.

The numerical methods described so far are sufficient to carry out steps (1)—(5) given at the end of Sec. V H to obtain the $\mathcal{M}$ matrix. Having $\mathcal{M}$, we begin the iteration of the generalized ring series by calculating $\bar{J}^{(3)}$ from Eq. (5.18). We apply $e_b^{-1}G_bQ$ to $\bar{J}^{(3)}$ by using Eqs. (5.23) and (5.24), and we then construct $\bar{S}_2^{(3)}$ according to Eq. (2.65). The energy $D_3^{\text{GR}} = D_3^c$ is calculated from Eqs. (5.25) and (5.26), and then we start the next iteration by applying $\mathcal{M}$ to $\bar{S}_2^{(3)}$.

The two-body average over the Fermi sea in Eq. (5.25) is defined by Eq. (5.5). When the quantity $F(k_0)$ to be averaged over $\vec{p}_1,\vec{p}_2$ depends only on $k_0 = \frac{1}{2}|\vec{p}_1 - \vec{p}_2|$, as is the case in Eq. (5.25), one finds

$$\langle F(k_0)\rangle_2 = 24k_F^{-1}\int_0^{k_F} dk_0 F(k_0) \times x^2(1 - \tfrac{3}{2}x + \tfrac{1}{2}x^3) \ , \quad (6.43)$$

where $x = k_0/k_F$. The integrand of Eq. (5.25) is calculated from Eq. (5.26) at $N(k_0)$ mesh points k_{0i}, which are taken to be Gauss points on the interval $(0,k_F)$. The result is fitted to a polynomial of $N(k_0)$ terms with leading power $k_0^{2l_0}$, and the integral in Eq. (6.43) is evaluated analytically.

After carrying out several iterations, we sum the entire generalized ring series. We evaluate Eq. (5.22), insert the result in Eq. (2.70), and invert the appropriate matrix to obtain $\bar{S}_2^{\text{tot}}$. Then $\bar{J}^{\text{tot}}$ is obtained from Eq. (2.71), and $D_{\text{tot}}^{\text{GR}}$ is obtained from $\bar{J}^{\text{tot}}$ in exactly the same way that D_3^{GR} was obtained from $\bar{J}^{(3)}$.

Besides the energy, the main quantities of interest are $S_2^{(n)}(f_0lkk_0)$ and $S_2^{\text{tot}}(f_0lkk_0)$. These are obtained by transforming from $\bar{S}_2^{(n)}(f_0lnm)$ to $\bar{S}_2^{(n)}(f_0lkk_0)$, as explained in Sec. III B, and multiplying by $Q(P_b,k)$, with a similar procedure for S_2^{tot}.

VII. TEST CALCULATIONS

A. Preliminary remarks

In any numerical calculation we must truncate all partial-wave expansions and choose a set of mesh parameters. We must constrain the calculation to a manageable size but still obtain reasonable numerical accuracy, preferably better than 1 MeV per particle in the energy. In this subsection we specify a standard set of truncations and mesh parameters. This set has been used in the production calculations of Sec. VIII. In later subsections of this section we describe test calculations that show what accuracy is attained with the standard parameters and

with other choices. Our approximations have forced us to use fixed average values of $K_{\min}$, P_b, $\mathcal{K}$, and ω_3, and we also explore the sensitivity of our results to variations in these quantities. Most numerical tests have been made at $k_F = 1.8$ fm^{-1}, which corresponds to a density more than twice the empirical saturation density. Because of the factor k_F^6 in Eq. (5.12) for D_3^c, we expect numerical errors to decrease quickly as k_F is decreased below 1.8 fm^{-1}.

To define any calculation we must specify the two-body potential v, the Fermi momentum k_F, and the parameters m^* and E_0 that define the single-particle spectrum through Eq. (4.10). The potentials v_2, v_6(Reid), and full Reid are defined in the Appendix. The values of m^* and E_0 obtained from self-consistent two-body calculations are given in Table III.

Additional parameters to be specified are (1) the mesh parameters $N(K)$, $N(k)$, $N(K_0)$, $N(k_0)$, $N_{\rm ex}(K_0)$, $n_{\max}$, $K_{\max}$, $k_{\max}$; (2) the fixed average values of $K_{\min}$, P_b, $\mathcal{K}$, and ω_3; (3) the sets of quantum numbers $\{\mathcal{J}\mathcal{P}\mathcal{T}\}$, $\{d_0,l_0\}$, $\{f_0,l\}$, $\{d,\beta\}$, and $\{d_1,\beta_1\}$ to be included (the set $\{d,\beta\}$ is treated by matrix inversion and the set $\{d_1,\beta_1\}$ by first-order perturbation theory). The standard values of most parameters are given in Table I. Some of these have been discussed earlier in Secs. IV and VI, and others are discussed below.

Relative orbital angular momenta l are especially important in truncation of partial-wave expansions. The relative two-body wave function for given relative momentum k and given l is $j_l(kr)$, which goes to zero as l increases for fixed k and r. Intuitively, this means that two particles with given relative momentum can be close enough to interact only for sufficiently small l. This is the physical reason that truncating partial-wave expansions is permissible. Various l values occur at several different places in the calculations. The l value corresponding to two particles in the Fermi sea is denoted l_0. The final-state l in $(kl\,|\,S_2\,|\,k_0l_o)$ or in $(kl\,|\,e_b^{-1}G_b\,|\,k_0l_0)$ is called l. We use l' or l' (jST) to represent the minimum l value corresponding to a two-body channel jST included in G_a, so that

$$l'(jsT) = j \quad \text{(uncoupled channels)}$$
$$= j - 1 \quad \text{(tensor-coupled channels)} . \quad (7.1)$$

TABLE III. Results of self-consistent two-body calculations for various two-body potentials and Fermi momenta. The quantity $\overline{T} = 0.3\ k_F^2$ is the average kinetic energy of a particle in the Fermi sea. In the calculation of D_2, the sum over channels $l_0S_0j_0T_0$ having $l_0 \geq 3$ is done analytically, using the approximation $G \approx v$ and Eqs. (6.41) and (6.42). For v_2 at $k_F = 1.8$ fm^{-1}, later and more accurate calculations gave $m^* = 1.09$, $E_0 = 1.40$ fm^{-2}, corresponding to an average single-particle potential energy of $0.3\ k_F^2(m^{*-1} - 1) - E_0 = -61.4$ MeV, compared with -61.1 MeV obtained from the values of m^*, E_0 given in the table. Since these average potential depths are nearly equal, our use of the less accurate values given in the table will not significantly affect the three-body calculations. Similar remarks apply to v_2 at $k_F = 1.4$ and 1.6 fm^{-1}.

k_F (fm^{-1})	m^*	E_0 (fm^{-2})	D_2 (MeV)	$\overline{T} + D_2$ (MeV)	κ_2
			Potential v_2		
1.4	1.185	0.857	−19.7	4.7	0.140
1.6	1.188	1.121	−25.7	6.1	0.197
1.8	1.189	1.319	−30.5	9.8	0.270
			Potential v_6(Reid)		
1.4	0.642	2.035	−35.39	−11.01	0.149
1.6	0.596	2.537	−41.81	−9.96	0.190
1.8	0.561	2.966	−45.73	−5.42	0.246
			Potential full Reid		
1.2	0.705	1.502	−27.40	−9.48	0.121
1.4	0.637	2.019	−34.91	−10.53	0.150
1.6	0.581	2.521	−40.78	−8.93	0.192
1.8	0.539	2.938	−43.69	−3.38	0.250

The quantum numbers L, L_0 are also relative orbital angular momenta, describing the motion of particle 3 relative to the center of mass of particles 1 and 2. Three-body states are labeled by $L(L_0)$ when particle 3 is above (below) the Fermi sea. It is intuitively clear that particle 3 must not be too far away from the center of mass of 1 and 2 if we are to have three-body correlations. Thus we expect partial-wave expansions in L,L_0 to converge (however, in some cases we find the convergence to be too slow for efficient computation—see Sec. VII B).

Let us now proceed to specify the standard sets of quantum numbers. We consider first the ring (R) and higher-order (H) terms. The 10 sets $f_0 = \{l_0 S_0 j_0 T_0\}$ with $l_0 \leq 2$ are included, and for each set f_0, all values of L_0 satisfying $L_0 + l_0 \leq 2$ and $\mathscr{P} = (-)^{L_0+l_0}$ are included. For each pair $f_0 L_0$, and a given $\mathscr{J}$, all J_0 consistent with the coupling $(J_0 j_0)\mathscr{J}$ are included. The requirement $L_0 + l_0 \leq 2$ implies $\mathscr{J} \leq \frac{7}{2}$. For odd parity, $\mathscr{P} = -$, only $L_0 + l_0 = 1$ is possible, so that $\mathscr{J} \leq \frac{5}{2}$ in this case. For each combination $\mathscr{J}\mathscr{P}$, the values $\mathscr{T} = \frac{1}{2}$ and $\frac{3}{2}$ are both included. The set $\{jST\beta\}$ depends on the two-body potential and is different for the ring (R) and higher-order (H) calculations. These sets are specified in Tables IV–VI for the potentials v_2, v_6(Reid), and full Reid, respectively. The notation $3R + 9A$ means that 3 positive λ_β's and 9 negative λ_β's are included. The $1R$ form factor corresponds to the largest positive λ_β, the $2R$ to the second largest, etc. The $1A$ form factor corresponds to the largest $|\lambda_\beta|$ among the negative λ_β, the $2A$ to the second largest, etc. For a given two-body channel jST, all pairs (L,J) are included that are compatible with the values of $\mathscr{J}$,$\mathscr{P}$. Note that if $\mathscr{T} = \frac{3}{2}$ only $T = T_0 = 1$ is allowed.

For the bubble (B) term, calculated by the method of Secs. V E and VI B, all sets f_0 having $l_0 \leq 2$ are included, and all jST are included, using the appproximation $G \approx v$ for $l'(jST) \geq 4$, as

TABLE IV. Standard sets $\{jST\beta\}$ and $\{jST\beta_1\}$ used in production calculations for the potential v_2. Since v_2 is a central potential with no spin or isospin dependence, we use the same set of β or β_1 for all jST having the same value of $l'(jST)$ defined in Eq. (7.1). The notation $3R + 9A$ means that 3 positive λ_β's and 9 negative λ_β's are included.

	Ring	Higher order	
$l'(jST)$	β	β	β_1
0	$3R + 9A$	$2R + 1A$	$1A$
1	$2R + 10A$	$1R + 1A$	$1R + 1A$
2	$2R + 10A$	$1A$	$1R$
3	$1R + 11A$		$1A$

TABLE V. Standard sets $\{jST\beta\}$ and $\{jST\beta_1\}$ used in production calculations for the v_6(Reid) potential. For the higher-order contribution, the sets $\{jST\beta\}$ (treated by matrix inversion) and $\{jST\beta_1\}$ (treated by first-order perturbation theory) depend on the value of $\mathscr{J}$. The channels jST are given in spectroscopic notation.

	Ring			Higher order		
		$\mathscr{J} = \frac{1}{2}$		$\mathscr{J} = \frac{3}{2}$ or $\frac{5}{2}$		$\mathscr{J} = \frac{7}{2}$
jST	β	β	β_1	β	β_1	β
$^1S_0$	$2R + 5A$	$2R + 1A$		$1R + 1A$	$1R$	$1R + 1A$
$^3S_1$-$^3D_1$	$6R + 5A$	$4R + 2A$		$3R + 1A$	$1R + 1A$	$3R + 1A$
$^1P_1$	$6R + 2A$	$3R$		$2R$	$1R$	$2R$
$^3P_0$	$2R + 4A$	$1R + 2A$		$1R + 1A$	$1A$	$1R + 1A$
$^3P_1$	$7R$	$3R$		$2R$	$1R$	$2R$
$^3P_2$-$^3F_2$	$8R + 5A$	$2R + 2A$		$1R + 1A$	$1R + 1A$	$1R + 1A$
$^1D_2$	$1R + 4A$		$2A$		$2A$	
$^3D_2$	$5A$	$1A$	$1A$	$1A$	$1A$	$1A$
$^3D_3$-$^3G_3$	$8R + 5A$	$1R + 1A$	$1R$	$1A$	$2R$	$1A$
$^1F_3$	$5R + 2A$		$1R$		$1R$	
$^3F_3$	$8R$		$2R$		$2R$	
$^3F_4$-$^3H_4$	$5R + 7A$		$1A$		$1A$	
$^1G_4$			$1A$		$1A$	
$^3G_4$			$1A$		$1A$	
$^3G_5$-$^3I_5$			$1A$		$1A$	

TABLE VI. Standard sets $\{jST\beta\}$ and $\{jST\beta_1\}$ used in production calculations for the full Reid potential. For the higher-order contribution, the sets $\{jST\beta\}$ (treated by matrix inversion) and $\{jST\beta_1\}$ (treated by first-order perturbation theory) depend on the value of $\mathcal{J}$. The channels jST are given in spectroscopic notation.

	Ring			Higher order							
		$\mathcal{J}=\frac{1}{2}$			$\mathcal{J}=\frac{3}{2}$			$\mathcal{J}=\frac{5}{2}$			$\mathcal{J}=\frac{7}{2}$
jST	β	β	β_1		β	β_1		β	β_1		β
$^1S_0$	$2R+5A$	$2R+1A$			$1R+1A$	$1R$		$1R+1A$	$1R$		$2R+1A$
$^3S_1$-$^3D_1$	$7R+4A$	$5R+2A$			$4R+1A$	$1R+1A$		$4R+1A$	$1R+1A$		$3R+1A$
$^1P_1$	$6R+2A$	$3R$			$2R$	$1R$		$2R$	$1R$		$2R$
$^3P_0$	$3R+2A$	$2R+1A$			$1R+1A$	$1R$		$2R+1A$			$2R+1A$
$^3P_1$	$6R$	$3R$			$2R$	$1R$		$2R$	$1R$		$2R$
$^3P_2$-$^3F_2$	$8R+5A$	$2R+1A$	$2R+1A$		$1R+1A$	$3R+1A$		$1R+1A$	$3R+1A$		$1R+1A$
$^1D_2$	$2R+3A$	$1A$				$1A$			$1A$		$1A$
$^3D_2$	$6A$	$1A$	$1A$		$1A$	$1A$		$1A$	$1A$		$1A$
$^3D_3$-$^3G_3$	$8R+4A$	$1A$	$3R$			$3R+1A$			$3R+1A$		
$^1F_3$	$5R+2A$										
$^3F_3$	$6R+2A$										
$^3F_4$-$^3H_4$	$5R+5A$		$2A$			$2A$			$2A$		
$^1G_4$											
$^3G_4$			$1A$			$1A$			$1A$		
$^3G_5$-$^3I_5$			$1A$			$1A$			$1A$		

described in Sec. VI B.

The dimensions of the square matrixes $\mathcal{M}$, $\bar{C}$, $\mathcal{O}$, and N are $N(f_0lnk_0)$, $N(d_0K_0nl)$, $N(d_0l_0K_0k_0)$, and $N(d\beta K)$, respectively, where

$$N(f_0nlk_0)=n_{\max}N(k_0)N(f_0l)\ , \tag{7.2}$$

$$N(d_0K_0nl)=n_{\max}N(K_0)N(d_0l)\ , \tag{7.3}$$

$$N(d_0l_0K_0k_0)=N(K_0)N(k_0)N(d_0l_0)\ , \tag{7.4}$$

$$N(d\beta K)=N(K)N(d\beta)\ . \tag{7.5}$$

Here, $N(ab\ldots)$ means the number of distinct sets of the variables $a,b\ldots$.

To get an idea of the sizes of these matrices we consider in detail the case $\mathcal{J}\mathcal{P}\mathcal{T}=\frac{3}{2}$, $+$, $\frac{1}{2}$. Table VII shows the calculations of $N(f_0l)$, $N(d_0,l_0)$, and $N(d_0l)$. The left-hand column gives in spectroscopic notation the 10 sets f_0 having $l_0\le 2$. The spectroscopic notation specifies $l_0S_0j_0$, and T_0 is determined by the requirement that $l_0+S_0+T_0$ be odd. The second column gives the contribution to $N(f_0l)$ from each two-body channel f_0. This is 1 for uncoupled channels and 2 for tensor-coupled channels (in this example we assume a tensor force is present). The sum of all contributions is $N(f_0l)=14$. This result is independent of $\mathcal{J}\mathcal{P}\mathcal{T}$ and enters Eq. (7.2) for the dimension of $\mathcal{M}$. The third and fourth columns give the allowed values of L_0,J_0, which must satisfy $L_0+l_0\le 2$ and $(-)^{L_0+l_0}=\mathcal{P}$ and be compatible with the angular momentum coupling $[(L_0\frac{1}{2})J_0j_0]\mathcal{J}$. The contribu-

TABLE VII. Calculation of $N(f_0l)$, $N(d_0l_0)$, and $N(d_0l)$ as described in the text for $\mathcal{J}\mathcal{P}\mathcal{T}=\frac{3}{2}$, $+$, $\frac{1}{2}$.

f_0	$N(f_0l)$	L_0	J_0	$N(d_0l_0)$	$N(d_0l)$
$^1S_0$	1	2	$\frac{3}{2}$	1	1
$^3S_1$	2	0	$\frac{1}{2}$	3	6
		2	$\frac{3}{2}$		
		2	$\frac{5}{2}$		
$^1P_1$	1	1	$\frac{1}{2}$	2	2
		1	$\frac{3}{2}$		
$^3P_0$	1	1	$\frac{3}{2}$	1	1
$^3P_1$	1	1	$\frac{1}{2}$	2	2
		1	$\frac{3}{2}$		
$^3P_2$	2	1	$\frac{1}{2}$	2	4
		1	$\frac{3}{2}$		
$^1D_2$	1	0	$\frac{1}{2}$	1	1
$^3D_1$	2	0	$\frac{1}{2}$	1	0(2)
$^3D_2$	1	0	$\frac{1}{2}$	1	1
$^3D_3$	2			0	0
Total	14			14	18(20)

TABLE VIII. Calculation of $N(d\beta)$ and $N(d_1\beta_1)$ for higher-order terms using the full Reid potential, as explained in the text, for $\mathscr{J}\mathscr{P}\mathscr{T} = \frac{3}{2}, +, \frac{1}{2}$.

jST	$N(L,J)$	β	$N(d\beta)$	β_1	$N(d_1\beta_1)$
$^1S_0$	1	$1R + 1A$	2	$1R$	1
$^3S_1$-$^3D_1$	3	$4R + 1A$	15	$1R + 1A$	6
$^1P_1$	3	$2R$	6	$1R$	3
$^3P_0$	1	$1R + 1A$	2	$1R$	1
$^3P_1$	3	$2R$	6	$1R$	3
$^3P_2$-$^3F_2$	4	$1R + 1A$	8	$3R + 1A$	16
$^1D_2$	4			$1A$	4
$^3D_2$	4	$1A$	4	$1A$	4
$^3D_3$-$^3G_3$	4			$3R + 1A$	16
$^1F_3$	4				
$^3F_3$	4				
$^3F_4$-$^3H_4$	4			$2A$	8
$^1G_4$	4				
$^3G_4$	4			$1A$	4
$^3G_5$-$^3I_5$	4			$1A$	4
Total			43		70

tions from each channel to $N(d_0l_0)$ are summed to give $N(d_0l_0) = 14$, which enters Eq. (7.4) for the dimension of $\mathscr{O}$.

The sixth column of Table VII gives the contribution from each channel f_0 to $N(d_0l)$. For example, the channel $f_0 = {}^3S_1$ has 3 pairs (L_0,J_0) and 2 values of l, giving 6 combinations in all. The sets (d_0l) corresponding to $({}^3S_1,L_0 = 0,J_0 = \frac{1}{2},l)$, $({}^3D_1,L_0 = 0,J_0 = \frac{1}{2},l)$ are identical because $^3S_1$ and $^3D_1$ have the same values of $j_0S_0T_0$. Therefore, the 2 sets $\{d_0l\}$ corresponding to $f_0 = {}^3D_1$ have already been included in the row labeled $^3S_1$, and this is indicated by the entries 0(2) for $f_0 = {}^3D_1$ and 18(20) for the total of $N(d_0l)$. In the computer program to evaluate $\overline{\mathscr{M}}^{\text{ex}}$ from Eq. (6.26), there is a loop on f_0', and for each new channel f_0' all matrix elements $(d_0K_0nl \mid \overline{C} \mid d_0'K_0'n'l')$ are read from a sequential dataset on disk. It is therefore convenient to treat the two identical sets $\{d_0,l\}$ mentioned above as distinct, even though this means that some matrix elements of $\overline{C}$ are stored twice. When this procedure is used, the size of the matrix $\overline{C}$ that is stored on disk is obtained by using $N(d_0l) = 20$.

Note that we cannot make a state with $\mathscr{J} = \frac{3}{2}$ using $f_0 = {}^3D_3$ and $L_0 + l_0 \lesssim 2$. Hence rows and columns of $\mathscr{M}$ corresponding to $f_0 = {}^3D_3$ receive no contribution from terms in Eq. (5.19) having $\mathscr{J} = \frac{3}{2}$. Similarly, rows and columns of $\mathscr{M}$ corresponding to $T_0 = 0$ receive no contribution from three-body states with $\mathscr{T} = \frac{3}{2}$.

Table VIII shows the calculation of $N(d\beta)$ and $N(d_1\beta_1)$ for $\mathscr{J}\mathscr{P}\mathscr{T} = \frac{3}{2}, +, \frac{1}{2}$. The first column gives jST in spectroscopic notation. For each jST all values of L,J consistent with $\mathscr{J},\mathscr{P} = \frac{3}{2}, +$ are included. The number of L,J pairs is simply the smaller of $2j + 1$ and $2\mathscr{J} + 1$ is shown in column 2. Column 3 gives the set of unperturbed β used in the calculation of higher-order terms for the full Reid potential (see Table VI). The contribution to $N(d\beta)$ from each jST is simply the number of β times the number of pairs $N(L,J)$. The last two columns show similar results for the set of β_1 that are treated by first-order perturbation theory.

Using Eqs. (7.2)–(7.5) and the results from Tables I, VII and VIII, we find the values shown in Table IX. To construct the higher-order contribution $\mathscr{M}_H$ we must invert the matrix $(d\beta K \mid N \mid d'\beta'K')$ of dimension 344. To sum the generalized ring series we must invert the matrix of

TABLE IX. Dimensions of various matrices for a calculation of higher-order terms using the full Reid potential with $\mathscr{J}\mathscr{P}\mathscr{T} = \frac{3}{2}, +, \frac{1}{2}$, as discussed in the text.

Variables	No. of combinations
$N(d\beta K) = \dim N$	344
$N(d_1\beta_1K)$	560
$N(d_0K_0k_0l_0) = \dim\mathscr{O}$	126
$N(d_0K_0ln) = \dim\overline{C}$	480
$N(f_0lnk_0) = \dim\mathscr{M}$	336

Eq. (2.70), whose dimension is $\dim\mathscr{M} = 336$. In order to use standard matrix-inversion programs, it is necessary for these matrices to fit into the fast memory of the computer. Since we use $(d\beta K \mid N \mid d'\beta' K')$ in symmetrized form, it requires $344 \times 345 \times \frac{1}{2} \approx 59\,000$ locations, while $\mathscr{M}$ requires $336 \times 336 \approx 113\,000$ locations. Our computer has 250 000 locations of fast memory, of which 40 000 are used for program instructions. Thus both matrices fit comfortably into core. However, the matrix $\bar{C}$ requires $480 \times 480 \approx 230\,000$ locations and has to be read from disk to core in small sections. The matrix $(d_1\beta_1 K \mid N \mid d'\beta' K')$ used in perturbation theory is 560×344, which is also quite large. However, this is not troublesome because the perturbation corrections from different $d_1\beta_1$ are not coupled but are purely additive. Thus we break $(d_1\beta_1 K \mid N \mid d'\beta' K')$ into several smaller matrices, all having right-hand dimension $N(d\beta K) = 344$, with the sum of the left-hand dimensions being $N(d_1\beta_1 K) = 560$. Each of these smaller matrices can then be treated separately in a first-order perturbation calculation.

B. Qualitative discussion of convergence in $L_0, l_0, l'(jST)$

In this subsection, using a combination of accurate numerical results and rough but reasonable formulas, we try to gain some intuitive understanding of what to expect for convergence in L_0, l_0, and $l'(jST)$.

Consider first the range of l_0 to be included. A measure of the size of S_2 is given by the parameter κ defined by

$$\kappa = A^{-1} \sum_{p_1 p_2} (p_1 p_2 \mid S_2^\dagger S_2 \mid p_1 p_2) \ , \tag{7.6}$$

which can be written

$$\kappa = \sum_{f_0} \nu(f_0) \hat{j}_0 \hat{T}_0 (k_F{}^3/12) \times \langle k_0{}^{-2} (k_0 f_0 \mid S_2^\dagger S_2 \mid k_0 f_0) \rangle_2 \tag{7.7}$$

[compare Eq. (5.4)], where

$$(k_0 f_0 \mid S_2^\dagger S_2 \mid k_0 f_0) = \tfrac{1}{2} \sum_l \int dk (kl \mid S_2 (j_0 S_0 T_0) \mid k_0 l_0)^2 . \tag{7.8}$$

The two-body approximation $\kappa \approx \kappa_2$ is obtained by replacing S_2 by $-(Q/e_b)G_b$ in these formulas. The approximation $\kappa \approx \kappa_{\rm GR}$ is defined by using $S_2 \approx Q_b \bar{S}_2^{\rm tot}$, where $\bar{S}_2^{\rm tot}$ is the sum of the generalized ring given by Eq. (2.70). Contributions to κ_2 and $\kappa_{\rm GR}$ for the full Reid potential at $k_F = 1.8$ fm^{-1}, using the single-particle spectrum specified by Table III are shown in Table X as functions of (f_0, l). These results are obtained from the production calculations of Sec. VIII.

A technical point must be mentioned here. In evaluating Eq. (7.8) we use the angle-average $Q_b(k)$ from Eq. (4.8). Putting $S_2 = Q_b \bar{S}_2$ into Eq. (7.8) would give a factor $[Q_b(k)]^2$ in the integrand. However, the exact Pauli operator Q satisfies $Q^2 = Q$, so that one power of Q is sufficient. In evaluating Eq. (7.8) we have used $Q_b(k)$ rather than $[Q_b(k)]^2$ in the integrand. This gives values of κ 5–10% larger than using $[Q_b(k)]^2$.

In Table X contributions from individual (f_0, l) are also summed over all variables except l_0 to get contributions from $l_0 = 0$, 1, and 2. The convergence in l_0 is seen to be very rapid. It will be seen later that contributions to D_3^c and $D_3^{\rm GR}$ also converge very fast in l_0, so that including only $l_0 = 0,1,2$ is an excellent approximation.

The rapid convergence in l_0 of $S_2^{(2)} = -(Q/e)G$ is understood intuitively as follows. If the two-body state $(k_0 f_0)$ is denoted ϕ, we have[2]

$$G\phi = v\psi \ , \tag{7.9}$$

where the correlated two-body wave function ϕ is

TABLE X. Contribution to κ_2 and $\kappa_{\rm GR}$ for the full Reid potential at $k_F = 1.8$ fm^{-1}, as discussed in the text.

f_0, l	κ_2		$\kappa_{\rm GR}$	
$^1S_0$	0.0479		0.0553	
$^3S_1 (l=0)$	0.0660	0.2102	0.0699	0.2566
$^3S_1 (l=2)$	0.0963		0.1314	
$^1P_1$	0.0108		0.0147	
$^3P_0$	0.0082		0.0074	
$^3P_1$	0.0099	0.0359	0.0178	0.0460
$^3P_2 (l=1)$	0.0031		0.0021	
$^3P_2 (l=3)$	0.0039		0.0040	
$^1D_2$	0.0004		0.0004	
$^3D_1 (l=2)$	0.0002		0.0002	
$^3D_1 (l=0)$	0.0001	0.0042	0.0008	0.0051
$^3D_2$	0.0008		0.0017	
$^3D_3 (l=2)$	0.0000		0.0000	
$^3D_3 (l=4)$	0.0027		0.0020	
Total	0.2503		0.3077	

defined by

$$\psi = \phi - (Q/e)G\phi \ . \tag{7.10}$$

The second term in Eq. (7.10) is $S_2^{(2)}$ and represents the difference between ϕ and ψ caused by the two-body potential. The wave function ϕ contains the factor $j_{l_0}(k_0 r)$ which, for $l_0 \geq 2$ and $k_0 < k_F$, is small at small r, where the potential is strong. Thus, for $l_0 \geq 2$, the strong part of v has little opportunity to deform the wave function, and we expect $\psi \approx \phi$ so that $S_2^{(2)} = \psi - \phi$ is small.

Note that this argument does not apply to the two-hole-line contribution D_2 to the energy. If $\psi \approx \phi$, then $G \approx v$, and the matrix element appearing in D_2 is

$$(k_0 f_0 \,|\, v^{j_0 S_0 T_0} \,|\, k_0 f_0) \propto \int r^2 dr v_{l_0}^{j_0 S_0 T_0}(r) j_{l_0}{}^2(k_0 r) \ . \tag{7.11}$$

The weak, long-ranged tail of v contributes appreciably to this integral, even though it is unable to deform the wave function and give a contribution to S_2. Equation (7.11) converges in l_0, but rather slowly. We illustrate this with results for the potential v_2. Contributions to D_2 in the approximation $G \approx v$ are given in Table XI as a function of l_0 for v_2 at $k_F = 1.8$ fm^{-1}. The convergence is seen to be slow. The observed odd-even staggering comes from the statistical weight of Eq. (5.4). Summing this over $j_0 S_0 T_0$ for fixed l_0 gives

$$\sum_{j_0 S_0 T_0} \nu(f_0)\hat{j}_0\hat{T}_0 = 6(2l_0+1),\ l_0 \text{ even}$$
$$= 10(2l_0+1),\ l_0 \text{ odd} \ . \tag{7.12}$$

Since v_2 has a one-pion exchange potential (OPEP) tail at large r, we expect qualitatively similar results for more realistic nucleon-nucleon potentials, except that the contributions from individual l_0 will alternate in sign, being negative for even l_0 and positive for odd l_0. In any practical calculation the sum over l_0 must be performed analytically using Eqs. (6.41) and (6.42).

Next we study convergence in L_0. Consider first the contribution $D_3^c(B)$ of the third-order bubble diagram calculated in an $\mathcal{O}$-type calculation. For

TABLE XI. Contributions to D_2 in the approximation $G = v$ for the potential v_2 at $k_F = 1.8$ fm^{-1}.

l_0	$D_2(l_0)$ (MeV)	l_0	$D_2(l_0)$ (MeV)
0	530.50	5	−2.16
1	−18.29	6	−0.85
2	−10.35	7	−0.91
3	−6.33	8	−0.34
4	−2.01	9 to ∞	−0.80

qualitative considerations spin and isospin are unnecessary, and we omit them. We also use unsymmetrized spatial states, and to avoid writing the subscript na repeatedly, we use the notation

$$|\ldots\rangle \equiv |\ldots)_{\rm na} \ . \tag{7.13}$$

We want to investigate the convergence in L_0 of

$$\sum_{L_0 M_0} M_B \equiv \sum_{L_0 M_0} \langle K_0 L_0 M_0 \vec{k}_0 \,|\, \mathcal{O}_B' \,|\, K_0 L_0 M_0 \vec{k}_0 \rangle, \tag{7.14}$$

where

$$\mathcal{O}_B' = G_B(Q/e_b)P_{132}G_a P_{123}(Q/e_b)G_b \ . \tag{7.15}$$

Here $\mathcal{O}_B'$ differs from $\mathcal{O}_B$ of Eq. (2.50) by replacement of $X = P_{123} + P_{132}$ by either P_{123} or P_{132}. Thus Eq. (7.15) is only one of four terms whose sum is $\mathcal{O}_B$, but the arguments to be given below apply equally well to any of these four terms.

In Eq. (7.15) we insert the completeness relation (4.49) to the left of P_{132} and to the right of P_{123}. Putting the result into Eq. (7.14) and using Eq. (3.7) gives

$$M_B = \int d\vec{K}'\, d\vec{k}'\, d\vec{K}\, d\vec{k} K_0{}^{-2} \delta(K' - K_0)$$
$$\times \delta(K - K_0) Y^*_{L_0 M_0}(\hat{K}') Y_{L_0 M_0}(\hat{K})$$
$$\times \langle \vec{k}_0 \,|\, G_b Q/e_b \,|\, \vec{k}' \rangle \langle \vec{k} \,|\, (Q/e_b) G_b \,|\, \vec{k}_0 \rangle$$
$$\times \langle \vec{K}'\vec{k}' \,|\, P_{132} G_a P_{123} \,|\, \vec{K}\vec{k} \rangle \ . \tag{7.16}$$

Using Eqs. (4.51)–(4.53) for P_{123}, and noting that $P_{132} = P_{123}^\dagger$, we find

$$\langle \vec{K}'\vec{k}' \,|\, P_{132} G_a P_{123} \,|\, \vec{K}\vec{k} \rangle = \delta(\vec{k} - \tfrac{1}{2}\vec{K} + \tfrac{1}{2}\vec{K}' - \vec{k}') \langle -\tfrac{3}{4}\vec{K}' - \tfrac{1}{2}\vec{k}' \,|\, G_a \,|\, \tfrac{1}{4}\vec{K}' - \vec{K} - \tfrac{1}{2}\vec{k}' \rangle \ . \tag{7.17}$$

This is put into Eq. (7.16) to get

$$M_B = \int d\vec{K}'\, d\vec{K}\, d\vec{k}'\, K_0^{-2}\delta(K'-K_0)\delta(K-K_0) Y^*_{L_0M_0}(\hat{K}') Y_{L_0M_0}(\hat{K}) \times \langle \vec{k}_0 | G_b Q/e_b | \vec{k}' \rangle \langle \vec{k}' - \tfrac{1}{2}\vec{K}' + \tfrac{1}{2}\vec{K} | (Q/e_b) G_b | \vec{k}_0 \rangle \langle -\tfrac{3}{4}\vec{K}' - \tfrac{1}{2}\vec{k}' | G_a | \tfrac{1}{4}\vec{K}' - \vec{K} - \tfrac{1}{2}\vec{k}' \rangle . \tag{7.18}$$

Since $\langle \vec{k}' | (Q/e_b) G_b | \vec{k}_0 \rangle$ is largest in the region $k' = 3-4$ fm^{-1} (see Fig. 8), and since $\frac{1}{2}K = \frac{1}{2}K' = \frac{1}{2}K_0$ is typically only about 1 fm^{-1}, it is reasonable in Eq. (7.18) to make the replacement

$$\langle \vec{k}' - \tfrac{1}{2}\vec{K}' + \tfrac{1}{2}\vec{K} | (Q/e_b) G_b | \vec{k}_0 \rangle \rightarrow \langle \vec{k}' | (Q/e_b) G_b | \vec{k}_0 \rangle . \tag{7.19}$$

For qualitative considerations we replace G_a in Eq. (7.18) by an effective two-body potential. We consider the two cases:

(1) $G_a \rightarrow v_W(r)$ (Wigner force, acting the same in all partial waves);

(2) $G_a \rightarrow v_M(r) P^r$, where P^r is the space exchange operator (Majorana force).

The two-body matrix elements of these effective potentials are given by

$$\langle \vec{q}' | v_W | \vec{q} \rangle = (2\pi)^{-3} \int d\vec{r}\, e^{-i(\vec{q}'-\vec{q})\cdot\vec{r}} v_W(r) , \tag{7.20}$$

$$\langle \vec{q}' | v_M P^r | \vec{q} \rangle = (2\pi)^{-3} \int d\vec{r}\, e^{-i(\vec{q}'+\vec{q})\cdot\vec{r}} v_M(r) . \tag{7.21}$$

When this approximation to G_a, along with Eq. (7.19), is put into Eq. (7.18), the angular integrals over $\hat{K}'$, $\hat{K}$ can be evaluated using

$$\int Y_{L_0M_0}(\hat{K}) e^{i\vec{K}\cdot\vec{r}} d\hat{K} = i^{L_0} 4\pi j_{L_0}(Kr) Y_{L_0M_0}(\hat{r}), \tag{7.22}$$

and the final result is

$$\sum_{L_0M_0} M_B = (2\pi^2)^{-1} K_0^2 \int d\vec{k}' \, | \langle \vec{k}' | (Q/e) G_b | \vec{k}_0 \rangle |^2 \times \sum_{L_0} (2L_0+1) \int d\vec{r} \begin{cases} j_{L_0}^2(K_0 r) v_W(r) \\ (-)^{L_0} j_{L_0}(\tfrac{1}{2}K_0 r) j_{L_0}(K_0 r) v_M(r) e^{i\vec{k}'\cdot\vec{r}} \end{cases} . \tag{7.23}$$

Equation (7.23) tells us what to expect for convergence of $D_3^c(B)$ in L_0. Consider first the Wigner force. Since L_0 ranges from 0 to $4k_F/3$, the integral in Eq. (7.23) is similar to that in Eq. (7.11), and the convergence in L_0 will be similar to the convergence in l_0 shown in Table XI, i.e., quite slow. This is why we avoid expanding $D_3^c(B)$ in L_0 and, instead, use the method of Sec. V E. For the Majorana force, Eq. (7.23) looks more favorable. There is an additional oscillating function $\exp(i\vec{k}'\cdot\vec{r})$ in the integrand, and the alternating signs will give cancellation between even and odd values of L_0. However, we have made a special selection of permutation operators in obtaining $\mathcal{O}_B'$ in Eq. (7.15) from $\mathcal{O}_B$. Other choices will give terms that converge badly for a Majorana force.

We next study the third-order ring contribution $D_3^c(R)$ with respect to convergence in L_0. Thus we consider

$$M_R = \langle K_0 L_0 M_0 \vec{k}_0 | \mathcal{O}_B' P_{123} | K_0 L_0 M_0 \vec{k}_0 \rangle , \tag{7.24}$$

where we have used P_{123} from the right-hand factor $X = P_{123} + P_{132}$ in Eq. (2.51) for $\mathcal{O}_R$. Proceeding as in the treatment of Eq. (7.14), we find

$$M_R = \int d\vec{K}'\, d\vec{k}'\, d\vec{K} \frac{\delta(K'-K_0)}{K_0} \frac{\delta(K-K_0)}{K_0} Y^*_{L_0M_0}(\hat{K}') Y_{L_0M_0}(\hat{K}) \langle \vec{k}_0 | G_b Q/e | \vec{k}' \rangle \times \langle \vec{k}' - \tfrac{1}{4}\vec{K}' - \tfrac{1}{2}\vec{K} + \tfrac{1}{2}\vec{k}_0 | (Q/e) G_b | -\tfrac{3}{4}\vec{K} - \tfrac{1}{2}\vec{k}_0 \rangle \times \langle -\tfrac{3}{4}\vec{K}' - \tfrac{1}{2}\vec{k}' | G_a | \tfrac{1}{4}\vec{K}' + \tfrac{1}{2}\vec{K} - \vec{k}_0 - \tfrac{1}{2}\vec{k}' \rangle . \tag{7.25}$$

For qualitative considerations we may replace the left-hand momentum in the matrix element of $(Q/e)G_b$ by $\vec{k}'$ [compare Eq. (7.19)]. Furthermore, this matrix element is largest when the inital state $|-\frac{3}{4}\vec{K}-\frac{1}{2}\vec{k}_0\rangle$ has $l_0=0$ (see Table X). For $l_0=0$ the matrix element varies slowly with the initial momentum $-\frac{3}{4}\vec{K}-\frac{1}{2}\vec{k}_0$ (see Fig. 36 of Ref. 8), so we replace this momentum by $-\frac{1}{2}\vec{k}_0$. Treating G_a the same as in the third-order bubble contribution, we obtain

$$\sum_{L_0M_0} M_R \approx (2\pi^2)^{-1}K_0{}^2\int d\vec{k}'\langle\vec{k}_0|G_bQ/\vec{e}|k'\rangle\langle\vec{k}'|(Q/e)G_b|-\tfrac{1}{2}\vec{k}_0\rangle$$

$$\times\sum_{L_0}(2L_0+1)\int d\vec{r}\begin{cases}(-)^{L_0}j_{L_0}(K_0r)j_{L_0}(\frac{1}{2}K_0r)v_W(r)e^{-i\vec{k}_0\cdot\vec{r}}\\ j_{L_0}{}^2(\frac{1}{2}K_0r)v_M(r)e^{i(\vec{k}'+\vec{k}_0)\cdot\vec{r}}\end{cases}. \tag{7.26}$$

Consider Eq. (7.26) for the Wigner force $v_W(r)$. Since the matrix elements of G_bQ/e and $(Q/e)G_b$ vary little with $\vec{k}_0$, we can average $e^{i\vec{k}_0\cdot\vec{r}}$ over two-body states in the Fermi sea, using Eq. (5.5) with $\vec{k}_0=(\vec{p}_1-p_2)/2$. The result is

$$\langle e^{i\vec{k}_0\cdot\vec{r}}\rangle_2 = l^2(\tfrac{1}{2}k_Fr)\ , \tag{7.27}$$

where the Slater function $l(y)$ is

$$l(y)=3y^{-1}j_1(y)\ . \tag{7.28}$$

Thus, for the Wigner force, the integrand in Eq. (7.26) differs from that of Eq. (7.23) for the third-order bubble by an additional factor $l^2(\frac{1}{2}k_Fr)$, which goes to zero at large r. Now, for $L_0\geq 2$ and $K_0<4k_F/3$, the integrand of Eq. (7.23) for M_B is small at small r and has a peak around $r\sim L_0/K_0$. But at this point, $l^2(\frac{1}{2}k_Fr)$ is small so that the contribution to M_R from a given L_0 is much less than the contribution to M_B. Also, the larger L_0 is, the larger is the value of r where the integrand for M_B is maximum, and the greater is the effect in M_R of the decreasing function $l^2(\frac{1}{2}k_Fr)$. We therefore conclude that (1) for a given $L_0\geq 2$, the contribution to M_R is much less than the contribution to M_B, and (2) the rate of convergence in L_0 is faster for M_R than for M_B. Thus it may well be efficient to expand in L_0 for M_R even though it is inefficient for M_B. Similar remarks apply to the Majorana force in Eq. (7.26) and to formulas obtained using other possible choices of the permutation operators in Eqs. (7.15) and (7.24).

Next we consider convergence in the two-body channels jST included in G_a. Truncation of jST is made according to the value of $l'=l'(jST)$ defined by Eq. (7.1). In the third-order bubble diagram of Fig. 1(a) the matrix element of G_a is $(bp_3|G_a|bp_3)$. For qualitative considerations we neglect spin and isospin and replace G_a by an effective potential $v_{l'}(r)$ that may depend on l'. Then the middle matrix element in $D_3^c(B)$ is

$$\langle\vec{q}'|v|\vec{q}\rangle=(2\pi^2)^{-1}\sum_{l'}(2l'+1)\times\int r^2dr\,j_{l'}(q'r)v_{l'}(r)\times j_{l'}(qr)P_{l'}(\hat{q}'\cdot\hat{q})\ , \tag{7.29}$$

where $\vec{q}'=\vec{q}=\frac{1}{2}(\vec{b}-\vec{p}_3)$. Since $\vec{q}'=\vec{q}$, the factor $P_{l'}(\hat{q}'\cdot\hat{q})$ in Eq. (7.29) is exactly unity, and since $q=q'$ can be larger than k_F, the convergence of Eq. (7.29) in l' will be slower than the convergence of D_2 in l_0 shown in Table XI. Thus convergence of $D_3^c(B)$ in $l'(jST)$ is quite slow. In practice, as described in Sec. VI B, we do the sum analytically for $l'\geq 4$, using the approximation $G\approx v$. Summing analytically over l' does not appear to be possible in an $\mathcal{O}$-type calculation using Eq. (5.58).

The situation is different for the third-order ring contribution $D_3^c(R)$, where the middle interaction is $(bp_3|G_a|cp_2)$ [see Fig. 2(a)]. Using momentum conservation $\vec{b}+\vec{p}_3=\vec{c}+\vec{p}_2$, we see that the middle interaction has the form of Eq. (7.29) with

$$\vec{q}'=\tfrac{1}{2}\vec{b}-\tfrac{1}{2}\vec{p}_3\ , \tag{7.30}$$

$$\vec{q}=\tfrac{1}{2}\vec{b}-\vec{p}_2+\tfrac{1}{2}\vec{p}_3\ . \tag{7.31}$$

In the approximation of zero hole momenta, i.e., all $p_i=0$, we have $\vec{q}'=\vec{q}$, and convergence in l' is the same as for $D_3^c(B)$. However, the zero-hole-momenta approximation is unlikely to be very accurate for $D_3^c(R)$ for the following reason. A typical value of b is $2-4$ fm^{-1}, so that $\frac{1}{2}b$ is of the order of k_F or a little larger. Therefore, as p_2 and p_3 range over the Fermi sea, the angle between $\vec{q}'$ and $\vec{q}$ will vary over an appreciable fraction of the interval $[0,\pi]$. When l' is large, this has two consequences: (1) The rapid variation of $P_{l'}(\hat{q}'\cdot\hat{q})$ in Eq.

(7.29) will tend to damp out the integrals over $\vec{p}_2$ and $\vec{p}_3$. (2) The average value of $P_{l'}(\hat{q}'\cdot\hat{q})$ will be closer to its rms value $(2l'+1)^{-1/2}$ than to the value unity that obtains when $\vec{q}\,' = \vec{q}$. Thus we expect that summing over momenta $\vec{p}_i$ in the Fermi sea will cause the third-order ring diagram to converge much faster in l' than the third-order bubble diagram. This is borne out by numerical calculations, where ring contributions from $l' = 3$ are already very small (see Sec. VII C).

As for higher-order contributions to D_3^c, we know that these arise from regions of configuration space where *all three* particles are close together.[21] Thus we expect that both L_0 and l_0 must be small, which in turn means that $\mathscr{J}$ is small. In intermediate states, where K and k are often $3-4$ fm^{-1}, larger values of L and l' will be important, and convergence in $l'(jST)$ will be studied numerically in Sec. VII D.

In summary, we expect rapid convergence of D_3^c in l_0. We expect $D_3^c(B)$ to converge only slowly in L_0 and $l'(jST)$, and these difficulties are overcome using the method of Secs. V E and VI B. The ring contribution $D_3^c(R)$ is expected to converge much better in L_0 and $l'(jST)$. $D_3^c(H)$ should converge well in L_0 and l_0, and convergence in $l'(jST)$ must be tested numerically.

C. Numerical study of convergence in $L_0,l_0,l'(jST)$

We first consider $\mathscr{O}$-type calculations of the bubble (B) and ring (R) contributions to D_3^c. Table XII shows results for the two-body potential v_2 at $k_F = 1.8$ fm^{-1}. Since v_2 is a central potential, each jST has a unique value of l', and all contributions from a given l' are summed and shown in the table. Comparing columns A and E, we see that for $l' \geq 2$ we have $|R(l')| << |B(l')|$, where $R(l')$ and $B(l')$ are the contributions from a particular value of l' to $D_3^c(R)$ and $D_3^c(B)$, respectively. Thus column A for $l' \geq 2$ essentially shows the convergence of B in l'. It is seen to be rather slow, as expected from the arguments in the preceding subsection.

Columns B, C, and D show the additional contributions to $D_3^c(B) + D_3^c(R)$ obtained by including $(L_0,l_0) = (4,0)$, (5,0), and (6,0), respectively. For the bubble contribution it is found that including $(L_0,l_0) = (3,1)$ has only 10—20% as much effect as including (4,0). Thus the pair (L_0,l_0) having $l_0 = 0$ gives the dominant effect on the bubble of pairs (L_0,l_0) having a given value of $L_0 + l_0$. This is found *not* to be true for the ring contribution, however. Inspection of columns A, B, C, and D shows

TABLE XII. Bubble (B) and ring (R) contributions to D_3^c for the two-body potential v_2 at $k_F = 1.8$ fm^{-1}, using $\mathscr{O}$-type calculations with various sets of (L_0,l_0). The contributions from individual l' in the middle G matrix of Figs. 1(a) and 2(a) are shown. For each l' the second column shows the rank of the separable approximation to G_a. Column A gives the contribution to the sum $B + R$ including $(L_0,l_0) = (3,0)$ plus all (L_0,l_0) having $L_0 + l_0 \leq 2$. Successively including $(L_0,l_0) = (4,0)$, (5,0), and (6,0) gives the *changes* in $B + R$ shown in columns B, C, and D, respectively. Column E gives the ring contribution including all (L_0,l_0) having $L_0 + l_0 \leq 2$. Column F gives the change in the ring contribution when the additional pairs $(L_0,l_0) =$ (3,0) and (2,1) are included. All energies are in MeV, and the standard parameters are used except for (L_0,l_0) as specified above. The values of m^* and E_0 are taken from Table III. In each case all states $\mathscr{J}\mathscr{P}\mathscr{T}$ permitted by the chosen set of pairs (L_0,l_0) are included.

l'	β	A $B+R$	B $\Delta(B+R)$	C $\Delta(B+R)$	D $\Delta(B+R)$	E R	F $\Delta(R)$
0	$3R + 9A$	55.65	−0.022	−0.007		18.62	0.010
1	$2R + 10A$	−2.70	−0.122	−0.060		−1.30	−0.036
2	$2R + 10A$	−8.80	−0.109	−0.047		0.020	−0.043
3	$1R + 11A$	−8.27	−0.202	−0.094		−0.137	0.012
4	$12A$	−2.04	−0.126	−0.065		0.015	−0.002
5	$12A$	−1.49	−0.201	−0.113			
6	$12A$	−0.48	−0.109	−0.068			
7	$12A$	−0.48	−0.157	−0.105	−0.077		
8	$12A$	−0.19	−0.078	−0.062			
9	$12A$	−0.21	−0.092	−0.095			
10	$12A$	−0.08	−0.042				
Total		30.91	−1.26	−0.72		17.22	−0.059

that convergence of $D_3^c(B)$ in L_0 is rather slow, as expected. The convergence in L_0 gets worse as l' increases.

Column E shows that $D_3^c(R)$ converges in l' much faster than $D_3^c(B)$, as was made plausible in the preceding subsection. In production calculations we have calculated $D_3^c(R)$ by including only $l' \leq 3$. To estimate the error caused by this truncation, we assume, in accord with the preceding subsection, that $D_3^c(R)$ converges faster in l' than $D_3(B)$ to write

$$\frac{|R(l')|}{|R(3)|} < \frac{|B(l')|}{|B(3)|}, \quad l' > 3 \tag{7.32}$$

so that

$$\sum_{l'>3} |R(l')| < |R(3)| \sum_{l'>3} |B(l')|/|B(3)| . \tag{7.33}$$

This upper bound on the omitted terms might be unrealistically small if $R(3)$ were accidentally very close to zero. In the present case we do not expect this to happen because $|R(3)|$ is the largest of $|R(l')|$ for $l' = 2,3,4$. Thus we expect Eq. (7.33) to give a safe upper bound. From columns A, B, and C of Table XII we find $B(l' \leq 3) + R(l' \leq 3) \approx 35$ MeV, and columns E and F give $R(l' \leq 3) \approx 17$ MeV, so that $B(l' \leq 3) \approx 18$ MeV. Detailed calculations using the method of Sec. V E give $B(\text{all } l') \approx 7$ MeV, so that $B(l' > 3) \approx -11$ MeV. Using $B(l' = 3) \approx -8.5$ MeV, we find that Eq. (7.33) gives

$$\sum_{l'>3} |R(l')| < (11/8.5)|R(3)| = 1.3|R(3)| , \tag{7.34}$$

which for v_2 is 0.18 MeV at $k_F = 1.8$ fm^{-1}.

The qualitative arguments of Sec. VII B that led to Eqs. (7.32) and (7.33) are also valid for more complicated potentials than v_2. Also, contributions from $l' \geq 3$ are dominated by the long-ranged OPEP tail of the potential, which has the same strength and range for v_2, v_6(Reid), and the full Reid potential. Thus we expect Eq. (7.34) also to be valid for the v_6(Reid) and full Reid potentials.

Table XIII shows contributions to $D_3^c(R)$ from individual *jST* for the v_6(Reid) and full Reid potentials at $k_F = 1.8$ fm^{-1}. Contributions obtained by summing over *jST* for fixed $l'(jST)$ are also shown. The convergence in l' is seen to be rapid. Summing the absolute values of contributions from $l' = 3$ and multiplying by 1.3 [as suggested by Eq. (7.34)] gives 0.11 and 0.07 MeV, respectively, for the v_6(Reid) and full Reid potentials. These are our estimates of the error in $D_3^c(R)$ caused by omission of contributions with $l' > 3$. The value 0.07 MeV is entered in

TABLE XIII. Contributions to $D_3^c(R)$ for individual two-body channels *jST* included in G_a, for the v_6(Reid) and full Reid potentials at $k_F = 1.8$ fm^{-1}. The calculations are $\mathcal{O}$-type, using the standard parameters, and m^*, E_0 are taken from Table III. For each *jST* the number of β's used is sufficient for numerical accuracy of 0.01 MeV or better.

	v_6(Reid)			v = full Reid		
jST	β	$D_3^c(R)$ (MeV)		β	$D_3^c(R)$ (MeV)	
$^1S_0$	$2R + 5A$	−1.01	−7.40	$2R + 6A$	−0.54	−6.42
$^3S_1$-$^3D_1$	$6R + 5A$	−6.39		$7R + 4A$	−5.88	
$^1P_1$	$6R + 2A$	−4.56		$6R + 2A$	−4.11	
$^3P_0$	$2R + 4A$	0.07	−12.67	$3R + 2A$	−1.16	−8.21
$^3P_1$	$7R$	−5.36		$6R$	−6.04	
$^3P_2$-$^3F_2$	$8R + 5A$	−2.82		$8R + 5A$	3.10	
$^1D_2$	$1R + 4A$	0.51		$2R + 3A$	0.19	
$^3D_2$	$5A$	1.13	1.50	$8A$	0.50	0.77
$^3D_3$-$^3G_3$	$8R + 5A$	−0.14		$8R + 4A$	0.08	
$^1F_3$	$5R + 2A$	−0.01		$5R + 2A$	0.02	
$^3F_3$	$8R$	−0.01	−0.08	$6R + 2A$	0.03	0.05
$^3F_4-^3H_4$	$5R + 7A$	−0.06		$5R + 5A$	−0.004	
$^1G_4$	$5A$	0.02		$3R + 9A$	0.003	
$^3G_4$	$5A$	−0.03	0.02	$2R + 10A$	−0.025	−0.01
$^3G_5-^3I_5$	$4R + 6A$	0.03		$8R + 8A$	0.011	
Total		−18.63			−13.82	

Table XXXII, which summarizes numerical errors from various sources for the full Reid potential at $k_F = 1.8$ fm^{-1}.

The convergence of $D_3^c(R)$ with respect to L_0 needs to be tested only for $l'(jST) \leq 3$. The results in Table XIII are calculated including (L_0,l_0) having $L_0 + l_0 \leq 2$. For the v_6(Reid) potential, the calculation was repeated, including in addition the pairs $(L_0,l_0) = (3,0),(2,1),(1,2)$ (all allowed sets $\mathcal{J}\mathcal{P}\mathcal{T}$ were included in the calculation). Including these additional pairs (L_0,l_0) causes a small change in the contribution to $D_3^c(R)$ from each channel jST. The absolute values of these changes were summed for all $l'(JST) \leq 3$ and came to 0.24 MeV. This process was repeated by including the additional pairs $(L_0,l_0) = (4,0)$, (3,1), (2,2), and the sum of the absolute values of the changes in $D_3^c(R)$ for $l'(jST) \leq 3$ was 0.08. Treating 0.24 and 0.08 as the first two terms in a geometric series, one finds the sum of the series to be 0.36 MeV. Since there is considerable cancellation of the contributions among different jST, this should be a substantial overestimate of the contribution to $D_3^c(R)$ from pairs (L_0,l_0) having $L_0 + l_0 \geq 3$. We take 0.3 MeV as a rather safe estimate of the error in $D_3^c(R)$ from this source, for v_6(Reid) at $k_F = 1.8$ fm^{-1}. We assume the same estimate holds for the full Reid potential. It is entered in Table XXXII.

So far we have omitted two-body states in the Fermi sea with $l_0 = 3$. That this is a good approximation was checked in the following way for the full Reid potential at $k_F = 1.8$ fm^{-1}. First, the contribution to $D_3^c(B)$ from two-body channels $f_0 = l_0 S_0 j_0 T_0$ having $l_0 = 3$ was calculated using the method of Sec. V E. It was found to be only 0.01 MeV. To save computer time, the effect on $D_3^c(R)$ of channels with $l_0 = 3$ was calculated using a reduced set of $jST\beta$, listed as set B in Table XIV. Set B gives $D_3^c(R) = -13.77$, in good agreement with the value -13.82 MeV obtained with a full set (see Table XIII). Thus set B is adequate for checking convergence in l_0. Using set B, $D_3^c(R)$ was calculated, including all pairs (L_0,l_0) having $L_0 + l_0 \leq 3$ except for (0,3). Then the calculation was repeated, but now including the pair $(L_0,l_0) = (0,3)$, and the resulting change in $D_3^c(R)$ was found to be 0.019 MeV. [Note that the pair $(L_0,l_0) = (0,3)$ contributes to $D_3^c(R)$ only in states having $\mathcal{P} = -$ and $\frac{3}{2} \leq \mathcal{J} \leq \frac{9}{2}$. Hence only this restricted set of $\mathcal{J}\mathcal{P}$ needs to be treated to obtain the effect of including $(L_0,l_0) = (0,3)$.] A similar pair of calculations showed that including $(L_0,l_0) = (1,3)$ changes $D_3^c(R)$ by only 0.002 MeV. Thus $D_3^c(R)$ converges rapidly in l_0, and for $l_0 = 3$ we find that $L_0 = 0$ is much more important than $L_0 = 1$. The error in $D_3^c(R)$ from the truncation $l_0 \leq 2$ is 0.02 MeV and is shown in Table XXXII.

Convergence in l_0 of $D_3^c(H)$ was tested in exactly the same way as just described for $D_3^c(R)$, except that set A of $jST\beta$ was used from Table XIV. Using set A with the four $\mathcal{J}\mathcal{P}\mathcal{T}$ sets $\frac{1}{2} + \frac{1}{2}$, $\frac{1}{2} - \frac{1}{2}$, $\frac{3}{2} - \frac{1}{2}$, $\frac{5}{2} - \frac{1}{2}$, gives $D_3^c(H) = -14.11$ MeV for the full Reid potential at $k_F = 1.8$ fm^{-1}. A full set of $jST\beta$ gives -15.32 MeV for the same set of $\mathcal{J}\mathcal{P}\mathcal{T}$. The contribution from set A of $jST\beta$ has not been compared with that from a full set for other sets $\mathcal{J}\mathcal{P}\mathcal{T}$, but these other sets give very small contribution sto $D_3^c(H)$ (see Table XXXVII). We conclude that set A is adequate for checking convergence of $D_3^c(H)$ in l_0. Addition of $(L_0,l_0) = (0,3)$ and (1,3) changed $D_3^c(H)$ by -0.007 and -0.001 MeV, respectively. In each case, all allowed sets of $\mathcal{J}\mathcal{P}\mathcal{T}$ were included. Thus the truncation $l_0 \leq 2$ causes an error of order 0.01 MeV in $D_3^{c(H)}$, and this error is shown in Table XXXII.

We now study convergence in L_0 of $D_3^c(H)$, and numerical results for the v_6(Reid) potential are shown in Table XV. The results shown include only contributions from odd-parity states, $\mathcal{P} = -$. Comparison of rows B and D shows that including $l_0 = 2$ changes the reslult by only -0.014 MeV. The same result follows from rows C and E. This is consistent with the rapid convergence in l_0 that

TABLE XIV. Reduced sets of $jST\beta$ used for test calculations with the full Reid potential at $k_F = 1.8$ fm^{-1}. Set A is used for calculations of $D_3^c(H)$, usually including only $\mathcal{J}\mathcal{P}\mathcal{T} = \frac{1}{2} + \frac{1}{2}$, $\frac{1}{2} - \frac{1}{2}$, $\frac{3}{2} - \frac{1}{2}$, and $\frac{5}{2} - \frac{1}{2}$. Sets B and C are used in test calculations of $D_3^c(R)$, usually including all allowed sets $\mathcal{J}\mathcal{P}\mathcal{T}$. Further discussion is given in the text.

jST	β (set A)	β (set B)	β (set C)
$^1S_0$	$1R + 1A$	$1R + 1A$	$1R + 1A$
$^3S_1$-$^3D_1$	$1R + 1A$	$2R + 1A$	$4R + 2A$
$^1P_1$	$1R$	$2R$	$3R$
$^3P_0$	$1R$	$1R$	$2R$
$^3P_1$	$1R$	$2R$	$3R$
$^3P_2$-$^3F_2$	$1R + 1A$	$1R + 1A$	$3R + 1A$
$^1D_2$			$1A$
$^3D_2$		$1A$	$1A$
$^3D_3$-$^3G_3$			$1R + 1A$
$^1F_3$		$1R$	
$^3F_3$			$1R$
$^3F_4$-$^3H_4$			$1A$

TABLE XV. Odd parity ($\mathscr{P} = -$) contributions to $D_3^c(H)$ for the v_6(Reid) potential at $k_F = 1.8$ fm^{-1}. the calculations are $\mathscr{O}$-type, and the standard parameters of Table I are used except for $N(K_0) = 4$ and $N(k_0) = 2$. Set A of $jST\beta$ from Table XIV is used. For each set of pairs (L_0,l_0), all sets $\mathscr{J},\mathscr{T}$ satisfying $\mathscr{J} \leq \frac{3}{2} + \max(L_0 + l_0)$ are included.

Row label	$D_3^c(H)$ (MeV)	Pairs (L_0,l_0) included
A	−5.169	(1,0), (0,1)
B	−5.1924	(1,0), (3,0), (0,1), (2,1)
C	−5.1925	(1,0), (3,0), (5,0), (0,1), (2,1), (4,1)
D	−5.2064	(1,0), (3,0), (0,1), (2,1), (1,2)
E	−5.2065	(1,0), (3,0), (5,0), (0,1), (2,1), (4,1), (1,2)

was found above. We also found above that the effect of $(L_0,l_0) = (1,3)$ was much less than that of (0,3). Similarly, we expect the effect of $(L_0,l_0) = (3,2)$ to be much less than that of (1,2), and for this reason $(L_0,l_0) = (3,2)$ is omitted from Table XV.

Comparing rows A and B or A and D in Table XV, we see that increasing $(L_0 + l_0)_{\max}$ from 1 to 3 changes $D_3^c(H)$ by −0.023 MeV (if $l_0 = 2$ is ommited) or −0.037 MeV (if $l_0 = 2$ is included). Increasing $(L_0 + l_0)_{\max}$ from 3 to 5 then gives a further change of only −0.001 MeV. This is seen by comparing rows B and C or rows D and E. This is excellent convergence in $(L_0 + l_0)_{\max}$, and in all further calculations of $D_3^c(H)$ we use $(L_0 + l_0)_{\max} = 2$. For $\mathscr{P} = -$ this means we use only $(L_0,l_0) = (1,0)$ and (0,1), expecting a resulting error of order −0.04 MeV in $D_3^c(H)$. For $\mathscr{P} = +$ we expect that increasing $(L_0 + l_0)_{\max}$ from 2 to 4 will produce a much smaller change. Thus, using $(L_0 + l_0)_{\max} = 2$, we expect an error of order 0.05 MeV in $D_3^c(H)$ for the v_6(Reid) potential at $k_F = 1.8$ fm^{-1}. Since v_2 and the full Reid potential have similar strength and range to v_6(Reid), we use the same error estimate for them as well, and the error 0.05 MeV is entered in Table XXXII for the truncation $L_0 + l_0 \leq 2$.

In summary, we plan to use $(L_0 + l_0)_{\max} = 2$ in production calculations, expecting errors of order 0.3 and 0.05 MeV in $D_3^c(R)$ and $D_3^c(H)$, respectively, at $k_F = 1.8$ fm^{-1}. For $D_3^c(B)$, L_0 is irrelevant, and omitting states with $l_0 \geq 3$ gives an error of 0.01 MeV. Using only $l'(jST) \leq 3$ gives an error in $D_3^c(R)$ of order 0.07 MeV. This truncation does not arise in $D_3^c(B)$, and it is discussed for $D_3^c(H)$ in Sec. VII D, along with truncation in β.

D. Convergence of $D_3^c(H)$ in $jST\beta$

In both $\mathscr{O}$- and $\mathscr{M}$-type calculations the matrix $N(d\beta K, d'\beta' K')$ of Eq. (5.52) must be inverted, and additional states $d_1\beta_1$ may be included by first-order perturbation theory (recall the notation $d \equiv LSjST$). In this subsection we investigate the accuracy obtainable using various sets of $d\beta$, treated either by matrix inversion or first-order perturbation theory. For a given channel jST we include all LJ consistent with given values of $\mathscr{J}\mathscr{P}$. Thus specifying a set of $jST\beta$ is equuivalent to specifying the set of $d\beta = LSjST\beta$. All calculations in this subsection are done with the full Reid potential at $k_F = 1.8$ fm^{-1}, using the standard parameters of Tables I and III. As discussed in Sec. VI, the matrix $N(d\beta K, d'\beta' K')$ between unperturbed states is calculated and then symmetrized. The numerical effect of symmetrization is given in Sec. VII E.

We first give results designed to learn how much each individual component $jST\beta$ contributes to the higher-order contribution $D_3^c(H)$. We start with a basic set of $jST\beta$, taken to be set A of Table XIV, that accounts for the bulk of $D_3^c(H)$. Then we successively include additional components $jST\beta$ and observe the resulting change in $D_3^c(H)$.

In Table XVI the contributions to $D_3^c(H)$ from set A are compared to those of the much larger set of Table VI that is used in production calculations. To save computing time we consider only the four sets $\mathscr{J}\mathscr{P}\mathscr{T}$ shown in Table XVI. These four sets account for −15.32 MeV, which is over 90% of the total contribution − 16.48 MeV from all sets of $\mathscr{J}\mathscr{P}\mathscr{T}$ (see Table XXXVII). Thus these four sets of $\mathscr{J}\mathscr{P}\mathscr{T}$ are sufficient for studying convergence in $jST\beta$. For the sum of $D_3^c(H)$ over these four sets

TABLE XVI. Contributions in MeV to $D_3^c(H)$ from set A of $jST\beta$ given in Table XIV and from the full set of $jST\beta$ given in Table VI. The full Reid potential is used at $k_F = 1.8$ fm^{-1} with standard parameters. The results using set A are obtained from $\mathscr{O}$-type calculations, and those using the full set from $\mathscr{M}$-type calculations (see Table XXXVII).

$\mathscr{J}\mathscr{P}\mathscr{T}$	$D_3^c(H)$ (set A)	$D_3^c(H)$ (Full set)
$\frac{1}{2} + \frac{1}{2}$	−10.78	−11.44
$\frac{1}{2} - \frac{1}{2}$	−1.84	−2.05
$\frac{3}{2} - \frac{1}{2}$	−1.12	−1.22
$\frac{5}{2} - \frac{1}{2}$	−0.37	−0.61
Sum	−14.11	−15.32

$\mathcal{JPT}$, Table XVI shows that set A of $jST\beta$ gives more than 90% of the result from the full set of $jST\beta$. To assign contributions to $D_3^c(H)$ from individual components $jST\beta$ in set A, we put Eq. (5.63) into Eq. (5.62), then Eq. (5.62) into Eq. (5.12), and sum or integrate over all variables except $jST\beta$. The results are shown in Table XVII in the column labeled Matrix inversion.

To assign contributions to $D_3^c(H)$ from individual components $jST\beta$ not included in set A, we proceed as follows. Consider the $^3S_1 - {}^3D_1$ channel. We perform a series of $\mathcal{O}$-type calculations of $D_3^c(H)$ using the $2R + 1A$, $3R + 1A$, $4R + 1A$,... separable representation of G_a in the $^3S_1 - {}^3D_1$ channel (set A is used in all other channels). The difference in $D_3^c(H)$ between the $3R + 1A$ and $2R + 1A$ calculations is taken to be the contribution from the individual component ($^3S_1 - {}^3D_1$,$3R$), etc. Then a similar series of calculations is done, using $1R + 2A$, $1R + 3A$,... in the $^3S_1 - {}^3D_1$ channel, to get the contributions from the individual components $2A$,$3A$,... . Analogous calculations are done for the jST channels not included in set A. The resulting contributions from individual components $jST\beta$ are given in Table XVII in the column labeled Matrix inversion.

The contributions to $D_3^c(H)$ from individual components $jST\beta$ not contained in set A can also be

TABLE XVII. Contributions to $D_3^c(H)$ from individual components $jST\beta$, including the four sets $\mathcal{JPT}$ of Table XVI, as described in the text. The full Reid potential is used at $k_F = 1.8$ fm^{-1} with standard parameters. The notation $2R$(*) means, for the given jST, that $2R$ is the last repulsive component, i.e., all further λ_β are negative. In the $^3P_1$ channel all λ_β are positive. All energies are in MeV.

jST	β	Matrix inversion	First-order perturbation	jST	β	Matrix inversion	First-order perturbation
				$^3P_1$	$1R$	−0.756	
$^1S_0$	$1R$	−3.827			$2R$	0.091	0.052
	$2R$(*)	−0.042	−0.045		$3R$	0.049	0.045
	$1A$	−0.207			$4R$	0.011	
	$2A$	−0.005			$1A$		
	$3A$	−0.003		$^3P_2 - {}^3F_2$	$1R$	−0.045	
	$4A$	0.000			$2R$	−0.013	−0.013
$^3S_1 - {}^3D_1$	$1R$	−6.411			$3R$	0.041	0.041
	$2R$	−0.131	−0.197		$4R$	0.044	
	$3R$	−0.023	−0.017		$5R$	0.005	
	$4R$	−0.013	−0.036		$6R$	−0.002	
	$5R$	0.042	0.041		$1A$	−0.157	
	$6R$	0.000			$2A$	−0.053	−0.056
	$7R$	0.001			$3A$	−0.009	
	$8R$	−0.001			$4A$	0.003	
	$1A$	−0.826		$^1D_2$	$1R$	−0.010	
	$2A$	−0.064	−0.067		$2R$(*)	0.000	
	$3A$	−0.002			$1A$	−0.315	−0.337
$^1P_1$	$1R$	−0.402			$2A$	0.005	
	$2R$	0.030	0.008		$3A$	0.002	
	$3R$	0.014	0.015	$^3D_2$	$1R$(*)	0.000	
	$4R$	0.009			$1A$	−0.208	−0.261
	$1A$	0.000			$2A$	−0.044	
	$2A$	0.000			$3A$	0.001	
$^3P_0$	$1R$	−1.480		$^3D_3 - {}^3G_3$	$1R$	−0.291	−0.296
	$2R$	−0.073	−0.087		$2R$	0.054	
	$3R$	−0.004			$3R$	0.035	
	$4R$(*)	0.000			$4R$	0.005	
	$1A$	−0.083	−0.075		$1A$	−0.293	−0.329
	$2A$	−0.008			$2A$	0.016	
	$3A$	0.000			$3A$	0.000	

TABLE XVII. *(Continued).*

jST	β	Matrix inversion	First-order perturbation
$^1F_3$	$1R$	0.011	
	$1A$	0.006	
	$2A$	0.001	
$^3F_3$	$1R$	0.008	
	$2R$	−0.001	
	$1A$	0.006	
	$2A$	0.001	
$^3F_4 - {}^3H_4$	$1R$	0.001	
	$2R$	0.000	
	$3R$	−0.001	
	$4R$	−0.001	
	$1A$	−0.093	−0.098
	$2A$	−0.040	
	$3A$	−0.002	
$^1G_4$	$1R$	0.006	
	$2R$	0.003	
	$1A$	−0.002	
	$2A$	0.002	
$^3G_4$	$1R$	0.000	
	$2R(*)$	0.000	
	$1A$	−0.054	−0.54
	$2A$	0.018	
$^3G_5 - {}^3I_5$	$1R$	−0.005	
	$2R$	−0.002	
	$3R$	0.005	
	$4R$	0.003	
	$1A$	−0.025	−0.025

calculated in first-order perturbation theory, using set A as unperturbed set. The contribution from an individual $j_1 S_1 T_1 \beta_1$ is obtained by summing over $L_1 J_1$ in Eq. (5.67) for $\delta\mathcal{O}_H$ or Eq. (5.71) for $\Delta\overline{C}_H$. Since we have not implemented perturbation theory in $\mathcal{O}$-type calculations, we have used $\mathcal{M}$-type calculations to evaluate the perturbation contributions to $D_3^c(H)$. The results are shown in the last column of Table XVII.

Comparison of the matrix inversion and perturbation columns of Table XVII determines the accuracy of first-order perturbation theory starting from the unperturbed set A of $jST\beta$. One small point must be mentioned here. Consider, for example, the individual component $(^3S_1 - {}^3D_1, 3R)$. Its matrix inversion contribution is the difference between two calculations using the $3R + 1A$ and $2R + 1A$ separable representations for G_a in the $^3S_1 - {}^3D_1$ channel. But its perturbation contribution is obtained using the $1R + 1A$ representation from set A in the unperturbed calculation, rather than the $2R + 1A$ representation. To the extent that components $jST\beta$ outside set A can be treated in first-order perturbation theory, their contributions are additive and this difference is negligible. We ignore it from now on because Table XVII shows that first-order perturbation theory is reasonably accurate for most components $jST\beta$ outside set A.

The accuracy of first-order perturbation theory, starting from set A, is seen from Table XVII to be far from perfect but still good enough to be useful. For a given jST, perturbation theory is more accurate for smaller $|\lambda_\beta|$, as is intuitively reasonable. The relative accuracy of perturbation theory is also seen to increase with increasing values of the quantity $l'(jST)$ defined in Eq. (7.1). In most cases where there is a substantial difference between the matrix-inversion and perturbation results, the difference is found to come almost entirely from $\mathcal{J}\mathcal{P}\mathcal{T} = \frac{1}{2} + \frac{1}{2}$. (This cannot be seen from Table XVII.) Therefore, for several components $jST\beta$, we use matrix inversion for $\mathcal{J} = \frac{1}{2}$ and perturbation theory for other values of $\mathcal{J}$ (see Table VI). This is feasible because, for $\mathcal{J} = \frac{1}{2}$, at most two combinations of L, J are allowed for any channel jST, so that the matrix to be inverted remains small enough to fit into the fast memory of the computer.

Table XVII allows us to test convergence of $D_3^c(H)$ in $l'(jST)$, defined by Eq. (7.1). Summing all contributions from the matrix inversion column of Table XVII, for a given value of $l'(jST)$, gives the results shown in Table XVIII. The convergence in $l'(jST)$ is rapid, and we assume the contribution to $D_3^c(H)$ from $l'(jST) \geq 5$ to be no larger in magnitude than 0.05 MeV for the four sets treated in

TABLE XVIII. Contributions to $D_3^c(H)$ for various values of l' (jST) for the full Reid potential at $k_F = 1.8$ fm^{-1}, as discussed in the text. Only the four sets $\mathcal{J}\mathcal{P}\mathcal{T} = \frac{1}{2} + \frac{1}{2}, \frac{1}{2} - \frac{1}{2}, \frac{3}{2} - \frac{1}{2}, \frac{5}{2} - \frac{1}{2}$ are included.

$l'(jST)$	Channels included	$D_3^c(H)$ (MeV)
0	$^1S_0, {}^3S_1 - {}^3D_1$	−11.512
1	$^1P_1, {}^3P_0, {}^3P_1, {}^3P_2 - {}^3F_2$	−2.788
2	$^1D_2, {}^3D_2, {}^3D_3 - {}^3G_3$	−1.043
3	$^1F_3, {}^3F_3, {}^3F_4 - {}^3H_4$	−0.104
4	$^1G_4, {}^3G_4, {}^3G_5 - {}^3I_5$	−0.051

TABLE XIX. Estimated errors in $D_3^c(H)$ from using sets $(jST\beta)$ and $(jST\beta)_1$ from Table VI for the full Reid potential at $k_F = 1.8$ fm^{-1}. The errors are in MeV, and further discussion is given in the text.

			$\mathcal{J}\mathcal{P}\mathcal{T} = \frac{1}{2}+\frac{1}{2}$		$\mathcal{J}\mathcal{P}\mathcal{T} = \frac{3}{2}-\frac{1}{2}$		$\mathcal{J}\mathcal{P}\mathcal{T} = \frac{5}{2}-\frac{1}{2}$	
jST	β	Error(1)	β_1	Error(2)	β_1	Error(2)	β_1	Error(2)
$^1S_0$	$2R + 1A$	0.008			$2R$	0.000	$2R$	0.001
$^3S_1 - {}^3D_1$	$5R + 2A$	0.007			$5R, 2A$	0.005	$5R, 2A$	0.002
$^1P_1$	$3R$	0.018			$3R$	0.002	$3R$	0.001
$^3P_0$	$2R + 1A$	0.012			$2R$	0.001		
$^3P_1$	$3R$	0.022			$3R$	0.001	$3R$	0.001
$^3P_2 - {}^3F_2$	$4R + 2A$	0.024	$3R, 4R, 2A$	0.009	$2R - 4R, 2A$	0.000	$2R - 4R, 2A$	0.001
$^1D_2$	$1A$	0.019			$1A$	0.000	$1A$	0.001
$^3D_2$	$2A$	0.002	$2A$	0.032	$2A$	0.007	$2A$	0.012
$^3D_3 - {}^3G_3$	$3R + 1A$	0.026	$1R - 3R$	0.006	$1R - 3R, 1A$	0.021	$1R - 3R, 1A$	0.004
$^1F_3$		0.030						
$^3F_3$		0.018						
$^3F_4 - {}^3H_4$	$2A$	0.008	$1A, 2A$	0.004	$1A, 2A$	0.004	$1A, 2A$	0.002
$^1G_4$		0.018						
$^3G_4$	$1A$	0.036	$1A$	0.003	$1A$	0.000	$1A$	0.001
$^3G_5 - {}^3I_5$	$1A$	0.043	$1A$	0.001	$1A$	0.001	$1A$	0.000
Total		0.291		0.055		0.042		0.026

Tables XVI–XVIII. To allow for contributions from other $\mathcal{J}\mathcal{P}\mathcal{T}$, we increase this by 20%, obtaining an error of order 0.06 MeV from neglect of contributions to $D_3^c(H)$ from $l'(jST) \geq 5$.

For any choice of sets $(jST\beta)$ and $(jST\beta)_1$, to be treated by matrix inversion and perturbation theory, respectively, Table XVII allows us to estimate the resulting error in $D_3^c(H)$. There are two sources of error: (1) Certain components $jST\beta$ are left out so that their contributions are missed, and (2) the contributions obtained in first-order perturbation theory differ from the correct ones obtained using matrix inversion. These errors are shown in Table XIX, using the sets $(jST\beta)$ and $(jST\beta)_1$ taken from Table VI for the full Reid potential. The left-hand column gives the channel jST, and the next column gives the corresponding β's, including both unperturbed and perturbation β's. The column labeled Error (1) is an estimate of the error from source (1) and is obtained as follows. For a given jST, the absolute values of the contributions from all β's appearing in Table XVII but not in Table XIX are summed, using the matrix inversion column of Table XVII. Also, the total contribution from all repulsive (attractive) β's not shown in Table XVII is assumed to equal the contribution of the last repulsive (attractive) β calculated, and this is added to the sum defined in the previous sentence. The result gives an estimate of the error from source (1) in the four sets $\mathcal{J}\mathcal{P}\mathcal{T}$ included in Table XVII.

The error from source (2) is estimated in the last six columns of Table XIX. For each $\mathcal{J}\mathcal{P}\mathcal{T}$ and jST, those β that are treated in first-order perturbation theory are listed. The absolute values of the differences between the perturbation contributions and those obtained from matrix inversion are summed, and this sum is listed in the column labeled Error (2) for each $\mathcal{J}\mathcal{P}\mathcal{T}$ and jST. (These results cannot be derived from Table XVII because Table XVII does not give contributions from individual $\mathcal{J}\mathcal{P}\mathcal{T}$. In Table XIX the contributions from $\mathcal{J}\mathcal{P}\mathcal{T} = \frac{1}{2} + \frac{1}{2}$ and $\frac{1}{2} - \frac{1}{2}$ are added together before listing.)

Adding together the errors in the last row of Table XIX gives a total of 0.41 MeV. To allow for additional sets of $\mathcal{J}\mathcal{P}\mathcal{T}$ we increase this by 20% to get 0.51 MeV. This is our estimate of the error in $D_3^c(H)$ caused by using the set of unperturbed β and perturbation β listed in Table VI, for the full Reid potential at $k_F = 1.8$ fm^{-1}. In addition we have the error of 0.06 MeV from neglect of jST having $l'(jST) \geq 5$. These error estimates are entered in Table XXXII.

E. Effect of transposed and symmetrized kernel

As explained in Sec. V I, all calculations of higher-order terms have been done using a symmetrized kernel, i.e., the matrix

$$(\alpha \,|\, XQ_a/e_a \,|\, \alpha') \tag{7.35}$$

of Eq. (5.52) is symmetrized before being used to calculated $\mathcal{O}_H$ or $\bar{C}_H$. The numerical effect of this on $D_3^c(H)$ is shown in Table XX, for the full Reid potential at $k_F = 1.8$ fm^{-1}. The calculations are $\mathcal{M}$-type, using standard parameters, except that $N(k_0) = 2$, set A of $jST\beta$ from Table XIV is used, and only the four sets $\mathcal{J}\mathcal{P}\mathcal{T} = \frac{1}{2} + \frac{1}{2}, \frac{1}{2} - \frac{1}{2}, \frac{3}{2} - \frac{1}{2}, \frac{5}{2} - \frac{1}{2}$ are included. It was shown in the preceding subsection that these sets of $jST\beta$ and $\mathcal{J}\mathcal{P}\mathcal{T}$ are adequate for test calculations of $D_3^c(H)$. In Table XX the values of $D_3^c(H)$ in the columns labeled Unsymmetrized, Transposed, and Symmetrized are obtained by using Eq. (7.35), its transpose, and the average of these two, respectively, in Eq. (5.52). The total spread of 0.023 MeV among the three calculations is entered in Table XXXII. The $\mathcal{M}$-type result $D_3^c(H) = -13.93$ MeV from Table XX differs slightly from the $\mathcal{O}$-type result of -14.11 MeV in Table XVI because the two types of calculation use different methods of integrating over the Fermi sea.

F. Convergence of $D_3^c(R)$ in β

In the calculation of $D_3^c(R)$ no matrix inversion is required, so that one can include as many sets $jST\beta$ as needed for any desired numerical accuracy. Nevertheless, it is of interest to know how many β's are needed for each jST, and in this subsection we give results that help to answer this question.

The results are shown in Table XXI. They are obtained from $\mathcal{O}$-type calculations using the full Reid potential at $k_F = 1.8$ fm^{-1}. The standard parameters of Tables I and III are used. Thus we have $L_0 + l_0 \leq 2$, and all sets consistent with this

TABLE XX. Values of $D_3^c(H)$ calculated using various treatments of the kernel of Eq. (5.52), for the full Reid potential at $k^F = 1.8$ fm^{-1}. Further discussion is given in the text.

$D_3^c(H)$(MeV)		
Unsymmetrized	Transposed	Symmetrized
-13.954	-13.957	-13.934

TABLE XXI. Contributions to $D_3^c(R)$ from individual components $jST\beta$ for the full Reid potential at $k_F = 1.8$ fm^{-1}, as described in the text. The notation 3(-7) means 3×10^{-7}. All energies are in MeV.

	$^1S_0$	$^3S_1 - {}^3D_1$	$^1P_1$	$^3P_0$	$^3P_1$	$^3P_2 - {}^3F_2$	$^1D_2$	$^3D_2$
1*R*	−0.5620	−2.2387	−3.2151	−1.0892	−4.4989	−0.2528	−0.0130	−1(−7)
2*R*	0.0026	−0.7254	−0.7518	−0.1152	−1.3990	−0.0585	−0.0003	
3*R*		−0.2704	−0.1242	−0.0211	−0.1800	−0.1287		
4*R*		0.1813	−0.0142	−0.0001	0.0210	−0.0432		
5*R*		0.0579	0.0006		0.0150	0.0291		
6*R*		0.0327	0.0002		−0.0010	−0.0032		
7*R*		−0.0151			−0.0014	−0.0016		
8*R*		0.0007			−0.0001	−0.0004		
9*R*		0.0016			−1(−5)			
10*R*		0.0003			0.0001			
11*R*					−0.0001			
12*R*					−0.0002			
1*A*	0.0056	−3.0999	−0.0030	0.0618		3.5012	0.1924	0.4605
2*A*	0.0137	0.1724	0.0002	0.0047		0.0785	0.0116	0.0504
3*A*	0.0043	0.0333		−0.0009		−0.0169	−0.0001	−0.0123
4*A*	−0.0002	−0.0066		−0.0001		−0.0008	0.0014	0.0023
5*A*	−0.0001	−0.0009		0.0001		0.0018	0.0005	0.0013
6*A*	0.0001	0.0008		−3(−5)		0.0003	−0.0001	0.0002
7*A*		0.0001		−3(−5)		0.0001	−0.0001	−0.0001
8*R*		−0.0001		−5(−6)		−0.0001	−1(−5)	−3(−5)
9*A*		−5(−7)		3(−5)			0.0001	−1(−5)
10*A*		2(−5)		4(−5)			0.0001	4(−5)
11*A*								0.0001
Total	−0.536	−5.876	−4.107	−1.160	−6.045	3.105	0.192	0.502

	$^3D_3 - {}^3G_3$	$^1F_3$	$^3F_3$	$^3F_4 - {}^3H_4$
1*R*	0.0915	0.0264	0.0314	−0.0008
2*R*	0.0724	−0.0044	0.0019	−0.0017
3*R*	0.0522	−0.0017	−0.0038	−0.0002
4*R*	0.0002	0.0003	−0.0004	−0.0019
5*R*	−0.0021	−5(−6)	0.0002	−0.0027
6*R*	−0.0037	−0.0003	−0.0002	−0.0007
7*R*	0.0018	−0.0003	−0.0005	0.0003
8*R*	0.0016	−0.0002	−0.0003	0.0004
9*R*		−0.0001		
1*A*	−0.1558	0.0008	0.0024	0.0241
2*A*	0.0263	0.0007	0.0012	−0.0069
3*A*	0.0022	0.0001	3(−5)	−0.0084
4*A*	−0.0015		−2(−6)	−0.0074
5*A*	0.0006			0.0018
6*A*	0.0003			0.0029
7*A*	−0.0003			0.0005
8*A*	−0.0004			−0.0005
Total	0.085	0.021	0.032	−0.001

are included (the calculations are done in the same way as those of Table XIII).

For each two-body channel *jST*, Table XXI gives the contribution to $D_3^c(R)$ as a function of β. For a given *jST*, convergence in β is initially very fast. The rate of decrease with increasing β eventually becomes very slow, but only after individual contributions have fallen to about 10^{-4} MeV in magnitude. Study of Table XXI also shows that the sets of β given in Table VI for the ring contribution are more

than adequate. The convergence of $D_3^c(R)$ in β is similar for the potentials v_2 and v_6 (Reid).

G. Numerical tests of mesh parameters

In this subsection we give results that show what accuracy can be obtained with various choices of mesh parameters. All results are calculated using the full Reid potential at $k_F = 1.8$ fm^{-1}. Similar but less complete tests using potentials v_2 and v_6(Reid) give results similar to the full Reid results. Thus the full-Reid results are expected to be a good guide in selecting mesh parameters for any reasonable nucleon-nucleon force. The error caused by a particular choice of mesh parameters is expected, because of the factor $k_F{}^6$ in Eq. (5.12), to decrease rapidly as k_F decreases below 1.8 fm^{-1}. As in earlier subsections, we sometimes use restricted sets of $jST\beta$ and $\mathcal{J}\mathcal{P}\mathcal{T}$ in order to save computer time.

Table XXII shows the variation of $D_3^c(R)$ and $D_3^c(H)$ with respect to $N(K)$ [the value of $N(K)$ does not affect $D_3^c(B)$, which is calculated as described in Secs. V E and VI C]. For $D_3^c(R)$ we use set C of $jST\beta$ from Table XIV. With this set, and with standard parameters [note that $N(k_0) = 2$ is used in Table XXII], one finds $D_3^c(R) = -14.2$ MeV, which is very close to the result -13.8 obtained from the full set of $jST\beta$ given in Table VI. Hence set C is adequate for test calculations. The convergence in $N(K)$ is seen from Table XXII to be poor, with fluctuations of 0.03 MeV even for $N(K)$ as large as 12. I attribute this to nonsmooth behavior of $F_0^{\rm dir}(d\beta K)$ and $(d\beta K\,|XQ_a/e_a|\,d'\beta'K')$ as functions of K,K'. One source of nonsmoothness is the lower limit L_0 of Eq. (6.6). If $L_0 = |K - K_0/2|$ were always valid, the variable y of Eq. (6.7) would always run from -1 to 1. But the angle-average Pauli operator causes L_0, and hence the range of y, to vary in a nonsmooth way as a function of K. Similar remarks apply to Eq. (6.14) for $(d\beta K\,|XQ_a/e_a|\,d'\beta'K')$. To confirm this idea, the calculations have been repeated with the factors $Q(P_b,K)$ and $Q_a(K,k)$ replaced by unity in Eqs. (6.3) and (6.14), respectively. Correspondingly, the right sides of Eqs. (6.6) and (6.16) are replaced by $|K - K_0/2|$ and $|K' - K/2|$, respectively. The reaction matrix G_b in Eq. (6.3) and the form factors g_β in Eq. (6.14) are calculated as usual, *not* with $Q = 1$. The results are shown in Table XXIII and the convergence in $N(K)$ is vastly improved. This comfirms that the poor convergence in Table XXII is caused by the Pauli operator. From Table XXII,

TABLE XXII. Variation of $D_3^c(R)$ and $D_3^c(H)$ with respect to $N(K)$ for the full Reid potential at $k_F = 1.8$ fm^{-1}. The calculation of $D_3^c(R)$ includes set C of form factors from Table XIV, and all sets $\mathcal{J}\mathcal{P}\mathcal{T}$ consistent with $L_0 + l_0 \leq 2$ are included. The calculation of $D_3^c(H)$ uses set A of form factors from Table XIV and includes $\mathcal{J}\mathcal{P}\mathcal{T} = (\frac{1}{2}+\frac{1}{2}), (\frac{1}{2}-\frac{1}{2}), (\frac{3}{2}-\frac{1}{2}), (\frac{5}{2}-\frac{1}{2})$. The value $N(k_0) = 2$ is used. Except for $N(K)$, all other parameters are the standard ones of Tables I and III. The calculations are $\mathcal{O}$-type.

$N(K)$	$D_3^c(R)$ (MeV)	$D_3^c(H)$ (MeV)
6	−13.941	−14.064
8	−13.806	−14.194
10	−13.765	−14.133
12	−13.792	−14.152

the numerical uncertainties using $N(K) = 8$ appear to be about 0.05 and 0.06 MeV, respectively, for $D_3^c(R)$ and $D_3^c(H)$. These values are entered in Table XXXII.

We next study convergence in the cutoff momenta $K_{\max}$ and $k_{\max}$. When $K_{\max}$ is changed, the Gauss grid in K also changes, and we expect fluctuations of order 0.05 MeV in $D_3^c(R)$ and $D_3^c(H)$ as discussed in the preceding paragraph. These fluctuations will obscure the convergence in $K_{\max}$. To avoid this, we study convergence in $K_{\max}$ by putting $Q = 1$ as discussed above in connection with Table XXIII.

While testing convergence with respect to $k_{\max}$ and $K_{\max}$, it is important to keep the functional forms of the g_β unchanged in Eqs. (6.3) and (6.14). This implies that the grid of relative momenta k used in calculating the g_β [see Eq. (4.33)] must remain fixed. While varying $k_{\max} = K_{\max}$, we use the grid

$$k_i = 0(0.25)5(0.5)12 \text{ fm}^{-1} , \tag{7.36}$$

TABLE XXIII. Same as Table XXII except that $Q = 1$ is used, as explained in the text.

$N(K)$	$D_3^c(R)$ (MeV)	$D_3^c(H)$ (MeV)
6	−17.432	−17.588
8	−17.398	−17.597
10	−17.394	−17.595
12	−17.394	−17.594

rather than Eq. (4.33). The grid of Eq. (7.36) allows $k_{max} = K_{max}$ to be as large as 12 fm^{-1}. When K_{max} is increased, a correspondingly larger value of $N(K)$ is required to achieve a given numerical accuracy. It is found, for $k_{max} = K_{max} = 12$ fm^{-1}, that convergence in $N(K)$ is achieved for $N(K) = 12$ to 0.002 and 0.005 MeV, respectively, for $D_3^c(R)$ and $D_3^c(H)$. Thus we use $N(K) = 12$ and observe the variation of $D_3^c(R)$ and $D_3^c(H)$ with $k_{max} = K_{max}$. The calculations are $\mathcal{O}$-type, and the results are shown in Table XXIV, using the same parameters as in Table XXIII except for $N(K)$, $k_{max} = K_{max}$, and the grid of Eq. (7.36). Both $D_3^c(R)$ and $D_3^c(H)$ are still changing slowly at $k_{max} = K_{max} = 12$ fm^{-1}. It is not clear whether these changes are caused by the change in the Gauss grid of points K_i or actually represent slow convergence with respect to $k_{max} = K_{max}$. As a reasonably safe bound on the error caused by using $k_{max} = K_{max} = 8$ fm^{-1}, we multiply the change between $k_{max} = K_{max} = 8$ fm^{-1} and 12 fm^{-1} by 3. The resulting uncertainties 0.04 and 0.09 MeV for $D_3^c(R)$ and $D_3^c(H)$ are entered in Table XXXII.

Next we test $D_3^c(B)$ for convergence in k_{max}, using the calculational method of Secs. V E and VI B. To save computer time only one mesh point in p_3 and two points in $\cos\theta(\vec{p}_3, \vec{k}_2)$ are used to evaluate Eq. (5.29) for $U(k_2,\delta E)$, and we also use $N(k_0) = 1$. Furthermore, we use the approximation $G_a \approx v$ for $l'(jST) \geq 3$, rather than the more standard choice $l'(jST) \geq 4$. All other parameters (except n_{max}, see below) are the standard ones of Sec. VI B and Tables I and III. These simplifications give $D_3^c(B) = 16.8$ MeV rather than the more accurate value 23.8 MeV from Table XXXIII, but this error will not appreciably affect convergence in k_{max}. For $k_{max} = 12$ fm^{-1}, it is found that $n_{max} = 12$ gives convergence to 0.001 MeV in n_{max}, and this value of n_{max} is used to obtain the results for $D_3^c(B)$ given in Table XXIV. The values of $D_3^c(B)$ for $k_{max} \geq 8$ fm^{-1} are fitted well by the formula $16.781 - 29.6\ k_{max}^{-3}$. Using this to extrapolate to $k_{max} = \infty$, we find that using $k_{max} = 8$ fm^{-1} causes an error of 0.06 MeV in $D_3^c(B)$. This value is entered in Table XXXII.

Convergence of $D_3^c(R)$ and $D_3^c(H)$ with respect to $N(K_0)$ is shown in Tables XXV and XXVI for $\mathcal{O}$- and $\mathcal{M}$-type calculations, respectively. To save computing time, only the most important sets $\mathcal{J}\mathcal{P}\mathcal{T}$ (see Table XXXVII) are included in the $\mathcal{M}$-type calculations of $D_3^c(R)$. The difference of order 0.25 MeV between the $\mathcal{O}$-type and $\mathcal{M}$-type calculations of $D_3^c(H)$ is caused by the different methods of integrating over the Fermi sea that are used in the two methods. Using the standard value $N(K_0) = 3$ gives error in $D_3^c(R)$ of about 0.12 and 0.03 MeV for $\mathcal{O}$- and $\mathcal{M}$-type calculations, respectively, and the larger of these is entered in Table XXXII. For $D_3^c(H)$ the error for $N(K_0) = 3$ is about 0.03 MeV for both types of calculation.

TABLE XXIV. Variation of three-body cluster contributions to the energy with the cutoff parameters $k_{max} = K_{max}$, as explained in the text. The Reid potential is used at $k_F = 1.8$ fm^{-1}. For $D_3^c(R)$ and $D_3^c(H)$ the sets of $jST\beta$ and $\mathcal{J}\mathcal{P}\mathcal{T}$ are the same as in Table XXII.

$k_{max} = K_{max}$ (fm^{-1})	$D_3^c(R)$ (MeV)	$D_3^c(H)$ (MeV)	$D_3^c(B)$ (MeV)
6	−17.149	−17.132	16.349
8	−17.402	−17.578	16.723
9	−17.406	−17.559	16.738
10	−17.408	−17.553	16.750
11	−17.409	−17.551	16.759
12	−17.414	−17.549	16.764

Convergence with respect to $N(k_0)$ is shown in Table XXVII. For $D_3^c(B)$ the calculations are similar to those of Table XXIV except that we use $n_{max} = 6$ to save computer time. Using $N(k_0) = 3$ is seen to give errors of 0.014, 0.005, and 0.002 MeV, respectively, in $D_3^c(B)$, $D_3^c(R)$, and $D_3^c(H)$, and these figures are entered in Table XXXII.

Convergence with respect to n_{max} is tested in Table XXVIII. The convergence of $D_3^c(B)$ is good, and using $n_{max} = 8$ gives an error of 0.003 MeV. The convergence of $D_3^c(R)$ and $D_3^c(H)$ is poor; there seems to be a "noise level" of order 0.01 MeV for $n_{max} = 8$, 10, 12. I attribute this to nonsmooth behavior of the functions being expanded in the

TABLE XXV. Convergence of $D_3^c(R)$ and $D_3^c(H)$ with respect to $N(K_0)$ for $\mathcal{O}$-type calculations with the full Reid potential at $k_F = 1.8$ fm^{-1}. Standard mesh parameters are used except that $N(k_0) = 2$ and $N(K_0)$ is varied. The sets of $jST\beta$ and $\mathcal{J}\mathcal{P}\mathcal{T}$ for $D_3^c(R)$ and $D_3^c(H)$ are the same as in Table XXII.

$N(K_0)$	$D_3^c(R)$ (MeV)	$D_3^c(H)$ (MeV)
2	−13.259	−14.012
3	−13.806	−14.194
4	−13.917	−14.169
5	−13.909	−14.173

TABLE XXVI. Convergence of $D_3^c(R)$ and $D_3^c(H)$ with respect to $N(K_0)$ for $\mathscr{M}$-type calculations with the Reid potential at $k_F = 1.8$ fm^{-1}. Standard mesh parameters are used except that $N(k_0) = 2$ and $N(K_0)$ is varied. For $D_3^c(H)$ the sets $jST\beta$ and $\mathscr{J}\mathscr{P}\mathscr{T}$ are the same as in Table XXII. For $D_3^c(R)$, set B of $jST\beta$ from Table XIV is used, and the sets $\mathscr{J}\mathscr{P}\mathscr{T}$ included are $(\frac{1}{2}+\frac{1}{2})$, $(\frac{1}{2}+\frac{3}{2})$, $(\frac{3}{2}+\frac{1}{2})$, $(\frac{1}{2}-\frac{1}{2})$, $(\frac{3}{2}-\frac{3}{2})$, $(\frac{5}{2}-\frac{1}{2})$.

$N(K_0)$	$D_3^c(R)$ (MeV)	$D_3^c(H)$ (MeV)
2	−13.588	−14.032
3	−13.388	−13.934
4	−13.406	−13.949
5	−13.408	−13.952

basic set $p_n(k)$. The situation is analogous to the one discussed earlier in connection with convergence in $N(K)$. In that case convergence in $N(K)$ was dramatically improved by putting $Q = 1$. For $D_3^c(H)$ I have checked that a similar improvement in convergence with respect to $n_{\max}$ takes place if Q is set equal to 1. The situation is presumably the same for $D_3^c(R)$, but this has not been checked by explicit calculation. For $n_{\max} = 8$, uncertainties of 0.03 MeV, i.e., 3 times the noise level, are assigned to both $D_3^c(R)$ and $D_3^c(H)$ and are entered in Table XXXII.

H. Sensitivity to $K_{\min}$, P, $\mathscr{K}$, and ω_3

In numerical calculations we have used fixed, average values of $K_{\min}$, P_b, $\mathscr{K}$, and ω_3 as discussed in Secs. IV A, IV B, and VI A. In an exact calculation all these quantities depend on $\vec{p}_1$, $\vec{p}_2$, $\vec{p}_3$. In this section we study the sensitivity of our numerical results to reasonable changes in the above parameters. This allows a rough estimate of the numerical uncertainty caused by using fixed average values. All calculations are for the Reid potential at $k_F = 1.8$ fm^{-1}.

TABLE XXVII. Convergence of three-body cluster energy with respect to $N(k_0)$ for the Reid potential at $k_F = 1.8$ fm^{-1}. for $D_3^c(R)$ and $D_3^c(H)$ the calculations are $\mathscr{O}$-type, standard parameters are used, and the sets $jST\beta$ and $\mathscr{J}\mathscr{P}\mathscr{T}$ are the same as in Table XXII. Further discussion is given in the text.

$N(k_0)$	$D_3^c(B)$ (MeV)	$D_3^c(R)$ (MeV)	$D_3^c(H)$ (MeV)
2	16.974	−13.806	−14.194
3	17.226	−14.206	−14.114
4	17.239	−14.205	−14.112
5	17.240	−14.201	−14.112

TABLE XXVIII. Convergence with respect to $n_{\max}$ for $\mathscr{M}$-type calculations with the Reid potential at $k_F = 1.8$ fm^{-1}. For $D_3^c(R)$ and $D_3^c(H)$, the standard parameters are used except that $N(k_0) = 2$. The sets $jST\beta$ and $\mathscr{J}\mathscr{P}\mathscr{T}$ are the same as in Table XXII. The calculation of $D_3^c(B)$ is the same as in Table XXVII except that $n_{\max}$ is varied and $N(k_0)$ is set equal to 1.

$n_{\max}$	$D_3^c(B)$ (MeV)	$D_3^c(R)$ (MeV)	$D_3^c(H)$ (MeV)
6	17.741	−13.548	−13.933
8	17.810	−13.588	−13.934
10	17.813	−13.591	−13.936
12	17.813	−13.594	−13.943

The calculation of $D_3^c(B)$ by the method of Sec. V E does not depend on $K_{\min}$. The variation of $D_3^c(R)$, $D_3^c(H)$, and their sum with $K_{\min}$ is shown in Table XXIX. The total variation in the sum over a wide range of $K_{\min}$ is seen to be 0.94 MeV. A somewhat arbitrary but reasonable estimate of the error from this source is 50% of this variation, or 0.47 MeV. Since this estimate and others to be made later in this section are rather rough, there is little point in increasing them by 10–20% to take account of the omitted sets of $\mathscr{J}\mathscr{P}\mathscr{T}$ and $jST\beta$ in Table XXIX.

The variations of $D_3^c(B)$, $D_3^c(R)$, $D_3^c(H)$, and their sum with P_b are shown in Table XXX. The sum is a function of $P_b = |\vec{p}_1 + \vec{p}_2|$ and can be

TABLE XXIX. Variation of $D_3^c(R)$, $D_3^c(H)$, and their sum with $K_{\min}$ for the full Reid potential at $k_F = 1.8$ fm^{-1}. The calculations are $\mathscr{O}$-type, using standard parameters except for $K_{\min}$, whose standard value at this value of k_F is 1.61 fm^{-1}. The sets $(jST\beta)$ and $(\mathscr{J}\mathscr{P}\mathscr{T})$ are the same as in Table XXII.

$K_{\min}$ (fm^{-1})	$D_3^c(R)$ (MeV)	$D_3^c(H)$ (MeV)	Sum (MeV)
0.41	−13.71	−13.88	−27.59
0.81	−14.14	−13.94	−28.08
1.21	−14.35	−14.16	−28.51
1.61	−14.21	−14.11	−28.23
2.01	−13.90	−13.67	−27.57

TABLE XXX. Variation with P_b of $D_3^c(B)$, $D_3^c(R)$, $D_3^c(H)$ and their sum for the Reid potential at $k_F = 1.8$ fm^{-1}. Standard parameters are used except that $G \approx v$ is used for $l'(jST) \geq 3$ in calculating $D_3^c(B)$. The calculations for $D_3^c(R)$ and $D_3^c(H)$ are $\mathcal{O}$-type, using the same sets $(jST\beta$ and $(\mathcal{J}\mathcal{P}\mathcal{T})$ as in Table XXII.

P_b (fm^{-1})	$D_3^c(B)$ (MeV)	$D_3^c(R)$ (MeV)	$D_3^c(H)$ (MeV)	Sum (MeV)
0.72	23.94	−14.98	−14.48	−5.52
1.44	24.25	−14.50	−14.29	−4.54
2.16	24.24	−14.05	−13.99	−3.79
2.88	23.88	−13.61	−13.66	−3.39

averaged over $\vec{p}_1$, $\vec{p}_2$ using Eq. (5.5) with $n = 2$. The result for this average is −4.22 MeV, while the sum at the standard value $P_b = (\frac{6}{5})^{1/2}k_F = 1.972$ fm^{-1} (obtained from Table XXX by interpolation) is −3.93 MeV. Table XXX does not cover the full range of P_b from 0 to $2k_F = 3.6$ fm^{-1}, but the probability of two particles having P_b less than 0.72 fm^{-1} or larger than 2.88 fm^{-1} is quite small. As a reasonable estimate of the error, we take 50% of the total variation in the sum shown in Table XXX. The resulting error estimate of 0.57 MeV is entered in Table XXXII.

The fixed average value of total momentum $\mathcal{K}$ does not affect the calculation of $D_3^c(B)$ using the method of Sec. V E. The value of $\mathcal{K}$ enters the calculation of $D_3^c(R)$ and $D_3^c(H)$ in two ways: it appears in the Pauli operator Q_a through Eqs. (4.4) and (4.5), and it appears in the energy denominator e_a through Eqs. (4.13) and (4.14). We first carry out calculations in which $\mathcal{K}$ and $\bar{\omega}_3$ are simultaneously varied, keeping $-\bar{\omega}_3 + \mathcal{K}^2/6$ constant. This has the effect of keeping Eqs. (4.13) and (4.14) for e_a and ${\gamma_a}^2$ unchanged and isolates the effect of $\mathcal{K}$ on Q_a through Eqs. (4.4) and (4.5). Varying $\mathcal{K}$ from 1.35 to 4.05 fm^{-1} is found to give a total variation of 0.18 MeV in $D_3^c(R) + D_3^c(H)$, and we assume the numerical error from this source to be 0.09 MeV, which is entered in Table XXXII.

The energy denominator e_a of Eqs. (4.13) and (4.14) is affected both by $\mathcal{K}$ and ω_3. We can vary e_a by keeping $\mathcal{K}$ fixed and varying ω_3. The results for $D_3^c(R)$, $D_3^c(H)$, and their sum are shown in Table XXXI. A fixed value of ω_3 is not used in evaluating $D_3^c(B)$ according to Sec. V E. If the sum in Table XXXI were linear in ω_3, then its average over $\vec{p}_1, \vec{p}_2, \vec{p}_3$ would be obtained *exactly* by doing a single calculation with average values of ω_3 and $\mathcal{K}^2$, which is precisely the calculation with standard parameters. The sum in Table XXXI is not quite linear, being fitted by $-27.172 + 0.384\omega_3 + 0.0143{\omega_3}^2$. This can be expressed as a function of $\vec{p}_1$, $\vec{p}_2$, $\vec{p}_3$ by using Eqs. (4.10) and (2.21). Averaging this expression over $\vec{p}_1$, $\vec{p}_2$, $\vec{p}_3$ gives −28.29 MeV, while a single calculation using $\bar{\omega}_3 = -3.404$ fm^{-2} gives −28.32 MeV. The complete range of ω_3 is from −8.81 to 0.20 fm^{-2}, and using the quadratic formula quoted above gives a variation in the sum of 2.35 MeV. A reasonable estimate of the error from using the average value of ω_3 is 25% of this total variation. This gives an error estimate of 0.59 MeV, which is entered in Table XXXII.

I. Estimate of numerical uncertainty in D_3^c

In the preceding subsections of Sec. VII we have studied in some detail the sensitivity of D_3^c to mesh parameters, truncations, the use of a symmetrized kernel, and values of $K_{\min}$, P_b, $\mathcal{K}$, and ω_3. In this subsection we put these results together to estimate the total numerical uncertainty in D_3^c. This estimate is made for the standard parameters that are used in the production calculations of Sec. VIII. By using the detailed results in the preceding subsections, one can make an analogous error estimate for other choices of parameters.

TABLE XXXI. Variation with ω_3 of $D_3^c(R)$, $D_3^c(H)$, and their sum for the Reid potential at $k_F = 1.8$ fm^{-1}. Standard parameters are used except for ω_3. The sets $(jST\beta)$ and $(\mathcal{J}\mathcal{P}\mathcal{T})$ are the same as in Table XXII.

ω_3 (fm^{-2})	$D_3^c(R)$ (MeV)	$D_3^c(H)$ (MeV)	Sum (MeV)
−7.011	−14.82	−14.34	−29.16
−4.306	−14.38	−14.18	−28.56
−1.600	−13.81	−13.94	−27.75

TABLE XXXII. Estimates of numerical uncertainty in D_3^c from various sources for the full Reid potential at $k_F = 1.8$ fm^{-1}. The entries in part A are discussed in Secs. VII C–VII G, those in part B in Sec. VII H, and those in parts C and D in Sec. VII I. Further discussion is given in Sec. VII I.

Parameter and value	Numerical uncertainty (MeV) $D_3^c(B)$	$D_3^c(R)$	$D_3^c(H)$
A. Mesh parameters and truncations			
$l'(jST) \leq 3(R)$		0.07	
$l'(jST) \leq 4(H)$			0.06
$l_0 \leq 2$	0.01	0.02	0.01
$L_0 + l_0 \leq 2$		0.30	0.05
β,β_1(Table VI)		0.00	0.51
Symmetrized kernel			0.023
$N(K) = 8$		0.05	0.06
$k_{max} = K_{max} = 8$ fm^{-1}	0.06	0.04	0.09
$N(K_0) = 3$		0.12	0.03
$N(k_0) = 3$	0.014	0.005	0.002
$n_{max} = 8$	0.003	0.03	0.03
$(\sum\delta_i^2)^{1/2} = 0.63$ (part A)			
B. Average values of $K_{min}, P_b, \mathscr{K}, \omega_3$			
$K_{min} = (k_F^2 - \mathscr{K}_0^2/9)^{1/2}$	0.47 (total for R,H)		
$P_b = (\frac{6}{5})^{1/2}k_F$	0.57 (total for B,R,H)		
$\mathscr{K}_0 = (\frac{9}{5})^{1/2}k_F$(effect on Q_a)	0.09 (total for R,H)		
$\omega_3 = 0.9k_F^2/m^* - 3E_0$	0.59 (total for R,H)		
$(\sum\delta_i^2)^{1/2} = 0.94$ (part B)			
C. Angle averaging			
Total error assumed equal to $(\sum\delta_i^2)^{1/2} = 0.94$ from part B.			
D. $(\sum\delta_i^2)^{1/2}$ from parts A–C is 1.47 MeV.			

The numerical uncertainties caused by use of the standard parameters are collected in Table XXXII, for the full Reid potential at $k_F = 1.8$ fm^{-1}. Part A gives the uncertainties coming from mesh parameters and truncations, as discussed in more detail in Secs. VII B through VII G. We assume these uncertainties are statistically independent. Thus the square root of the sums of the squares of all entries in part A gives the total error from part A. This result is given as $(\sum\delta_i^2)^{1/2}$ and equals 0.63 MeV for part A. Part B gives the uncertainties estimated in Sec. VII H due to use of fixed, average values of K_{min}, P_b, $\mathscr{K}$, and ω_3. These are combined in the same way as for part A to give a total uncertainty from part B of 0.94 MeV.

Additional numerical uncertainty comes from our use of angle-average Pauli operator and from the angle-average approximations used to obtain Eqs. (5.11) and (5.17). These angle-average approximations give an oversimplified treatment of the geometry of the Fermi sphere in momentum space. It is the same kind of oversimplification that leads to the use of fixed, average values for K_{min}, P_b, $\mathscr{K}$, and ω_3. Therefore, we take the uncertainty from this latter source to be an estimate of the uncertainty due to angle-average approximations, and this is indicated in part C of Table XXXII. This assumption is intuitively reasonable but can only be established by doing more detailed calculations. For example, one could treat the difference between the exact and angle-average Pauli operators in first-order perturbation theory.

In part D of Table XXXII the square root of the sums of squares from parts A, B, and C is calculated to be 1.47 MeV. This is our estimate of the numerical uncertainty in D_3^c for the full Reid potential at $k_F = 1.8$ fm^{-1}. I believe the probability is better than 50% that the value $D_3^c = -6.57$ MeV obtained with standard parameters (see Table XXXIII) has a numerical error less than 1.47 MeV. However, it will require better calculations to ascertain the error with more certainty.

TABLE XXXIII. Three-body cluster contributions $D_3^c(B)$, $D_3^c(R)$, $D_3^c(H)$, and their sum D_3^c for different two-body potentials and Fermi momenta. All energies are in MeV and k_F is in fm^{-1}. For v_2 and v_6 (Reid) the columns headed 1.8*A* and 1.8*B* give results at $k_F = 1.8$ fm^{-1} with shifted energy denominators. In column 1.8*A* the spectrum of states above the Fermi sea is shifted up by the constant amount $\Delta = 0.2$ fm$^{-2} = 8.3$ MeV. This is equivalent to replacing E_0 of Eq. (4.10) by $E_0 + 0.2$ fm^{-2} everywhere in the calculation. In column 1.8*B*, all energy demonimators e_a (including those occurring inside the calculation of G_a) are increased by 0.6 fm$^{-2} = 24.9$ MeV, while all energy denominators e_b are left unchanged. In the calculation of $D_3^c(B)$, for some channels $lSjT$ in the G_a matrix, fewer than seven values of δE were used (see Sec. VI B). This accounts for the small differences in $D_3^c(B)$ between this table and Table XXXV.

			Potential v_2			
	k_F:	1.4	1.6	1.8	1.8*A*	1.8*B*
$D_3^c(B)$		−0.96	0.76	6.86	8.11	8.06
$D_3^c(R)$		4.55	9.13	17.20	16.82	17.45
$D_3^c(H)$		−7.65	−16.88	−33.69	−33.25	−33.95
D_3^c		−4.06	−6.99	−9.63	−8.32	−8.44
$\kappa_2 D_2$		−2.76	−5.06	−8.24		
			Potential v_6(Reid)			
	k_F:	1.4	1.6	1.8	1.8*A*	1.8*B*
$D_3^c(B)$		3.34	9.52	22.18	22.51	23.01
$D_3^c(R)$		−5.74	−10.90	−18.64	−18.19	−18.75
$D_3^c(H)$		−3.96	−8.52	−17.06	−16.73	−17.11
D_3^c		−6.36	−9.90	−13.52	−12.41	−12.85
$\kappa_2 D_2$		−5.27	−7.94	−11.25		
			Potential full Reid			
	k_F:	1.2	1.4	1.6	1.8	
$D_3^c(B)$		0.72	3.68	10.32	23.83	
$D_3^c(R)$		−2.14	−4.57	−8.39	−13.90	
$D_3^c(H)$		−1.81	−4.07	−8.51	−16.50	
D_3^c		−3.23	−4.96	−6.58	−6.57	
$\kappa_2 D_2$		−3.32	−5.24	−7.83	−10.92	

The absolute value of the numerical error is expected to be about the same for all three potentials at $k_F = 1.8$ fm^{-1}. Taking D_3^c from Table XXXIII, one then finds relative errors at $k_F = 1.8$ fm^{-1} of 23%, 11%, and 15% for the potentials full Reid, v_6(Reid), and v_2, respectively. If we go to smaller k_F for the full Reid potentials, the numerical error will certainly decrease since the individual contributions from B, R, and H all decrease in magnitude faster than k_F^4 (see Table XXXIII). Thus it seems safe to assume that the error in D_3^c decreases as fast as k_F^4. This assumption produces relative errors for the full Reid potential of 14%, 11%, and 9% for $k_F = 1.6$,1.4, and 1.2 fm^{-1}, respectively. From the preceding numbers, it appears that the relative uncertainty in D_3^c is no larger than 15% for any potential or k_F except for the full Reid potential at $k_F = 1.8 fm^{-1}$. Thus we will take the numerical uncertainty in D_3^c to be 15% for all potentials and all values of k_F considered in this paper except for the full Reid potential at $k_F = 1.8$ fm^{-1}, where we use 1.47 MeV.

VIII. NUMERICAL RESULTS

In this section we give numerical results for the two-body potentials, v_2, v_6(Reid), and full Reid. These potentials are defined in Appendix A. The three-body calculations are $\mathcal{M}$-type, using the standard parameters of Tables I and III–VI, as discussed in Sec. VII.

The three-body cluster results are given in Table XXXIII. The rough estimate $D_3^c \approx \kappa_2 D_2$ is seen to give the correct order of magnitude for all three potentials, and over a range of densities.

From Tables III and XXXIII the results for v_6(Reid) and full Reid are seen to be similar. More detailed comparisons between the two potentials are given in Tables XXXIV, XIII, and XXXV. The results for D_2 in Table XXXIV show that v_6(Reid) and full Reid give substantially different results for individual partial waves, even though the sum over partial waves differs very little in the two cases. At $k_F = 1.8$ fm^{-1} the main difference in D_3^c between v_6(Reid) and full Reid comes from the ring contribution (see Table XXXIII). Contributions to $D_3^c(R)$ from individual two-body channels jST in the G_a matrix are shown in Table XIII. The biggest difference between the two potentials occurs in the $^3P_2$-$^3F_2$ channel. Table XXXV shows contributions to $D_3^c(B)$ from individual two-body channels $lSjT$ in the G_a matrix. A big difference between v_6(Reid) and full Reid is again found in the $^3P_2$ channel.

The results from Table XXXIII using shifted energy denominators are useful for two reasons. First, they provide necessary data for estimating the result of a three-body coupled-cluster calculation using the Bochum truncation[4–6,11] [we call this a CC(3) calculation]. In a CC(3) calculation the generalized ring series is summed, certain less important classes of diagrams are summed, and the single-particle potential energy $U(p_1)$ of states in the Fermi sea is modified. Comparison of columns 1.8 and 1.8B shows how much of the shift comes from the three-body denominators e_a. This information is useful in estimating certain four- and five-hole-line terms that appear in the CC(3) approximation.[27]

A second use for column 1.8A in Table XXXIII is to apply a test of the hole-line expansion described in Ref. 3. As discussed in Ref. 3, a necessary condition for the validity of the hole-line expansion is

$$\left| \frac{\partial(D_2 + D_3)}{\partial \Delta} \right| << \frac{\partial D_2}{\partial \Delta} = \kappa_2 , \tag{8.1}$$

TABLE XXXIV. Contributions to D_2 from individual channels $f_0 = l_0 S_0 j_0 T_0$ for the v_6(Reid) and full Reid potentials at $k_F = 1.8$ fm^{-1}. The same values of m^* and E_0 are used for both potentials [they are self-consistent ones for v_6(Reid) from Table III]. The contribution from channels with $l_0 \geq 3$ is calculated in the approximation $G \approx v$. The total of -45.53 MeV for v_6(Reid) differs by 0.2 MeV from that given in Table III because coarser mesh parameters are used here.

	D_2(MeV)	
f_0	v_6(Reid)	Full Reid
$^1S_0$	−23.51	−23.51
$^3S_1$	−20.05	−14.81
$^1P_1$	9.42	9.42
$^3P_0$	−12.16	−5.78
$^3P_1$	21.10	28.35
$^3P_2$	−3.60	−20.82
$^1D_2$	−9.74	−8.26
$^3D_1$	4.82	4.01
$^3D_2$	−12.18	−12.51
$^3D_3$	0.73	−0.48
$l_0 \geq 3$	−0.36	1.95
Total	−45.53	−42.44

TABLE XXXV. Contributions to $D_3^c)B)$ from individual $lSjT$ in the middle G matrix for the two-body potentials v_6(Reid) and full Reid at $k_F = 1.8$ fm^{-1}. The method of calculation is described in Sec. VI B.

$lSjT$	v_6(Reid)	Full Reid
$^1S_0$	5.16	4.66
$^3S_1$	10.58	12.00
$^1P_1$	9.68	9.70
$^3P_0$	−3.25	4.36
$^3P_1$	14.05	17.99
$^3P_2$	7.56	−11.62
$^1D_2$	−9.41	−6.20
$^3D_1$	2.81	2.06
$^3D_2$	−9.24	−6.92
$^3D_3$	−0.35	0.61
$^1F_3$	0.89	1.35
$^3F_2$	−2.52	−0.72
$^3F_3$	3.63	3.42
$^3F_4$	−2.15	−3.51
$l > 3$	−5.14	−3.22
Total	22.31	23.97

where Δ is a momentum-independent shift of the single-particle energy of states above the Fermi level. When the very small hole-hole term is neglected, condition (8.1) can be written to a good approximation as[3]

$$\left| \frac{\partial D_3^c}{\partial \Delta} - 2\kappa_2{}^2 \right| << \kappa_2 \, . \tag{8.2}$$

Using the results for D_3^c in columns 1.8 and 1.8*A* of Table XXXIII to evaluate $\partial D_3^c/\partial\Delta$, one finds the results shown in Table XXXVI. The condition (8.2) is seen to be well satisfied at $k_F = 1.8$ fm^{-1} for both v_2 and v_6(Reid).

The three-body cluster contributions from individual sets $\mathcal{J}\mathcal{P}\mathcal{T}$ are shown in Table XXXVII, for the full Reid potential at $k_F = 1.8$ fm^{-1}. The results for $D_3^c(H)$ are from the complete $\mathcal{M}$-type calculation. Those for $D_3^c(R)$ are from an $\mathcal{O}$-type calculation using set *C* of $jST\beta$ from Table XIV. These results are expected to differ by less than 5% from those of the full calculation. The results for $D_3^c(B)$ are calculated in the same way as those for $D_3^c(R)$. [The more accurate method of Sec. V E for $D_3^c(B)$ does not yield separate contributions from individual $\mathcal{J}\mathcal{P}\mathcal{T}$.] The truncations $l'(jST) \leq 3$ and $L_0 + l_0 \leq 2$ are inaccurate for $D_3^c(B)$, and these results are therefore only roughly correct, probably with errors of 10–30%. For $D_3^c(H)$ the dominant contribution comes from $\mathcal{J}\mathcal{P}\mathcal{T} = \frac{1}{2} + \frac{1}{2}$, and all other even-parity contributions are practically negligible. The total odd-parity contribution is about 40% of the dominant one. The same remarks apply to the sum $D_3^c(B) + D_3^c(R)$ but not to $D_3^c(B)$ or $D_3^c(R)$ individually.

Results for the generalized ring series are given in Tables XXXVIII and XXXIX for the energy and for κ, respectively. In Table XXXVIII the rows

TABLE XXXVI. Test of Eq. (8.2) for the two-body potentials v_2 and v_6(Reid) at $k_F = 1.8$ fm^{-1}, as described in the text.

Potential	$\partial D_3^c/\partial\Delta - 2\kappa_2{}^2$	κ_2
v_2	0.012	0.270
v_6(Reid)	0.013	0.246

TABLE XXXVII. Three-body cluster contributions from individual $\mathcal{J}\mathcal{P}\mathcal{T}$ for the full Reid potential at $k_F = 1.8$ fm^{-1}, as described in the text. Note that the results for $D_3^c(B)$ are only accurate to 10–30%.

$\mathcal{J}\mathcal{P}\mathcal{T}$	$D_3^c(B)$ (MeV)	$D_3^c(R)$ (MeV)	$D_3^c(H)$ (MeV)
$\frac{1}{2} + \frac{1}{2}$	10.38	1.02	−11.44
$\frac{1}{2} + \frac{3}{2}$	3.17	−3.00	−0.03
$\frac{3}{2} + \frac{1}{2}$	14.02	−14.21	−0.13
$\frac{3}{2} + \frac{3}{2}$	0.05	−0.02	−0.05
$\frac{5}{2} + \frac{1}{2}$	−0.20	0.16	−0.14
$\frac{5}{2} + \frac{3}{2}$	−0.15	0.10	−0.01
$\frac{7}{2} + \frac{1}{2}$	−0.15	0.04	−0.001
$\frac{7}{2} + \frac{3}{2}$	−0.02	0.02	−0.001
$\frac{1}{2} - \frac{1}{2}$	2.38	2.84	−2.05
$\frac{1}{2} - \frac{3}{2}$	0.99	0.30	−0.58
$\frac{3}{2} - \frac{1}{2}$	1.07	−0.14	−1.22
$\frac{3}{2} - \frac{3}{2}$	0.01	−0.58	−0.22
$\frac{5}{2} - \frac{1}{2}$	−0.76	−0.62	−0.61
$\frac{5}{2} - \frac{3}{2}$	0.12	−0.12	0.0001
Total	30.91	−14.21	−16.48

n = 3,4,5,6 give the values of $D_3^{GR} \equiv D_3^c$, $D_4^{GR} \equiv D_4(B1)$ (notation of Ref. 8), D_5^{GR}, and D_6^{GR}. The next row gives the sum of these four contributions. The row labeled Sum to ∞ gives D_{tot}^{GR} obtained from Eqs. (2.70)–(2.72). In Table XXXIX row n gives κ_n calculated by putting

$$S_2 \approx Q_b \sum_{i=2}^{n} \bar{S}_2{}^{(i)} \tag{8.3}$$

into Eq. (7.7) for κ. [Note that Q_b rather than $Q_b{}^2$ is used in the evaluation of κ. See the paragraph following Eq. (7.7).] The row labeled ∞ gives the result of putting $S_2^{tot} = Q_b \bar{S}_2^{tot}$ into Eq. (7.7), where $\bar{S}_2^{tot}$ is obtained from Eq. (2.70).

The main feature of Table XXXVIII is that the generalized ring series converges quite rapidly. This is true for all three two-body potentials and for all densities considered. There is a slight but clear tendency for the convergence to be slower at lower density. The rapid convergence means that (1) we are not compelled by these results to modify the hole-line expansion, and (2) these results give no in-

TABLE XXXVIII. Energies D_n^{GR} from the generalized ring series for different potentials and k_F. The columns headed 1.8*A* and 1.8*B* have the same meaning as in Table XXXIII. All energies are in MeV and k_F is in fm^{-1}. Further discussion is given in the text.

		Potential v_2				
n	k_F:	1.4	1.6	1.8	1.8*A*	1.8*B*
3		−4.06	−6.99	−9.63	−8.32	−8.44
4		−0.41	−0.98	−2.13	−1.93	−2.11
5		−0.043	0.004	0.44	0.51	0.59
6		−0.018	−0.050	−0.28	−0.28	−0.34
Sum		−4.53	−8.02	−11.61	−10.02	−10.30
Sum to ∞		−4.56	−8.04	−11.55	−9.93	−10.21
		Potential v_6(Reid)				
n	k_F:	1.4	1.6	1.8	1.8*A*	1.8*B*
3		−6.36	−9.90	−13.52	−12.41	−12.85
4		−1.00	−1.50	−2.01	−1.71	−1.83
5		−0.23	−0.28	−0.28	−0.19	−0.22
6		−0.073	−0.077	−0.071	−0.044	−0.057
Sum		−7.66	−11.76	−15.88	−14.35	−14.96
Sum to ∞		−7.74	−11.81	−15.90	−14.36	−14.98
		Potential full Reid				
n	k_F:	1.2	1.4	1.6	1.8	
3		−3.23	−4.96	−6.58	−6.57	
4		−0.62	−0.91	−1.24	−1.51	
5		−0.17	−0.20	−0.18	−0.018	
6		−0.065	−0.063	−0.060	−0.077	
Sum		−4.08	−6.13	−8.06	−8.18	
Sum to ∞		−4.17	−6.19	−8.10	−8.18	

dication that long-range correlations are important in nuclear matter.

All calculations in this paper use the "conventional" single-particle spectrum of Eq. (4.10), i.e., the single-particle potential energy $U(k)$ is set equal to zero for $k > k_F$. Interesting suggestions for nonzero choices of $U(k)$ for states above the Fermi sea have been made. It is important to test the convergence of the generalized ring series for such choices of U. The methods developed in this paper could be used to do this. Note that a nonzero $U(k)$ for $k > k_F$ gives an explicit contribution to the $\mathcal{M}$ matrix. This contribution is obtained from Eqs. (5.45), (5.47), and (5.48) with $U(k_2, \delta E)$ in Eq. (5.45) being replaced by the negative of the chosen nonzero $U(k_2)$ for $k_2 > k_F$.

Table XXXIX shows that the generalized ring series modifies κ substantially from the two-body approximation κ_2. This is presumably because κ_n involves cross terms from products such as $S_2^{\dagger(2)} S_2^{(n)}$. However, the convergence of κ_n is still quite fast. The difference $\kappa_\infty - \kappa_2$ is nearly independent of density, even though κ_2 varies roughly as $k_F{}^2$.

Table XL shows contributions to D_3^c and to D_{GR}^{tot} from individual channels $(f_0 l) \equiv (l_0 S_0 j_0 T_0 l)$, for the full Reid potential at $k_F = 1.8$ fm^{-1}. These results are obtained by putting Eq. (5.26) into

TABLE XXXIX. Approximations to κ from the generalized ring series as described in the text. The columns headed 1.8*A* and 1.8*B* have the same meaning as in Table XXXIII.

		Potential v_2				
n	k_F:	1.4	1.6	1.8	1.8*A*	1.8*B*
2		0.140	0.197	0.270	0.261	0.270
3		0.159	0.224	0.300	0.283	0.293
4		0.163	0.231	0.310	0.290	0.303
5		0.165	0.233	0.309	0.288	0.300
6		0.166	0.234	0.311	0.289	0.303
∞		0.170	0.237	0.312	0.289	0.303
		Potential v_6(Reid)				
n	k_F:	1.4	1.6	1.8	1.8*A*	1.8*B*
2		0.149	0.190	0.246	0.236	0.246
3		0.199	0.249	0.312	0.293	0.307
4		0.214	0.263	0.326	0.302	0.318
5		0.219	0.267	0.328	0.304	0.321
6		0.222	0.269	0.329	0.304	0.322
∞		0.227	0.271	0.331	0.304	0.323
		Potential full Reid				
n	k_F:	1.2	1.4	1.6	1.8	
2		0.121	0.150	0.192	0.250	
3		0.164	0.196	0.241	0.296	
4		0.179	0.209	0.252	0.304	
5		0.185	0.213	0.256	0.306	
6		0.189	0.215	0.257	0.307	
∞		0.200	0.220	0.259	0.308	

TABLE XL. Contributions to D_3^c and D_{GR}^{tot} from individual $f_0\, l$ for the full Reid potential at $k_F = 1.8$ fm^{-1}, as described in the text.

f_0, l	D_3^c (MeV)	D_{GR}^{tot} (MeV)
$^1S_0$	−1.483	−1.820
$^3S_1(l=0)$	−1.074	−1.602
$^3S_1(l=2)$	−4.308	−4.730
$^1P_1$	−0.033	−0.086
$^3P_0$	0.372	0.310
$^3P_1$	−0.300	−0.388
$^3P_2(l=1)$	0.195	0.139
$^3P_2(l=3)$	−0.025	−0.048
$^1D_2$	0.025	0.017
$^3D_1(l=2)$	0.015	0.010
$^3D_1(l=0)$	−0.009	−0.016
$^3D_2$	−0.026	−0.036
$^3D_3(l=2)$	−0.001	−0.000
$^3D_3(l=4)$	0.087	0.074
Total	−6.57	−8.18

(5.25) and summing or integrating over all variables except $f_0 l$. The rapid convergence with increasing l_0 is clear.

The quantity

$$(kl \mid S_2(j_0 S_0 T_0) \mid k_0 l_0) = Q(P_b,k)\bar{S}_2(f_0 l k k_0) \tag{8.4}$$

is plotted against k in Fig. 8 for the full Reid potential at $k_F = 1.6$ fm^{-1}. All the curves have $f_0 = {}^3S_1$, $k_0 = 0.8$ fm^{-1}. The dashed curves give the two-body approximation $S_2^{(2)}$, and the solid curves give the sum of the generalized ring series S_2^{tot}, both in units of fm. The sharp corners at $k = 2.48$ fm^{-1} in the curves for $l = 2$ come from the factor $Q(P_b,k)$, which has a sharp corner at $k = k_F + \frac{1}{2}P_b = 2.48$ fm^{-1}. The factor $Q(P_b,k)$ is also present in the curves for $l = 0$, but its effect is not so apparent in the figure. The effect of three-body correlations, and of higher-order terms in the generalized ring series, is to enhance $S_2(k)$ in the region 2–4 fm^{-1}. However, the enhancement is quite moderate, which is consistent with the rapid convergence of the generalized ring series.

Since three-body calculations are fairly complicated, and since the two-body approximation is clearly inadequate, it is of great interest to find a simple way to reproduce the effect of three-body correlations. This is one of the motivations of nonzero choices for $U(k > k_F)$. [28,29] A successful choice, when inserted into Eq. (5.45), will have the effect that Eq. (5.47) is a good approximation to $\mathcal{M}\bar{S}_2$ for the exact $\mathcal{M}$ matrix. We can look at this from another point of view. Putting $\bar{S}_2 = \bar{S}_2^{\text{tot}}$ in Eq. (5.47), we replace $\mathcal{M}_B\bar{S}_2^{\text{tot}}$ by $\mathcal{M}\bar{S}_2^{\text{tot}}$, where $\mathcal{M}$ is the full $\mathcal{M}$ matrix. Then we solve for $\bar{U}(k,k_0)$ [we call the solution $U_{\text{eff}}(k)$]. This tells us what function $U_{\text{eff}}(k)$ is required to reproduce the effect of $\mathcal{M}$ on the function of interest, $\bar{S}_2^{\text{tot}}$. The result will depend on $f_0 l$ as well as on k,k_0. Hence it cannot be reproduced by any single-particle potential, because any such potential would give through Eq. (5.45) a result $\bar{U}(k,k_0)$ that is independent of $f_0 l$. This is not really a problem however. If we can find *any* function $U_{\text{eff}}(k)$, depending on $k_0 f_0 l$ or not, that reproduces the effect of $\mathcal{M}$ on $\bar{S}_2^{\text{tot}}$, we will have succeeded in reproducing the effect of three-body correlations in a simple way. There is no reason to require that $U_{\text{eff}}(k,k_0 f_0 l)$ be associated with a single-particle potential.

Figure 9 shows the functions $U_{\text{eff}}(k)$ that are required to reproduce the effect of $\mathcal{M}$ on the function $\bar{S}_2^{\text{tot}}$. The full Reid potential is used with $k_F = 1.6$ fm^{-1} and $k_0 = 0.8$ fm^{-1}. The three channels (f_0,l) shown are $({}^3S_1,l = 0)$, $({}^3S_1,(l = 2)$, and $({}^1S_0,l = 0)$. For a given channel (f_0,l), $U_{\text{eff}}(k)$ is obtained by solving Eq. (5.47) for $\bar{U}(k,k_0)$ with $\mathcal{M}_B\bar{S}_2$ replaced by $\mathcal{M}\bar{S}_2^{\text{tot}}$. For comparison, the

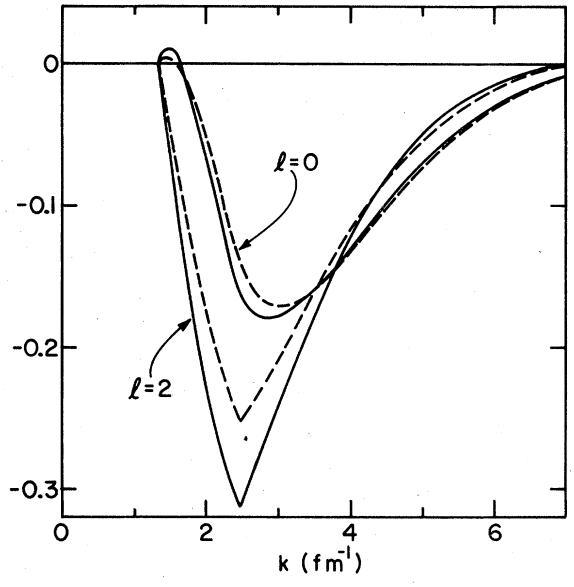

FIG 8. Plots of $S_2^{(2)}$ (dashed lines) and S_2^{tot} (solid lines) in fm as functions of k for the ${}^3S_1 - {}^3D_1$ channel. The full Reid potential is used at $k_F = 1.6$ fm^{-1}, with $k_0 = 0.8$ fm^{-1}.

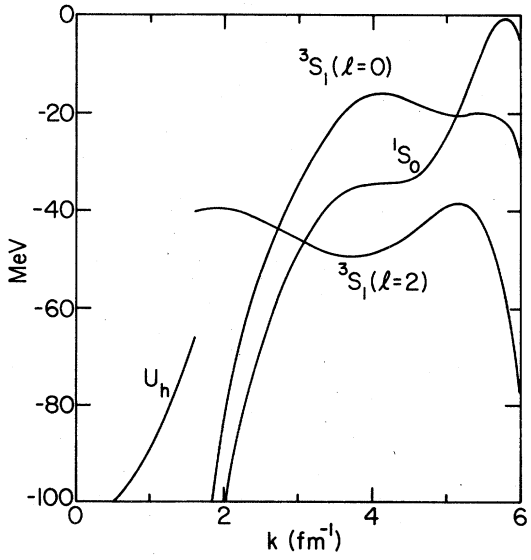

FIG 9. Effective potentials $U_{\text{eff}}(k)$ for the full Reid potential, as discussed in the text.

curve labeled U_h in Fig. 9 is the single-particle energy of states in the Fermi sea, using m^* and E_0 from Table III, and treating k as a single-particle momentum.

The behavior of $U_{\rm eff}(k)$ at large k is not very important because the energy denominators are so large that the ratio $\overline{U}/e_b$ in Eq. (5.47) is very small. Thus the region $k = 2$ to 4 fm^{-1}, where e_b is not too large and $\overline{S}_2^{\rm tot}$ is large, is probably the most important. For the $^3S_1(l=2)$ case, one sees from Fig. 9 that a constant $U_{\rm eff} \approx -45$ MeV will reproduce the effect of $\mathscr{M}$ quite well. In the $^1S_0$ and $^3S_1(l=0)$ cases, $U_{\rm eff}(k)$ goes to $-\infty$ as $k \to 1.6$ fm^{-1} because $\overline{S}_2^{\rm tot}(k)$ vanishes at $k = 1.6$ fm^{-1} (see Fig. 8). For 2 fm$^{-1} < k < 4$ fm^{-1}, $U_{\rm eff}(k, l=0)$ rises sharply from -85 to -15 MeV. This behavior is quite different from that in the $^3S_1(l=2)$ case.

Let us now use our results to calculate the binding energy of nuclear matter. To do this, we use our three-body results to estimate the contributions from all three- and four-hole-line contributions to the energy. An alternative procedure is to use the Bochum truncation of the coupled-cluster equations.[4-6,11] Our three-body results allow us to estimate the results of coupled-cluster calculations at the three- and four-body levels. This will be reported elsewhere,[27] but we note here that the hole-line and coupled-cluster results are numerically very close,[27,11] differing by only 1–2 MeV even at the high density corresponding to $k_F = 1.8$ fm^{-1}.

All three- and four-hole-line diagrams are enumerated, and many are numerically calculated, in Ref. 8, which gives simple scaling formulas for most of the terms. The quantities entering these scaling formulas are D_2, $\overline{U} \equiv 2D_2$, D_3^c, and κ_2. Also, the four-hole-line term of class B1 in Ref. 8 is simply the second term $D_4^{\rm GR}$ of the generalized ring series in our present notation. Probably the four-hole-line term with the largest numerical uncertainty is the four-body cluster term D_4^c, which was called W_4 in Ref. 8. There, a rough numerical calculation using central forces gave a result of order $\kappa_2^2 D_2$ for D_4^c (see also the work of Lassey and Sprung[30]). Here we take D_4^c to be zero with a numerical uncertainty of $\pm\kappa_2^2 D_2$. This is consistent with the only available numerical calculation[8,30] but can only be firmly established by further numerical work.

The three-hole-line terms are D_3^c and the hole-hole term D_3^{hh} (called W_3^{hh} in Ref. 8). The four-hole-line terms are designated $A1, A2, \ldots, A9$, $B1, B2, \ldots, B6$, and D_4^c, where we follow the notation of Ref. 8 except for D_4^c. Diagrams $A3$ and $A4$ are identical except for an exchange of hole lines,[5,6] and it is found numerically that they nearly cancel each other.[8] Therefore, we omit terms $A3$ and $A4$ here. The terms $A7$ and $A9$ are also omitted because they nearly cancel and are individually extremely small.

Our method of estimating the three- and four-hole-line contributions is illustrated in Table XLI, for the full Reid potential at $k_F = 1.6$ fm^{-1}. Column 1 lists all the diagrams except $A3$, $A4$, $A7$, and $A9$, whose sum is assumed to be zero. Column 2 gives the scaling formulas for the various diagrams, obtained from the results of Ref. 8. Scaling formulas are not needed for D_3^c and $B1 = D_4^{\rm GR}$ because these are calculated in this paper. Column 3 gives an estimate of the percentage error in each term. The error in D_4^c was discussed above, and the error in D_3^c was discussed in Sec. VII I. We assume the same relative error for $D_4^{\rm GR}$ as for D_3^c. The other error estimates are based on a careful reading of Ref. 8. They are reasonably conservative but are not backed up by any firm numerical results. Column 4 gives numerical values and uncertainties for each term. The values of D_3^c and $B1 = D_4^{\rm GR}$ are taken from the rows $n = 3$ and 4, respectively, of Table XXXVIII. The other numerical values are obtained from the scaling formulas of column 2. The values of D_2, $\overline{U} \equiv 2D_2$, and κ_2 needed in the formulas are found in Table III. The error in the total three- or four-hole-line contribution is taken to be the square root of the sums of the squares of the individual errors. However, the error in the sum $D_3 + D_4$ is not the square root of sums of squares of individual errors because the error in D_3^c is correlated with the error in $B3 + B4 \approx -(8\kappa_2/3)D_3^c$, and similarly for D_3^{hh} and $A2$. The errors for these four terms are marked with asterisks in Table XLI, and error estimates for them are discussed in the next paragraph.

In the estimate

$$D_3^c + B3 + B4 \approx (1 - 8\kappa_2/3)D_3^c \ , \tag{8.5}$$

there are two sources of error: the uncertainty in D_3^c and the uncertainty in the formula

$$B3 + B4 \approx (8\kappa_2/3)D_3^c \ . \tag{8.6}$$

According to Table XLI, the latter uncertainty exists even when D_3^c is known precisely. We assume the error in Eq. (8.5) to be the sum of two independent errors δ_1 and δ_2 given by

$$\delta_1 = (1 - 8\kappa_2/3)\delta D_3^c \ , \tag{8.7}$$

$$\delta_2 = 0.20(-8\kappa_2/3)D_3^c \ , \tag{8.8}$$

TABLE XLI. Estimates of the three- and four-hole-line terms and numerical uncertainties for the full Reid potential at $k_F = 1.6$ fm^{-1}, as discussed in the text. In the formulas for $A5 + A6 + A8$ and $B6$, $\overline{U}$ and D_3^c are to be expressed in MeV to obtain a result in MeV.

Term	Scaling formula	Error	Numerical Value (MeV)
D_3^{hh}	$\kappa_2\overline{U}/26$	$\pm 50\%$(*)	-0.60 ± 0.30
D_3^c		$\pm 15\%$(*)	-6.58 ± 0.99
Total $= D_3$			-7.18 ± 1.03
$A1$	$\kappa_2^2 D_2$	$\pm 20\%$	-1.50 ± 0.30
$A2$	$-4\kappa_2 D_3^{hh}$	$\pm 50\%$(*)	0.46 ± 0.23
$A5 + A6 + A8$	$-\kappa_2\overline{U}^2/3270$	$\pm 50\%$	-0.39 ± 0.20
$B1$		$\pm 15\%$	-1.24 ± 0.19
$B2$	D_3^{hh}	$\pm 100\%$	-0.60 ± 0.60
$B3 + B4$	$-(8\kappa_2/3)D_3^c$	$\pm 20\%$(*)	3.37 ± 0.67
$B5$	$\kappa_2^2\overline{U}/7$	$\pm 100\%$	-0.43 ± 0.43
$B6$	$-\overline{U}D_3^c/2000$	$\pm 100\%$	-0.27 ± 0.27
D_4^c	zero	$\pm \kappa_2^2 D_2$	0 ± 1.50
Total $= D_4$			-0.60 ± 1.88

where δD_3^c is the uncertainty in D_3^c and the factor 0.20 in Eq. (8.8) comes from the 20% uncertainty in Eq. (8.6). Then we take the error in $D_3^c + B3 + B4$ to be $(\delta_1^2 + \delta_2^2)^{1/2}$. A similar procedure is applied to $D_3^{hh} + A2$. To estimate the error in $D_3 + D_4$ we sum the squares of the errors of all terms not marked with asterisks in Table XLI. We add to this the squares of the errors in $(D_3^c + B3 + B4)$ and $(D_3^{hh} + A2)$ and take the square root. In this way we obtain the results given in Table XLII. In this table the rows labeled $BB(2)$, $BB(3)$, and $BB(4)$ correspond, respectively, to $\overline{T} + D_2$, $\overline{T} + D_2 + D_3$, and $\overline{T} + D_2 + D_3 + D_4$, where $\overline{T} = 3k_F^2/10$ is the average kinetic energy of the Fermi-gas state. The uncertainties quoted in Table XLII are the numerical uncertainties discussed above. We have assumed that the contributions from higher-order terms in

TABLE XLII. Different approximations to the energy per particle of nuclear matter for various potentials and values of k_F. All energies are in MeV and k_F is in fm^{-1}. Further discussion is given in the text.

k_F:	1.2	1.4	1.6	1.8
		Potential v_2		
$BB(2)$		4.7	6.1	9.8
$BB(3)$		0.4 ± 0.6	-1.2 ± 1.1	-0.5 ± 1.5
$BB(4)$		0.8 ± 0.7	-0.2 ± 1.5	0.9 ± 2.9
		Potential v_6(Reid)		
$BB(2)$		-11.0	-10.0	-5.4
$BB(3)$		-17.8 ± 1.0	-20.5 ± 1.5	-19.8 ± 2.1
$BB(4)$		-17.9 ± 1.2	-19.9 ± 2.2	-17.8 ± 3.7
		Potential full Reid		
$BB(2)$	-9.5	-10.5	-8.9	-3.4
$BB(3)$	-13.0 ± 0.5	-15.9 ± 0.8	-16.1 ± 1.0	-10.8 ± 1.5
$BB(4)$	-13.4 ± 0.7	-16.4 ± 1.1	-16.7 ± 1.9	-12.3 ± 3.2

the hole-line expansion are negligible compared to the numerical uncertainties in the rows labled $BB(4)$ in Table XLII. This assumption is consistent with the observed rapid convergence of the first three terms D_2, D_3, D_4 of the hole-line expansion. The Bochum truncation of the coupled-cluster equations is found to converge as well or better.[27]

For each of the three potentials considered, the $BB(4)$ result in Table XLII gives our best estimate of the energy per particle of nuclear matter as a function of k_F. The results for v_2 and v_6(Reid) are consistent[9,10] with variational calculations. Variational results are not yet available for the full Reid potential. The approximations $BB(2)$, $BB(3)$, and $BB(4)$ are plotted in Fig. 10 for the full Reid potential. The dashed curves give the estimated numerical uncertainty in the $BB(4)$ result. The empirical saturation point is believed[3] to lie inside the rectangular box that extends between -15 and -17 MeV and between 1.28 and 1.44 fm^{-1}.

The $BB(4)$ curve saturates at $E/A = 17.3$ MeV, $k_F = 1.52$ fm^{-1}, i.e., at a reasonable energy but too high a density. It is important to estimate the uncertainty in this calculated saturation point. The curves labeled L and H in Fig. 10 have been constructed for this purpose. Curve L is drawn by eye with the requirement that it remain inside the dashed curves but saturate at the lowest possible value of k_F, consistent with smooth and reasonable behavior. Curve H is obtained in the same way, except that we aim for saturation at the highest possible value of k_F. The curves, L, $BB(4)$, and H have minima at $k_F = 1.43$, 1.52, and 1.63 fm^{-1}, respectively. Thus the uncertainty in the calculated saturation point is of the order of 0.1 fm^{-1} in k_F and 1.5 MeV in energy.

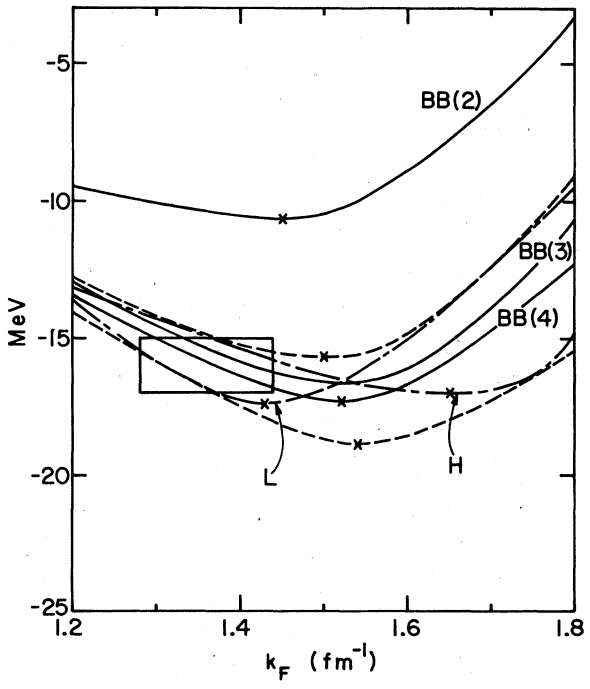

FIG 10. Saturation curves for the full Reid potential, as discussed in the text.

The compressibility parameter K is defined by

$$K = k_{F0}^2 \left. \frac{d^2E/A}{dk_F^2} \right|_{k_{F0}}, \tag{8.9}$$

where k_{F0} is the value of k_F at saturation. Fitting the $BB(4)$ results of Table XLII with a cubic in k_F, one finds $K = 226$ MeV, which is consistent with the empirical value $K = 210-230$ MeV deduced by Blaizot, Gogny, and Grammaticos,[31] using a random-phase approximation (RPA) analysis of measured monopole excitations in nuclei.

IX. SUMMARY AND DISCUSSION

We have seen that it is feasible to solve the three-body equation in nuclear matter for interesting phenomenological potentials, such as the Reid potential. Two types of calculation are made possible by solution of the three-body equation. The simpler calculation (called $\mathcal{O}$-type) gives the three-body cluster energy D_3^c, which is the leading correction to the lowest-order two-body Brueckner-Bethe result. The more elaborate calculation (called $\mathcal{M}$-type) gives not only the three-hole-line term D_3^c, but also a series of terms involving four, five,...hole lines. This series is called the generalized ring series and is the most likely place to look for long-range correlations in nuclear matter.

The method is suitable for two-body potentials that are defined independently in each two-body channel jST. Hence there is no difficulty in treating the complicated state dependence of the nuclear force. Also, since we calculate the two-body reaction matrix in momentum space, there is no requirement that the potential in a given two-body channel by only a function of r. An arbitrary nonlocality can be treated, and the method should therefore be applicable to potentials such as those of the Paris[32] and Bonn[33] groups. The method may be less effective for a potential with an infinitely repulsive core. In that case, the two-body reaction matrix can of course be calculated, but it will decrease more slowly with momentum than for a potential such as

Reid. Using a momentum cutoff of 8 fm^{-1}, which was found to be accurate for the Reid potential, might cause appreciable error when a hard core is present. This question remains to be studied.

The numerical accuracy for various choices of mesh parameters and cutoffs has been studied in detail and is satisfactory. The numerical error caused by the various angle-average approximations that have been made is less well determined. It is plausible from the numerical results that the total numerical error in D_3^c is no greater than 15%, but this can only be established by better calculations. In particular, one could try to treat the difference between the exact and angle-average Pauli operators by first-order perturbation theory.

The calculations require substantial computer resources. The $\mathscr{M}$-type production calculations for the Reid potential take about two hours for each value of k_F, using the very fast IBM 370-195 computer, which is roughly as fast as the CDC 7600. This time could be reduced in several ways. One could use coarser meshes, such as reducing $N(k_0)$ from 3 to 2, or $n_{\max}$ from 8 to 6, without seriously affecting the accuracy. Omitting two-body states in the Fermi sea having $l_0 = 2$ would save substantial computing time and cause only small errors. One could also do the simpler $\mathscr{O}$-type calculation instead of the $\mathscr{M}$-type calculation. This would be sufficient to obtain the three-hole-line approximation to the energy, and the omitted four-hole-line contribution is only 1—2 MeV per particle. Finally, all our calculations have been done in double precision, so that about 14 significant figures are stored in the computer for each variable. It seems quite likely that a single-precision calculation (about seven significant figures for each variable) would be sufficiently accurate. This would save a factor of 2 in storage requirements and thus make the calculation less expensive. So far this possibility has not been tested.

For each two-body potential to be treated, one has to explore in each two-body channel the accuracy of the separable representation of the off-energy-shell reaction matrix. The separable representation is not used for the bubble contribution to $\mathscr{M}$ or D_3^c, but it *is* used for the ring and higher-order contributions. For the ring contribution, one can use as many separable terms as required for the desired accuracy. For the higher-order terms, in order to keep the matrices to a manageable size, one has to use a judicious choice of separable terms, based on the results of test calculations. These test calculations may require several man days of effort, but this seems unavoidable in the present method.

The main conclusions that emerge from the numerical calculations follow: (1) The three-body cluster term D_3^c is attractive. Its magnitude is typically 4—5 MeV near the empirical saturation density and increases with density. (2) The generalized ring series converges rapidly for all three two-body potentials studied, and over a wide range of density. Conclusion (1) means that the lowest-order two-body calculation is inadequate: the three-body cluster term must be taken into account. A simple way of doing this would be valuable. One possibility is the use of a nonzero single-particle potential energy for momenta above the Fermi sea.[28,29] We have argued, however, that other methods may be simpler and more accurate. Remarkably, the simple formula $D_3^c \approx \kappa_2 D_2$ is usually accurate to 20%. However, at present we have no good understanding of why any of these prescriptions should accurately reproduce the value of D_3^c. Conclusion (2) that the generalized ring series converges rapidly means that long-range correlations are not very important for the energy of nuclear matter. Rapid convergence of the generalized ring series is also consistent with the validity of the hole-line expansion because each term in the generalized ring series has one more hole line than its predecessor. In this paper we have used the hole-line expansion to calculate the energy per particle of nuclear matter. The Bochum truncation of the coupled cluster equations provides an equally plausible approximation scheme. This scheme has been applied elsewhere[27] and gives results consistent with the hole-line expansion.

The hole-line expansion and the Bochum truncation are both approximation schemes for solving the system of coupled cluster equations, which are equivalent to the many-body Schrödinger equation. The two schemes are based on similar physical ideas and give similar numerical results. This paper has been devoted to the technical matter of solving the three-body equation, which is necessary to carry out either scheme. The question arises of whether these schemes lead to an accurate approximation to the many-body Schrödinger equation. We certainly have no proof that this is so. However, the following results are consistent with the validity of the approximation scheme. (1) The numerical convergence is good (see Table XLII). (2) The most important source of long-range correlations has been investigated by studying the generalized ring series. (3) The hole-line expansion and the Bochum truncation give results that are consistent with each other.[27] (4) The results are stable with respect to small changes in the single-particle spectrum above

the Fermi sea. (5) The results are consistent with variational calculations.[9,10]

Assuming the hole-line expansion and Bochum truncation to be valid approximation methods, the accuracy attainable is limited by our ability to carry out the calculations. For the Reid potential, the numerical uncertainty in the calculated saturation point is about 0.1 fm^{-1} in k_F and 1.5 MeV in energy. To improve on this accuracy will require coming to grips with the four-body cluster term, which requires solving a four-body equation. This is sufficiently difficult that alternative schemes should be investigated first, such as attempting to combine[34] the coupled cluster equations with the powerful hypernetted-chain techniques that have been developed for variational calculations.

Although the present accuracy of the calculations is limited, it seems to be good enough to draw interesting conclusions. For example, we find that the Reid potential predicts saturation at about the right energy but at too high a density. It is important to make similar calculations for other two-body potentials that are fitted to nucleon-nucleon scattering data and to deuteron properties.

ACKNOWLEDGMENTS

I am extremely grateful to F. Coester, and J. Zabolitzky for many discussions of nuclear-matter theory over a long period of time. Frequent consultation with S. Pieper was invaluable in getting the computer programs running. I am indebted to R. V. Reid for the two-body potentials in higher partial waves and for correspondence about nucleon-nucleon phase shifts. This work was performed under the auspices of the U. S. Department of Energy.

APPENDIX

Here we define the three two-body potentials v_2, v_6(Reid), and full Reid that are used in this paper. We use the notation

$$x = 0.7r \ , \tag{A1}$$

where r is the distance between two nucleons and is measured in fm. All potentials are given in units of MeV.

The potential v_2 is a central potential with no spin or isospin dependence. Its radial shape is that of the central part of the Reid[12] soft-core potential in the $^3S_1$ - $^3D_1$ channel, namely

$$v_2(r) = -10.463e^{-x}/x + 105.468e^{-2x}/x - 3187.8e^{-4x}/x + 9924.3e^{-6x}/x \ . \tag{A2}$$

The v_6(Reid) potential is specified separately in each of the four spin-isospin channels.

$(a)(S = 0, T = 1)$. $v_6(\text{Reid}) = v_C(r)$, where

$$v_c(r) = -10.463e^{-x}/x - 1650.6e^{-4x}/x + 6484.2e^{-7x}/x \ . \tag{A3}$$

$(b)(S = 0, T = 0)$. $v_6(\text{Reid}) = v_C(r)$, where

$$v_c(r) = 31.389e^{-x}/x - 634.39e^{-2x}/x + 2163.4e^{-3x}/x \ . \tag{A4}$$

$(c)(S = 1, T = 0)$, $v_6(\text{Reid}) = v_C(r) + v_T(r)S_{12}$, where S_{12} is the tensor operator of Eq. (4.25), and

$$v_c(r) = -10.463e^{-x}/x + 105.468e^{-2x}/x - 3187.8e^{-4x}/x + 9924.3e^{-6x}/x \ , \tag{A5}$$

$$v_T(r) = -10.463[(1 + 3/x + 3/x^2)e^{-x}/x - (12/x + 3/x^2)e^{-4x}/x] + 351.77e^{-4x}/x - 1673.5e^{-6x}/x \ . \tag{A6}$$

$(d)(S = 1, T = 1)$. $v_6(\text{Reid}) = v_C(r) + v_T(r)S_{12}$, where

$$v_c(r) = (10.463/3)e^{-x}/x - 933.48e^{-4x}/x + 4152.1e^{-6x}/x \ , \tag{A7}$$

$$v_T(r) = 10.463[(\tfrac{1}{3} + 1/x + 1/x^2)e^{-x}/x - (4/x + 1/x^2)e^{-4x}/x] - 34.925e^{-3x}/x \ . \tag{A8}$$

The v_6(Reid) potential defined in Eqs. (A3)–(A8) is related to the Reid soft-core potential as follows. In all $(S = 0, T = 1)$ channels the Reid $^1S_0$ potential is used. In all $(S = 0, T = 0)$ channels the Reid $^1P_1$ potential is used. In all $(S = 1, T = 0)$ channels the Reid $^3S_1$ -$^3D_1$ potential is used with spin-orbit force omitted. In all $(S = 1, T = 1)$ channels the Reid $^3P_2$-$^3F_2$ potential is used with spin-orbit force omitted.

We now turn to the full Reid potential. In all two-body channels with $j \leq 2$ the Reid soft-core potential from Reid's paper is used (we do not repeat these formulas here). In two-body channels

with $j \geq 3$ we use potentials kindly supplied by Reid. In some cases I have made small modifications in these potentials, and any responsibility for possible inadequacy of the potentials rests with me. In tensor-coupled channels the potential has the form $v_C(r) + v_T(r)\, S_{12} + v_{LS}(r)\, \vec{l} \cdot \vec{S}$, and in uncoupled channels it is simply $v_C(r)$. The explicit formulas are

$^3D_3$-$^3G_3$:

$$v_c(r) = -10.463e^{-x}/x - 103.4e^{-2x}/x - 419.6e^{-4x}/x + 9924.3e^{-6x}/x \ , \tag{A9}$$

$$v_T(r) = -10.463[(1 + 3/x + 3/x^2)e^{-x}/x - (12/x + 3/x^2)e^{-4x}/x] + 351.77e^{-4x}/x - 1673.5e^{-6x}/x \ , \tag{A10}$$

$$v_{LS}(r) = 650e^{-4x}/x - 5506e^{-6x}/x \ . \tag{A11}$$

The tensor component of Eq. (A10) is identical to that used in the $^3S_1$-$^3D_1$ channel.

$^1F_3$ and $^1H_5$:

$$v_c(r) = 31.389(e^{-x}/x - 16e^{-4x}/x) \ . \tag{A12}$$

$^3G_4$:

$$v_c(r) = -31.389[(1 + 2/x + 2/x^2)e^{-x}/x - (16 + 8/x + 2/x^2)e^{-4x}/x] + 3133.04e^{-6x}/x \ . \tag{A13}$$

$^3G_5$-$^3I_5$: Use v_6(Reid) from Eqs. (A5) and (A6), with $v_{Ls} = 0$.

$^3F_3$:

$$v_c(r) = 10.463[(1 + 2/x + 2/x^2)e^{-x}/x - (8/x + 2/x^2)e^{-4x}/x] - 729.25e^{-4x}/x + 219.8e^{-6x}/x \ . \tag{A14}$$

$^3F_4$-$^3H_4$: v_C and v_T are the same as in $^3P_2$-$^3F_2$, which is the same as v_6(Reid) ($S = 1$, $T = 1$), Eqs. (A7) and (A8).

$$v_{LS}(r) = -1037.05e^{-6x}/x \ . \tag{A15}$$

Equation (A15) for v_{LS} is exactly one half the v_{LS} used in the $^3P_2$-$^3F_2$ channel.

$^1G_4$:

$$v_c(r) = -10.463e^{-x}/x - 39.025e^{-2x}/x + 6484.2e^{-7x}/x \ . \tag{A16}$$

$^3H_5$:

$$v_c(r) = 10.463[(1 + 2/x + 2/x^2)e^{-x}/x - (8/x + 2/x^2)e^{-4x}/x] \ . \tag{A17}$$

In all channels not explicitly specified, the v_6(Reid) potential is used.

[1]B. H. Brandow, Phys. Rev. 152, 863 (1966).
[2]B. D. Day, Rev. Mod. Phys. 39, 719 (1967).
[3]B. D. Day, Rev. Mod. Phys. 50, 495 (1978).
[4]K. H. Lührmann, Ann. Phys. (N. Y.) 103, 253 (1977).
[5]K. H. Lührmann and H. Kümmel, Nucl. Phys. A194, 225 (1972).
[6]H. Kümmel, K. H. Lührmann, and J. G. Zabolitzky, Phys. Rep. 36C, 1 (1978).
[7]F. Coester, in *Lectures in Theoretical Physics: Quantum Fluids and Nuclear Matter,* edited by K. T. Mahanthappa and W. E. Brittin (Gordon and Breach, New York, 1969), Vol. XI B.
[8]B. D. Day, Phys. Rev. 187, 1269 (1969).
[9]B. D. Day, Nucl. Phys. A328, 1 (1979).
[10]B. D. Day, in *The Meson Theory of Nuclear Forces and Nuclear Matter,* edited by D. Schütte, K. Holinde, and K. Bleuler (Bibliographisches Institut, Zurich, 1980), p. 1.
[11]B. D. Day, in Proceedings of the International School of Physics "Enrico Fermi," Varenna, 1980.
[12]R. V. Reid, Ann. Phys. (N.Y.) 50, 411 (1968).
[13]T. K. Dahlblom, Proceedings of the Abo Academy, Ser. B, Vol. 29, No. 6. Available from NORDITA, Blegdamsvej 17, Copenhagen, Denmark.
[14]P. Grangé, Phys. Lett. 56B, 439 (1975).
[15]P. Grangé and M. A. Preston, Nucl. Phys. A204, 1 (1973).
[16]J. G. Depp, Ph. D. thesis, Carnegie-Mellon University, 1969 (unpublished), available from University Microfilms, Inc., order No. 70-17139.

[17]B. D. Day, F. Coester and A. Goodman, Phys. Rev. C 6, 1992 (1972).
[18]M. Gell-Mann and K. A. Brueckner, Phys. Rev. 106, 364 (1957).
[19]K. A. Brueckner and K. Sawada, Phys. Rev. 106, 1117 (1957).
[20]J. Goldstone, Proc. R. Soc. London, Ser. A 239, 267 (1957).
[21]R. Rajaraman and H. A. Bethe, Rev. Mod. Phys. 39, 745 (1967).
[22]N. M. Hugenholtz, Physica (Utrecht) 23, 481 (1957).
[23]K. A. Brueckner and J. L. Gammel, Phys. Rev. 109, 1023 (1958).
[24]W. Legindgaard, Nucl. Phys. A297, 429 (1978).
[25]R. Balian and E. Brézin, Nuovo Cimento 61B, 403 (1969).
[26]A. H. Stroud and D. Secrest, *Gaussian Quadrature Formulas* (Prentice-Hall, Englewood Cliffs, 1966).
[27]B. D. Day and J. G. Zabolitzky Nucl. Phys. (to be published)
[28]H. S. Köhler, Nucl. Phys. A204, 65 (1973).
[29]A. Lejeune and C. Mahaux, Nucl. Phys. A295, 189 (1978).
[30]K. R. Lassey and D. W. Sprung, Nucl. Phys. A177, 125 (1971).
[31]J. P. Blaizot, D. Gogny and B. Grammaticos, Nucl. Phys. A265, 315 (1976).
[32]M. Lacombe, B. Loiseau, J. M. Richard, R. Vinh Mau, J. Côté, P. Pirès, and R. de Tourreil, Phys. Rev. C 21, 861 (1980).
[33]K. Holinde and R. Machleidt, Nucl. Phys. A247, 495 (1975).
[34]E. Krotscheck, H. Kümmel and J. G. Zabolitzky, Phys. Rev. A 22, 1243 (1980).